KEK 83-12
July 1983
T/E

PROCEEDINGS OF THE WORKSHOP

ON

"MONOPOLES AND PROTON DECAY"

18-20 October 1982
Kamioka, Japan

Edited by

J. ARAFUNE
H. SUGAWARA

NATIONAL LABORATORY FOR
HIGH ENERGY PHYSICS

Preface

Workshop on "Monopoles and the Proton Decay" was held October 18th through 20th at the site of proton decay experiment: Kamioka. Morning of 18th was devoted to theoretical talks and the rest to experimental talks. We had the chance to see the experimental hall in the morning of 19th. The organizers wish to express their sincere appreciation to the speakers and to all the participants for their active participation.

Organizers

J. Arafune and H. Sugawara

Contents

An Introduction to Monopole-Fermion Dynamics

Yoichi Kazama

Department of Physics, Kyoto University, Kyoto 606, JAPAN

(Slightly expanded version of the talk given at the workshop on "Proton Decay and Monopoles", Oct. 18 - 20, 1982, Kamioka, JAPAN. To be published in the Proceedings.)

Monopoles are elusive yet fascinating objects. While their existence leads to the celebrated charge quantization rule [1], their possible abundance is a nuisance for big-bang cosmology [2]. From the field theoretical point of view, they also occupy an enthralling role in that they reflect one of the most characteristic features of local gauge theories —— an intimate interplay between space-time symmetry and internal symmetry —— through global topology of gauge (and Higgs)fields. The recent discovery by Rubakov [3] that, in the presence of light fermions, they lead to a dramatic physical effect of catalyzing baryon number violation with large rate has added to their charm

The purpose of this lecture is to give a rudimentary account of monopoles with emphasis on their interaction with fermions, which should help understand the subsequent talks. The Rubakov syndrome and some more aspects of monopole theory will be discussed by Professors Kobayashi and Arafune.

1. An Abelian Monopole and a Charged Particle without Spin

Even in the era of non-abelian gauge theories and their monopoles, the role of abelian monopoles is not diminished. They survive as the asymptotic form of the non-abelian counterparts and most of the interesting physics can be analyzed in the abelian setting. So let us begin with an abelian monopole.

1-1. Monopole and Dirac String.

A monopole of course is characterized by the spherically symmetric magnetic field $H=g\hat{r}/r^2$, where g is the magnetic charge. When we try to express this as the curl of a vector potential $\vec{A}$, however, we immediatedly find that $\vec{A}$ must have a string of singularities [4] emanating from the monopole. The argument is simple: Assume that we can take a singularity-free potential. Then the total outward magnetic flux through a sphere is obtained, via Stokes' theorem, by the sum of line intergrals $\oint A_\mu dx^\mu$ around the equator in opposite directions. Since such a sum is obviously zero, not $4\pi g$, our assumption fails and $\vec{A}$ must have a singularity on every sphere around the monopole. In this way, one finds that a Dirac string is unavoidable.

Let us see this more explicitly by deriving a typical monopole potential in spherical coordinates. If we set $A_r=A_\theta=0$ and choose the Coulomb gauge, the equation $\vec{\nabla}\times\vec{A}=g\vec{r}/r^3$ reduces to

$$\begin{cases} \partial_r(A_\varphi r)=0 \\ \partial_\theta(A_\varphi \sin\theta)=g\sin\theta/r \\ \partial_\varphi A_\varphi = 0 \end{cases} , \qquad (1.1)$$

where the last is the Coulomb gauge condition. This is immediately solved to give

$$A_\varphi = g\frac{(c-\cos\theta)}{r\sin\theta} , \qquad (1.2)$$

where c is an arbitrary constant of integration. Now the Dirac string appears explicitly as the singularity of $1/r\sin\theta = 1/\sqrt{x^2+y^2}$, which cannot be exorcised by any choice of c. In fact, we have cheated a little. If we compute $\vec{\nabla}\times\vec{A}$ carefully with $\vec{A}$ given by (1.2), we not only get $g\vec{r}/r^3$ but also an extra piece

$$\vec{H}_s = 4\pi g\tfrac{1}{2}\left[(1+c)\theta(-z)-(1-c)\theta(z)\right]\delta(x)\delta(y) , \qquad (1.3)$$

which is there to keep the equation $\vec{\nabla}\cdot(\vec{\nabla}\times\vec{A})=0$ intact. Thus the potential (1.2) does not really describe an isolated monopole, but rather a monopole with an infinitely long string of magnetic flux.

1-2. Wu-Yang Formulation. [5]

That such an annoying string can be completely removed was pointed out by Wu and Yang. The idea after all is quite simple. Note that by choosing c to be 1 or -1, we can at least remove half of the string, the part along the positive z axis for c=1 and the part along the negative z axis for c=-1. So, if we devide the region around the monopole into two overlapping regions R_a and R_b (see Fig. 1) and define

$$\begin{aligned} (A_\varphi)_a &= g(+1-\cos\theta)/r\sin\theta \qquad \text{in } R_a \\ (A_\varphi)_b &= g(-1-\cos\theta)/r\sin\theta \qquad \text{in } R_b \end{aligned} , \qquad (1.4)$$

$(A_\varphi)_{a,b}$ in their respective domain of validity are entirely free of string singularities. A_φ, considered as a pair $((A_\varphi)_a, (A_\varphi)_b)$, is called a section, a concept borrowed from the mathematics of fibre bundles. [6] (A Little more about this later.)

What about in the overlap R_{ab}? To be consistent, $(A_\varphi)_a$ and $(A_\varphi)_b$ must describe the same physics, i.e., they must differ only by a gauge transformation. That this is indeed so stems from the fact that the arbitrariness of c is in fact a gauge freedom within the Coulomb gauge. Within the Coulomb gauge, we can still make a gauge transformation $\vec{A} \to \vec{A}' = \vec{A} + \vec{\nabla} f$ provided that the gauge function is harmonic, $\nabla^2 f = 0$. If we choose f to depend only on φ, so that $A_r = A_\theta = 0$ remain true, this condition reduces to $(\partial/\partial\varphi)^2 f(\varphi) = 0$. This gives $f(\varphi) = a\varphi + b$, and $(\vec{\nabla} f)_\varphi = a/r\sin\theta$, which precisely corresponds to the arbitrainess of c. Thus we see that

$$\begin{cases} (A_\varphi)_b = (A_\varphi)_a + \frac{1}{e}(\vec{\nabla} f)_\varphi \\ \qquad\quad = (A_\varphi)_a + \frac{1}{ie} e^{-if} \vec{\nabla} e^{if} \\ f = -2eg\varphi \end{cases} \tag{1.5}$$

The U(1) phase e^{if} is called a transition function and in quantum mechanical context will appear as the multiplicative phase for the wave function of a charged particle under the above gauge transformation. It can also be interpreted as the change in the phase of such a wave function when the charged particle encircles the Dirac string (1.3) by the amount φ.

In Wu-Yang formalism, one demands that the transition function is mathematically well-behaved, i.e., it should be single-valued. In Dirac's formulation, one requires that the string is undetectable by Bohm-Aharonov type experiment, which amounts to the single valuedness of the wave function in the presence of the string.

By either reasoning, we arrive at the famous quantization rule of Dirac [1].

$$2eg = \text{integer} . \tag{1.6}$$

1-3. Extra Angular Momentum

What makes the physics of the charge-monopole system extra-ordinary is the appearance of, in general half integral, extra angular momentum. This can be seen in three ways. (The fourth will be added when we come to SU(2) monopole.)

(A) The simplest is to consider the equation of motion of a charged particle in the monopole field in non-relativistic classical mechanics [7]. It reads

$$m\frac{d\vec{v}}{dt} = e\vec{v}\times\vec{H} = eg\vec{v}\times\frac{\vec{r}}{r^3} . \tag{1.7}$$

Multiplying from left by $\vec{r}\times$, we get

$$\vec{r}\times m\frac{d\vec{v}}{dt} = eg\vec{r}\times(\vec{v}\times\vec{r})\frac{1}{r^3} = \frac{eg}{r^3}\left[\vec{v}r^2 - \vec{r}(\vec{v}\cdot\vec{r})\right]$$
$$= eg\left(\frac{1}{r}\frac{d\vec{r}}{dt} - \frac{\vec{r}}{r^2}\frac{dr}{dt}\right) .$$

Noting that $\vec{r}\times\frac{d\vec{v}}{dt} = \frac{d}{dt}(\vec{r}\times\vec{v})$ and $\frac{d\hat{r}}{dt} = \frac{1}{r}\frac{d\vec{r}}{dt} - \frac{\vec{r}}{r^2}\frac{dr}{dt}$, we easily get

$$0 = \frac{d}{dt}\left(\vec{r}\times\vec{p} - eg\hat{r}\right) \equiv \frac{d\vec{J}}{dt} . \tag{1.8}$$

Thus we see that the conserved angular momentum has an extra piece $-eg\hat{r}$. It is perpendicular to the ordinary piece $\vec{r}\times\vec{p}$ and due

to the Dirac condition its magnitude $|eg|$ is quantized to be integral or half integral, like a spin.

(B) The extra angular momentum above can be interpreted also as a field angular momentum. If we denote $\vec{r}$, $\vec{E}(\vec{r}, \vec{r}')$, $\vec{H}(\vec{r}, \vec{r}')$ as the vector from the pole to the charge, the electric field at $\vec{r}'$ due to the charge, and the magnetic field at $\vec{r}'$ due to the pole, respectively, the angular momentum stored in such a field configuration is given by

$$\vec{L}_{field} = \int d^3r' \frac{1}{4\pi} \vec{r}' \times \left(\vec{E}(\vec{r}, \vec{r}') \times \vec{H}(\vec{r}, \vec{r}') \right).$$

The integral is easy (but not trivial) and again gives the answer $-eg\hat{r}$.

(C) Let us turn to non-relativistic quantum mechanics. The Hamiltonian and the stationary Schrödinger equation are

$$\begin{cases} H = \frac{1}{2m} (\vec{p} - e\vec{A})^2 \\ \frac{1}{2m} (\vec{p} - e\vec{A})^2 \Psi = E\Psi \end{cases} \qquad (1.9)$$

The latter is form-invariant under the gauge transformation $\vec{A} \to \vec{A}' = \vec{A} + \frac{1}{e} \vec{\nabla} f$, $\Psi \to \Psi' = (\exp if)\Psi$. Since the monopole field $\vec{A}$ is defined in R_a and R_b separately, Ψ must also be defined similarly, with the transition in the overlap R_{ab} given by

$$(\Psi)_b = e^{if} (\Psi)_a = e^{-i2egg} (\Psi)_a . \qquad (1.10)$$

Would the ordinary angular momentum $\vec{L} = \vec{r} \times (\vec{p} - e\vec{A})$ be still correct in this system? The answer is, as expected, no. An elementary calculation gives

$$[L_i, L_j] = i\varepsilon_{ijk} L_k + ieg\varepsilon_{ijk} \hat{r}_k , \qquad (1.11)$$

i.e., the Lie algebra is violated by the extra piece. This, however, can be easily cured. Noting that $\hat{r}_j$ still transforms like a vector, $[L_i, \hat{r}_j] = i\varepsilon_{ijk}\hat{r}_k$, we are tempted to define a new operator

$$\tilde{L} = \vec{r} \times (\vec{p} - e\vec{A}) - eg\hat{r} . \qquad (1.12)$$

Then

$$\begin{aligned} [\tilde{L}_i, \tilde{L}_j] &= [L_i, L_j] - eg \{ [L_i, \hat{r}_j] + [\hat{r}_i, L_j] \} \\ &= i\varepsilon_{ijk} L_k + ieg\varepsilon_{ijk}\hat{r}_k - 2ieg\varepsilon_{ijk}\hat{r}_k \\ &= i\varepsilon_{ijk} (L_k - eg\hat{r}_k) = i\varepsilon_{ijk}\tilde{L}_k . \end{aligned} \qquad (1.13)$$

Indeed L_i's satisfy the correct angular momentum algebra. It is also a simple matter to check that $\tilde{L}_i$'s commute with H. So $\tilde{L}$ has every right to be called the system's angular momentum operator.

1-4. Monopole Harmonics [8]

Because of the extra piece in the angular momentum, angular eigenfunctions are different from the ordinary spherical harmonics. They will be called monopole harmonics and are defined by

$$\begin{aligned} \tilde{L}^2 Y_{q,\tilde{\ell},\tilde{m}} &= \tilde{\ell}(\tilde{\ell}+1) Y_{q,\tilde{\ell},\tilde{m}} \\ \tilde{L}_z Y_{q,\tilde{\ell},\tilde{m}} &= \tilde{m} Y_{q,\tilde{\ell},\tilde{m}} \end{aligned} \qquad (1.14)$$

$$q_b \equiv eg$$

Before we go on, let us make a space-saving comment. As has been emphasized, all the quantities which depend on $\vec{A}$ must be defined in R_a and R_b separately. $\tilde{L}$ and $Y_{q,\ell,m}$ are such quantities. This nevertheless does not complicate the calculation. Once $Y_{q,\ell,m}$ is obtained in R_a, the corresponding expression in R_b is obtained simply by the general rule of (1.10). So from now on, we will only deal with the expressions for R_a.

Now the construction of $Y_{q,\ell,m}$ is a standard exercise in elementary quantum mechanics once we write down $\tilde{L}_z$ and $\tilde{L}_\pm$, the raising and lowering operators,

$$\tilde{L}_z = (\vec{r}\times\vec{p})_z - eg = \frac{1}{i}\frac{\partial}{\partial\varphi} - eg$$

$$\tilde{L}_\pm = (\vec{r}\times\vec{p})_\pm - eg\,A_\varphi e^{\pm i\varphi} = e^{\pm i\varphi}\left(\pm\frac{\partial}{\partial\theta} + i\cot\theta\frac{\partial}{\partial\varphi} - eg\frac{1-\cos\theta}{\sin\theta}\right). \quad (1.15)$$

Starting from the state $Y_{q,\tilde{\ell},\tilde{\ell}}$ with the highest weight, which is gotton by solving $\tilde{L}_+ Y_{q,\tilde{\ell},\tilde{\ell}} = 0$, repeated applications of $\tilde{L}_-$ give all the $Y_{q,\tilde{\ell},\tilde{m}}$'s. Just for the sake of completeness, we give the result:

$$Y_{q_b,\tilde{\ell},\tilde{m}} = e^{i\alpha}\frac{1}{2^{\tilde{\ell}}}\left[\frac{(2\tilde{\ell}+1)!\,(\tilde{\ell}+\tilde{m})!}{4\pi\,(\tilde{\ell}-\tilde{m})!\,(\tilde{\ell}+\tilde{q}_b)!\,(\tilde{\ell}-\tilde{q}_b)!}\right] e^{i(\tilde{m}+q_b)\varphi}$$

$$\times\frac{1}{(\sin\theta)^{\tilde{m}}\,(\tan\frac{\theta}{2})^{q_b}}\left(\frac{d}{d\cos\theta}\right)^{\tilde{\ell}-\tilde{m}}\left(\sin^{2\tilde{\ell}}\theta\,\tan^{2q_b}\theta/2\right), \quad (1.16)$$

where α is an arbitrary phase set by convention.

More important and useful than the explicit form above are some properties of $Y_{q,\tilde{\ell},\tilde{m}}$, which we shall list below.

1° $Y_{q,\tilde{\ell},\tilde{m}}$, as a section, is everywhere analytic. $\{Y_{q,\tilde{\ell},\tilde{m}}\}$ for any fixed q form a complete orthonormal system, i.e., one can expand any continuous section belonging to class q in terms of $Y_{q,\tilde{\ell},\tilde{m}}$.

2° $\tilde{\ell}$ takes the values $|q|$, $|q|+1$, ...

3° $Y_{q,\tilde{\ell},\tilde{m}}$ is related to the familiar rotation function $\mathcal{D}^{(j)}_{m'm}(\alpha,\beta,\gamma)$ by $Y_{q,\tilde{\ell},\tilde{m}}(\beta,\alpha) = \sqrt{\frac{2\tilde{\ell}+1}{4\pi}}(-1)^{q+\tilde{m}}\mathcal{D}^{(\tilde{\ell})}_{q,-m}(\alpha,\beta,-\alpha)$.

This is due to the fact that, for fixed m', $\mathcal{D}^{(j)}_{m'm}$, regarded as a vector indexed by m, form a basis of the irreducible representation specified by j and moreover for $\gamma=-\alpha$ they form a basis for functions on a sphere. Because of this, various formulae for the rotation functions can be readily utilized for $Y_{q,\tilde{\ell},\tilde{m}}$.

4° For the purpose of this lecture, all we shall encounter are the forms for $q=\pm 1/2$, $\tilde{\ell}=1/2$, which are very simple:

$$Y_{\frac12,\frac12,\frac12} = -\frac{1}{\sqrt{2\pi}}e^{i\varphi}\sin\frac{\theta}{2}, \qquad Y_{\frac12,\frac12,-\frac12} = \frac{1}{\sqrt{2\pi}}\cos\frac{\theta}{2}$$

$$Y_{-\frac12,\frac12,\frac12} = \frac{1}{\sqrt{2\pi}}\cos\frac{\theta}{2}, \qquad Y_{-\frac12,\frac12,-\frac12} = \frac{1}{\sqrt{2\pi}}e^{-i\varphi}\sin\frac{\theta}{2}. \quad (1.17)$$

2. A Dirac Fermion in the Field of an Abelian Monopole

2-1. Helicity Flip Scattering and Zero Energy Bound State [9]

Already for a system of a spinless charged particle and a monopole, the extra angular momentum alluded to above brings forth an intriguing circumstance. Although we shall not discuss it in detail, it can easily be shown [10] that aggregate of such "dyons" obey Fermi-Dirac statistics; fermions are created out of bosons.

Now when such an extra angular momentum is coupled to the spin of a charged Dirac particle, it leads to further novel phenomena. Namely, for the state with the lowest total angular momentum, helicity flip scattering occurs and also we will find a dyon-like bound state with exactly zero energy.

In the basis where γ^0 is diagonal, the Dirac equation of the form

$$\begin{bmatrix} -E+m & \vec{\sigma}\cdot(\vec{p}-e\vec{A}) \\ \vec{\sigma}\cdot(\vec{p}-e\vec{A}) & -E-m \end{bmatrix} \Psi = 0 \qquad (2.1)$$

The conserved angular momentum of the system is

$$\vec{J} = \vec{L} + \tfrac{1}{2}\vec{\Sigma} = \vec{L} - eq\hat{r} + \tfrac{1}{2}\vec{\Sigma} \qquad (2.2)$$

For the purpose of partial wave decomposition it sufficies to construct two-component angular eigenfunctions, which can be easily gotten via

$$|jm\rangle = \sum_{\tilde{\ell},\tilde{m},m_s} |\tilde{\ell},\tilde{m}\rangle \otimes |\tfrac{1}{2},m_s\rangle \langle \tilde{\ell},\tilde{m}:\tfrac{1}{2}m_s|jm\rangle \qquad (2.3)$$

Here $|\tilde{\ell},\tilde{m}\rangle$ denotes the monopole harmonics obtained in the previous section and $\langle \tilde{\ell}\,\tilde{m}:\tfrac{1}{2}m_s|jm\rangle$ are the Clebsch-Gordan coefficients. We then find that there are two types of independent eigenfunctions $\Phi^{(1)}_{jm}$ and $\Phi^{(2)}_{jm}$ given by

$$\Phi^{(1)}_{jm} = \begin{bmatrix} \left(\frac{j+m}{2j}\right)^{1/2} Y_{q,j-1/2,m-1/2} \\ \left(\frac{j-m}{2j}\right)^{1/2} Y_{q,j-1/2,m+1/2} \end{bmatrix} \quad \text{for } j=|q|+\tfrac{1}{2},|q|+\tfrac{3}{2},\cdots \qquad (2.4)$$

$$\Phi^{(2)}_{jm} = \begin{bmatrix} -\left(\frac{j-m+1}{2j+2}\right)^{1/2} Y_{q,j+1/2,m-1/2} \\ \left(\frac{j+m+1}{2j+2}\right)^{1/2} Y_{q,j+1/2,m+1/2} \end{bmatrix} \quad \text{for } j=|q|-\tfrac{1}{2},|q|+\tfrac{1}{2},\cdots \qquad (2.5)$$

Notice that for states with $j \geq |q|+1/2$, $\Phi^{(2)}_{jm}$ and $\Phi^{(2)}_{jm}$ occur pairwise for each j. This corresponds, in the familiar case of $q=0$, to parity even and odd states. The lowest angular momentum state with $j=|q|-1/2$ is an exception. Since $\tilde{\ell}_{min}=|q|$, the type (1) state for which $\tilde{\ell}=j-1/2$ cannot exist, and we only have a type (2) wave function. From now on, both because of simplicity and of its relevance to the Rubakov effect, we shall concentrate on the j_{min} state in the field of a fundamental monopole, i.e., we set $|q|=1/2$ and $j=0$, and use the symbol η to denote $\Phi^{(2)}_{00}$.

That a peculiar phenomenon may occur for this state can be seen without looking into the dynamics. It is earily checked that $\vec{\sigma}\cdot\hat{r}$ is conserved and commutes with $\vec{J}^2$ and J_z. Since η is an isolated state, and $(\vec{\sigma}\cdot\hat{r})^2=1$, η must be an eigenstate of $\vec{\sigma}\cdot\hat{r}$

with eigenvalues ±1. What is significant is that this sign depends upon the sign of q. To see this, we note that for η, $\hat{r}\cdot\vec{J}=-eg+\frac{1}{2}\vec{\sigma}\cdot\hat{r}$ vanishes because j=0. Thus we immediately get the key result

$$(\vec{\sigma}\cdot\hat{r})\eta = \frac{q}{|q|}\eta \quad . \tag{2.6}$$

Physical implication of this relation is readily appreciated once we recognize that $\vec{\sigma}\cdot\hat{r}$ is (minus) the helicity for the outgoing (incoming) wave in the asymptotic region. That is, the helicity of the outgoing (and incoming) wave is completely correlated with the sign of e for fixed g. This means that in the scattering process for this partial wave, the helicity must flip. (See Fig. 2). Consider, for instance, the case of positive q. If we send in a particle with helicity h=-1, and look at the outgoing particle, while the spin $\vec{\sigma}$ is still radially outward, parallel with $\hat{r}$, the momentum $\vec{p}$, which was initially inward, is of course changed into an outward vector. We see that the helicity has been flipped.

Does this process actually occur with finite amplitude? We now must look at the Dirac equation, which for this state becomes enormously simplified. Let us write

$$\psi = \begin{pmatrix} f(r)\eta \\ g(r)\eta \end{pmatrix} \quad . \tag{2.7}$$

Then the Dirac equation becomes

$$\begin{cases} (E-m)f\eta = \vec{\sigma}\cdot(\frac{1}{i}\vec{\nabla}-e\vec{A})g\eta \\ (E+m)g\eta = \vec{\sigma}\cdot(\frac{1}{i}\vec{\nabla}-e\vec{A})f\eta \end{cases} \quad . \tag{2.8}$$

If we now put

$$f = \frac{q}{|q|}\frac{1}{r}F \quad , \quad g = \frac{1}{i}\frac{1}{r}G \quad , \tag{2.9}$$

and use

$$\vec{\sigma}\cdot(\frac{1}{i}\vec{\nabla}-e\vec{A})(f\eta) = \frac{1}{i}\frac{q}{|q|}(\partial_r+\frac{1}{r})f\eta \quad , \tag{2.10}$$

(2.8) reduces to

$$\begin{cases} (m-E)F = \frac{d}{dr}G \\ (m+E)G = \frac{d}{dr}F \end{cases} \quad . \tag{2.11}$$

Combining these, we finally arrive at trivial equations,

$$\begin{cases} \left[\left(\frac{d}{dr}\right)^2+k^2\right]F = 0 \\ G = \frac{1}{m+E}\frac{d}{dr}F \\ k^2 = E^2-m^2 \end{cases} \tag{2.12}$$

(i) Scattering Solution: For scattering solution, $k^2>0$ and we obtain

$$\psi = \begin{bmatrix} \frac{q}{|q|}\frac{1}{r}\sin(kr+\delta)\eta \\ \frac{1}{i}\frac{k}{E+m}\frac{1}{r}\cos(kr+\delta)\eta \end{bmatrix} \tag{2.13}$$

δ = arbitrary phase .

This solution unfortunately is troublesome. For any choice of δ the probability amplitude for the particle to pass through the pole sitting at the origin does not vanish. In the Hilbert space

containing such a state vector, we have the so called Lipkin-Weisberger-Peshkin problem [11], namely that the following Jacobi identity fails:

$$\begin{cases} [P_1,[P_2,P_3]] + \text{cyclic} = -4\pi q \delta^3(\vec{r}) \neq 0 \\ P_i \equiv p_i - eA_i \quad . \end{cases} \tag{2.14}$$

This is related to the fact that the extra piece of the angular momentum, $-eq\hat{r}$, is not well defined at the origin.

An essentially unique cure [12] is provided by the introduction of an anomalous magnetic moment for the Dirac particle, (which is there anyway for the physical electron), which turns out to give the necessary suppression around the origin. Using the modified Hamiltonian

$$H_{new} = H_{old} - \frac{\kappa q}{2m} \gamma^0 \vec{\Sigma} \cdot \frac{\hat{r}}{r^2} \quad , \tag{2.15}$$

one earily finds that

$$-G = F \sim \exp\left(-\frac{|\kappa q|}{2mr}\right) \to 0 \quad \text{as } r \to 0 \quad . \tag{2.16}$$

This sets the boundary condition at the origin

$$-G/F \xrightarrow[r\to 0]{} 1 \tag{2.17}$$

and determines the phase to be $\delta = -\frac{\kappa}{|\kappa|}\frac{k}{E+m}$.

The scattering amplitude is now readily obtained by the usual procedure, i.e., by projecting the $j=j_{min}$ partial wave from the incoming plane wave, matching this to the incoming part of the scattering solution and so on. The result confirms the previous kinematical argument. For $q>0$ and κ infinitesimal, the scattering amplitude is given by

$$\begin{cases} f_{-\to+} = \frac{q}{ik}(\sin\theta)^{2|q|-1} e^{i\varphi+2i\delta} \\ f_{+\to-} = 0 \end{cases} \tag{2.18}$$

where $\pm$ refer to the helicities.

May be it is helpful, at this point, to make a comment on the relation between this result and the chiral anomaly [13]. At first sight, one may think that the chiral anomaly is not at work here since we have dealt only with a pure monopole, not with a dyon configuration. This is actually false; we do have a dyonic configuration in the problem. This becomes clear when we write down the matrix element of the relevant operator $\vec{E}\cdot\vec{B}$ between the initial and the final scattering states, i.e., ${}_{out}\langle e_R^-, M|\vec{E}\cdot\vec{B}|e_L^-, M\rangle_{in}$, where M stands for a monopole. Inserting the intermediate state $|\psi_s, M\rangle$ corresponding to the scattering solution obtained above, we have

$${}_{out}\langle e_R^-, M|\vec{E}|\psi_s, M\rangle\langle\psi_s, M|\vec{B}|e_L^-, M\rangle_{in} \quad . \tag{2.19}$$

There are two points to make. First, we are dealing with states containing an electron as well as a monopole. $\vec{E}$ can have non-vanishing expectation value. Second, as can be easily verified, the intermediate scatteirng state $|\psi_s, M\rangle$ contains components with both chiralities, even in the limit of vanishing electron

mass. (The proper limit is to send κ to zero and then set m=0) Thus each of the matrix element in (2.19) is non-vanishing. That the chirality flip scattering is due to the anomaly, not to the mass term, is also seen from the expression (2.18). The amplitude $f_{-\to+}$ does not vanish as we send m to zero.

(ii) Zero Energy Bound State: Now we set E=0 in (2.12). Then, $k^2=-m^2$, and we immediately get a normalizable solution

$$\begin{cases} F = e^{-mr} \\ G = -e^{-mr} \end{cases} \qquad (\text{for } m>0) \tag{2.20}$$

Notice that F and G satify the relation -G/F=1, which is identical with (2.17). This is the reason why we did not need to introduce $\kappa \neq 0$ first and then send κ to zero for this solution. This is a peculiar bound state. It is a boson, according to the spin-statistics relation mentioned before, and although it carries an electric charge, it is exactly degenerate in energy with the pure monopole. In the following subsection, we will understand better why such a state may exist.

2-2. Topology of Dirac Equation in the Monopole Field.

Previously we saw that the state with the lowest angular momentum, which exhibited peculiar properties, came into being because of the extra angular momentum. We now wish to show that the existence of such a state can also be understood in topological terms. In fancy language, the monopole field is a non-trivial

connection on the U(1) principal fiber bundle over S^2 and the raison d'être for the j_{min} state is a consequence of the Atiyah-Singer index theorem [14] (i.e., integrated "chiral anomaly") for it. We shall however work everything out explicitly in an earthly manner.

For simplicity, we will deal with the massless case. As is well known the massless Dirac equation $i\gamma^\mu(\partial_\mu + ieA_\mu)\Psi = 0$ can be decomposed into a set of decoupled equations for the two-component Weyl spinors. In γ_5 diagonal basis, they are of the form

$$\begin{cases} [i\partial_0 - A_0 \pm i\vec{\sigma}\cdot(\vec{\nabla} - ie\vec{A})]u_\pm = 0 \\ \Psi = \begin{pmatrix} u_+ \\ u_- \end{pmatrix} \end{cases} \tag{2.21}$$

where $\pm$ refer to chiralities. We now consider a configuration for which $A_0=A_0(r)$, $\vec{A} \propto \hat{\varphi}$, with $r\vec{A}$ being a function of θ and φ only. This includes a dyon configuration as well as that of a monopole. What we intend to do is to decompose the equation (2.21) into a part responsible for the dynamics in the r-t plane and a part which describes the physics on a sphere, i.e., in the $\theta - \varphi$ plane. Defining the Pauli matrices in spherical coordinates by

$$\begin{aligned} \sigma_r &\equiv \vec{\sigma}\cdot\hat{r} = \begin{pmatrix} \cos\theta & e^{i\varphi}\sin\theta \\ e^{i\varphi}\sin\theta & -\cos\theta \end{pmatrix} \\ \sigma_\theta &\equiv \vec{\sigma}\cdot\hat{\theta} = \begin{pmatrix} -\sin\theta & e^{-i\varphi}\cos\theta \\ e^{i\varphi}\cos\theta & \sin\theta \end{pmatrix} \\ \sigma_\varphi &\equiv \vec{\sigma}\cdot\hat{\varphi} = \begin{pmatrix} 0 & -ie^{-i\varphi} \\ ie^{i\varphi} & 0 \end{pmatrix} , \end{aligned} \tag{2.22}$$

and setting, for convenience,

$$u_\pm = \frac{1}{r}\chi_\pm \tag{2.23}$$

we easily achieve this goal and obtain

$$\begin{cases} \frac{1}{r}\left(i\partial_0 - eA_0 \pm i\sigma_r \frac{\partial}{\partial r}\right)\chi_\pm \pm \frac{1}{r^2} D_\Omega \chi_\pm = 0 \\ D_\Omega \equiv i\sigma_\theta \frac{\partial}{\partial\theta} + i\sigma_\varphi \frac{1}{\sin\theta}\frac{\partial}{\partial\varphi} - i\sigma_r + \sigma_\varphi (reA_\varphi) \end{cases} \tag{2.24}$$

Now a key observation is, that, by direct computation, one can show that

$$\{\sigma_r , D_\Omega\} = 0 \tag{2.25}$$

namely σ_r acts like γ_5 for the 2 dimensional Dirac-like operator D_Ω ; σ_r defines the "chirality" on a sphere. This imediately allows us to make the following familiar argument for the spectrum of D_Ω : If ϕ_λ is an eigenfunction of D_Ω with non zero eigenvalue λ , $\sigma_r\phi_\lambda$ is also an eigenfunction with eigenvalue $-\lambda$, i.e., non-vanishing eigenvalues and eigenfunctions come in pairs. On the other hand, the so called zero mode ϕ_0 with $\lambda = 0$, if it exists at all must be an eigenstate of the chirality operator σ_r with eigenvalue 1 or -1.

We have in fact explicitly verified these statements before when we constructed angular eigenstates $\varphi^{(1)}_{jm}$ and $\varphi^{(2)}_{jm}$. The relevant connection is provided by the relation (again directly verifiable)

$$D_\Omega^2 = \vec{J}^2 + \frac{1}{4} - (eg)^2$$

with

$$\vec{J} = \vec{r} \times (\vec{p} - e\vec{A}) - eg\hat{r} + \frac{1}{2}\vec{\sigma} \tag{2.26}$$

which shows that the eigenfunctions of D_Ω with eigenvalues $\pm\lambda$ have the same angular momentum and also, since $(|q|-1/2)(|q|+1/2) + \frac{1}{4} - q^2 = 0$, the state with $j = j_{min} = |q| - 1/2$ corresponds to the zero mode of D_Ω . Note that for the fundamental monopole ($|eg| = 1/2$). D_Ω is exactly the "square root" of $\vec{J}^2$.

Having identified $\vec{\sigma}\cdot\hat{r}$ as the "chirality" operator on a sphere, it is natural to go to the basis where it is diagonal. This is achieved by the unitary transformation

$$u = e^{i\theta\frac{\sigma_2}{2}} e^{i\varphi\frac{\sigma_3}{2}} , \tag{2.27}$$

which gives

$$\begin{aligned} u\sigma_\theta u^+ &= \sigma_1 \equiv \gamma^1 \\ u\sigma_\varphi u^+ &= \sigma_2 \equiv \gamma^2 \\ u\sigma_r u^+ &= \sigma_3 = \frac{1}{i}\gamma^1\gamma^2 \equiv \gamma^5 \end{aligned} \tag{2.28}$$

where γ^μ's are a set of gamma matrices in Euclidean two dimensions. In this basis, D_Ω takes the form

$$\begin{aligned} D'_\Omega = uD_\Omega u^+ = i\Big(&\gamma^1\frac{\partial}{\partial\theta} + \gamma^2\frac{1}{\sin\theta}\frac{\partial}{\partial\varphi} + \gamma^1\frac{1}{2}\frac{\cos\theta}{\sin\theta}\Big) \\ &+ \gamma^2(reA_\varphi) \end{aligned} \tag{2.29}$$

Now we are ready to show that D_{Ω}' is nothing other than the genuine Dirac operator on the unit sphere S^2. As we all know, the metric on S^2 is $g_{\mu\nu}$ =diag (1, $\sin^2\theta$), where μ=1, 2 refers to θ and φ respectively. To write down the Dirac operator, we need the zweibein $e^a{}_\mu$, related to $g_{\mu\nu}$ by $g_{\mu\nu}$ =$e^a{}_\mu e^a{}_\nu$, and its inverse $E_a^{\ \mu}$. Then non-vanishing components can be taken to be e^1_1=1, e^2_2=sinθ , E^1_1=1, and E^2_2=1/sinθ . The Dirac operator is then written as

$$D = i\gamma^a E_a^{\ \mu} \mathcal{D}_\mu \tag{2.30}$$

where $\mathcal{D}_\mu$ is the derivative which is gauge covariant as well as generally covariant, given by

$$\mathcal{D}_\mu = \partial_\mu + \frac{1}{4}[\gamma_b, \gamma_c]\omega_\mu^{bc} + ieA_\mu \tag{2.31}$$

$\omega_\mu^{\ bc}$ here is the spin connection and its sole non-vanishing component is ω_2^{21}=-cosθ . Putting these together, the explicit form of D is obtained as

$$D = i\left(\gamma^1\frac{\partial}{\partial\theta} + \gamma^2\frac{1}{\sin\theta}\frac{\partial}{\partial\varphi} + \gamma^1\frac{1}{2}\frac{\cos\theta}{\sin\theta}\right) - \gamma^2\frac{eA_2}{\sin\theta} \tag{2.32}$$

where

$$A_2 = A_{\mu=2} = A_a e^a{}_2 = -A_\varphi \sin\theta \ .$$

Thus, indeed D_{Ω}'=D.

Let us now look at the Atiyah-Singer index theorem on S^2. It reads

$$\nu_+ - \nu_- = \frac{1}{2\pi}\int_{S^2} F_{\mu\nu}dx^\mu dx^\nu \ , \tag{2.33}$$

where $\nu_\pm$ are the number of normalizable zero modes with two-dimensional chirality equal to $\pm$1. We can easily evaluate the right hand side for the monopole field, which is given by

$$A_\mu = \begin{cases} (0, \ -eg(1-\cos\theta)) & \text{for } R_a \\ (0, \ eg(1+\cos\theta)) & \text{for } R_b \end{cases} \tag{2.34}$$

The magnetic field now looks like an "electric" field in Euclidean 2 dimension and is given by

$$F_{12} = \frac{\partial}{\partial\theta}A_2 = -eg\sin\theta \qquad \text{for both } R_a \text{ and } R_b \tag{2.35}$$

Thus

$$\frac{1}{2\pi}\int F_{\mu\nu}dx^\mu dx^\nu = \frac{1}{2\pi}(-eg)\int \sin\theta \, d\theta d\varphi$$
$$= 2eg = 2\frac{q}{b} \ , \tag{2.36}$$

which is $q/|q|$ for the fundamental monopole. This clearly gives the promised topological reason why we had only one lowest angular momentum state η with $\sigma_r\eta = q/|q|\eta$. (Normalizability on S^2 is trivial since it is compact.)

Let us finally take a look at the equation in the r-t plane. For the angular zero mode, in σ_r-diagonal basis, Eq.(2.24) simplifies to

$$(i\partial_0 \pm i\sigma_3\frac{\partial}{\partial r} - eA_0)\chi_\pm = 0 \tag{2.37}$$

Multiplying from left by σ_1 and identifying $\sigma_1 = \bar{\gamma}^0$, $i\sigma_2 = \bar{\gamma}^1$, this can be written as

$$\begin{cases} i\bar{\gamma}^r(\partial_\mu + ieA_\mu)\chi_\pm = 0 \\ A_0 = A_0(r), \quad A_1 = 0 \quad . \end{cases} \tag{2.38}$$

We have found a remarkable thing: The fact that we have an angular zero mode, which is precisely due to the presence of the monopole, cast the equation into nothing but the two dimensional Dirac equation in the presence of an electric field. Due to this feature, when the system is fully second quantized, we will be dealing effectively with a Schwinger like model [15] and its famous quantum anomaly will lead to the Rubakov effect. In other words it is an interplay of two 2-dimensional anomalies, one in $\theta - \varphi$ plane and the other in r-t plane, which will be responsible for the exotic physics.

3. Non Abelian Monopoles

As was announced in the prologue, one of the main purposes of this talk is to lay a helpful ground work for understanding the Rubakov's effect. For this purpose, except for the all important boundary condition at the origin, to be discussed in the next section, we need not talk about non-abelian monopoles; the size of the core, within which non-abelian nature becomes

manifest, will never enter into the problem. Nevertheless for a pedagogical review, we cannot skip this fundamental subject. Descriptions will, however, be brief.

3-1. 't Hooft-Polyakov Monopole and Julia-Zee Dyon [16], [17]

Take an SU(2) gauge theory with a triplet of Higgs scalars. The Lagrangian is given by

$$\mathcal{L} = -\frac{1}{4}F^a_{\mu\nu}F^{\mu\nu}_a + \frac{1}{2}(D_\mu\phi)^a(D^\mu\phi)_a - \frac{1}{e^2}U(e\phi) \tag{3.1}$$

$$\begin{aligned} F^a_{\mu\nu} &= \partial_\mu A^a_\nu - \partial_\nu A^a_\mu + e\,\varepsilon^{abc}A^b_\mu A^c_\nu \ , \\ (D_\mu\phi)^a &= \partial_\mu\phi^a + e\,\varepsilon^{abc}A^b_\mu\phi^c \ , \end{aligned} \tag{3.2}$$

where the potential is chosen to effect the spontaneous breaking of SU(2) down to U(1), i.e.

$$U(e\phi) = \frac{\hbar^2}{4}(M_W^2 - e^2\phi^a\phi^a)^2 . \tag{3.3}$$

It is sometimes convenient to rescale the fields and define $eA^a \equiv a^a$, $e\phi^a \equiv \Phi^a$, in which case

$$\mathcal{L} = \frac{1}{e^2}\left\{-\frac{1}{4}F^a_{\mu\nu}F^{\mu\nu}_a + \frac{1}{2}(D_\mu\Phi)^2 - \frac{\hbar^2}{4}(M_W^2 - \Phi^a\Phi^a)^2\right\} . \tag{3.4}$$

This form shows that expansion in e is that in $\hbar$. The gauge boson mass matrix takes the form

$$\mathcal{M}^2_{ab} = M_W^2 (\delta_{ab} - \hat{\phi}_a \hat{\phi}_b)$$
$$\hat{\phi}_a \equiv \phi_a / |\phi| \quad . \tag{3.5}$$

Clearly $\mathcal{M}^2_{ab} \hat{\phi}_b$ vanishes, meaing that the rotation around the direction of the vacuum Higgs field corresponds to the unbroken "electromagnetic" U(1).

't Hooft gave a gauge invariant expression for the corresponding electromagnetic field strength tensor [16],

$$F_{\mu\nu} = \frac{\phi^a}{|\phi|} F^a_{\mu\nu} - \frac{1}{e|\phi|^3} \varepsilon^{abc} \phi^a (D_\mu \phi)^b (D_\nu \phi)^c \quad . \tag{3.6}$$

The second term is necessary to remove the non-abelian part. $F_{\mu\nu}$ can also be written as

$$F_{\mu\nu} = f_{\mu\nu} + H_{\mu\nu}$$
$$f_{\mu\nu} = \partial_\mu B_\nu - \partial_\nu B_\mu \quad , \quad B_\mu = \hat{\phi}^a A^a_\mu \quad , \tag{3.7}$$
$$H_{\mu\nu} = \frac{1}{e} \varepsilon^{abc} \hat{\phi}_a \partial_\mu \hat{\phi}_b \partial_\nu \hat{\phi}_c \quad .$$

The gauge invariant electric and magnetic currents are given by

$$j^e_\mu = \partial^\nu F_{\mu\nu} \qquad \text{(equation of motion)}$$
$$j^m_\mu = \partial^\nu \tilde{F}_{\mu\nu} \qquad \text{(definition)} \tag{3.8}$$

where $\tilde{F}_{\mu\nu} = \frac{1}{2} \varepsilon_{\mu\nu\rho\sigma} F^{\rho\sigma}$. Monopoles are the objects with non-vanishing magnetic charge $g = \frac{1}{4\pi} \int d^3x \, j^m_0$. What makes non-abelian monopoles conceptually much more fundamental than the abelian ones is that they exist as regular finite energy solutions of the field equation.

Before looking into specific solutions, however, we can see by topological reasoning [18] that eg is quantized. For a regular solutions, due to the abelian Bianchi identity, $f_{\mu\nu}$ part (see (3.7)) does not contribute to the magnetic current and j^m_μ consists entirely of Higgs field,

$$j^m_\mu = \frac{1}{2e} \varepsilon_{\mu\nu\rho\sigma} \partial^\nu \hat{\phi}^a \partial^\rho \hat{\phi}^b \partial^\sigma \hat{\phi}^c \varepsilon_{abc} \tag{3.9}$$

Then the magnetic charge is given by

$$g = \frac{1}{4\pi} \int d^3x \, j^m_0 = \lim_{R\to\infty} \frac{1}{8\pi e} \int_{S^2_R} \varepsilon_{ijk} \varepsilon_{abc} \hat{\phi}^a \partial_j \hat{\phi}^b \partial_k \hat{\phi}^c (d^2\sigma)_i \tag{3.10}$$

where $(d^2\sigma)_i$ is the unit area vector on the large sphere S^2_R. If we regard $\hat{\phi}^a$ as giving a coordinate on a sphere, the above expression can be rewritten in terms of the metric $g_{\alpha\beta} = \partial_\alpha \hat{\phi}^a \partial_\beta \hat{\phi}^a$ on the sphere

$$g = \lim_{R\to\infty} \pm \frac{1}{4\pi e} \int \sqrt{\det(g_{\alpha\beta})} \, d^2\xi$$
$$\xi_\alpha = \text{an independent coordinate on } S^2_R \tag{3.11}$$

The right hand side gives $\pm\frac{1}{e}$ times the number of times $\hat{\phi}^a$ covers the unit sphere as ξ_α sweeps S^2_R once. Thus one gets the quantization condition,

$$eg = n = \text{integer winding number} \quad , \tag{3.12}$$

or, in terms of the minimum charge $e' = \frac{e}{2}$ allowed for the SU(2) doublet field, $e'g = \frac{n}{2}$, which is precisely the Dirac quantization condition.

To get an explicit monopole solution, or more generally, a dyon solution, one tries to solve the field equation with a simplifying ansatz. The simplest one, of course, is the ansatz with spherical symmetry, which is also expected to be of lowest energy. In gauge theories, the spherical symmetry means invariance of the configuration under rotation plus global guage transformations. This restricts the form of A_0^a and ϕ^a to be $\propto x^a$ and that of A_i^a to be $\propto \delta_{ai}$, $\varepsilon_{aij}\hat{x}_j$, or $\hat{x}_a\hat{x}_i$. If one chooses the Coulomb gauge, as we shall do, $\varepsilon_{aij}\hat{x}_j$ will be the only allowed structure for A_i^a. With the additional requirement of time independence (again up to a gauge transformation), the ansatz may be written in the form

$$\begin{cases} A_o^a = \hat{x}_a \dfrac{J(r)}{er} \quad , \qquad \phi^a = \hat{x}_a \dfrac{H(r)}{er} \\ A_i^a = \varepsilon_{aij}\hat{x}_j \dfrac{A(r)}{er} \quad , \quad A(r) = 1 - K(r) \end{cases} \tag{3.13}$$

Substituting those into the energy functional and minimizing with respect to the unknown radial functions J(r), H(r) and A(r), one obtains the coupled non-linear equations

$$\begin{cases} r^2K'' = K\left(K^2 - J^2 + H^2 - 1\right) \\ r^2H'' = 2HK^2 - h^2e^2M_w^2r^2H\left(1 - \dfrac{H^2}{M_w^2r^2}\right) \\ r^2J'' = 2JK^2 \end{cases} , \tag{3.14}$$

where the double prime denotes $(d/dr)^2$. Except for a special limiting case called Prasad-Sommerfield limit [19], which is

obtained by sending h to zero with M_w fixed, (3.14) cannot be solved analytically and one must resort to numerical means. A typical result [17] is sketched in Fig. 3. A smooth monopole (dyon) indeed exists, and has a core of radius $\sim M_w^{-1}$ (if h=O(1)) outside of which it looks just like an abelian monopole (dyon). Asymptotically, for large r, the radial functions behave like

$$\begin{cases} K \sim e^{-ar} \\ \dfrac{J}{r} \sim M + \dfrac{b}{r} \\ \dfrac{H}{r} \sim M_w \end{cases} \quad (M, a, b \text{ are constants}) \tag{3.15}$$

The gauge invariant electric field $E_i = F_{oi}$, the electric charge Q, and the magnetic field B_i are given by

$$\begin{cases} E_i = -\hat{x}_i \dfrac{d}{dr}\left[\dfrac{J(r)}{er}\right] \\ Q = \dfrac{1}{4\pi}\int d^3x\, \partial_i F_{oi} = \dfrac{b}{e} \\ B_i = \hat{x}_i \dfrac{1}{er} \end{cases} \tag{3.16}$$

There are two points of particular importance;

(i) Inside the core, the fields diminish and become exactly zero at the origin, unlike the abelian coounterparts, which blow up. As a consequence, the total energy (the mass) is finite and is of the order $M_w/\alpha \sim 137M_w$.

(ii) At the classical level, the electric charge of the dyon is not quantized. Quantization requires the existence of a "periodicity" (or compactness) of some sort. When we demand that

the physical motion be identical after one period, quantization of the spectrum of the generator of such a motion occurs. For the magnetic charge, this periodicity is provided by the non-trivial topology of the sphere. What about for the electric charge?

There is actually a hidden periodicity which is non-topological. This can be most easily seen by going to a gauge in which the asymptotically constant part of A_0^a (see (3.15)) is absent. It is achieved by a time-dependent gauge transformation around the direction of the Higgs field

$$U_\lambda = \exp i\lambda \hat{r}\cdot\frac{\vec{\tau}}{2}$$

with $\lambda = -Mt$. Then A_i^a exhibits the following periodic structure in time:

$$A_i^a = \frac{A}{er}\varepsilon_{aij}\hat{x}_j + \frac{1}{er}(1-A)(1-\cos Mt)\varepsilon_{aij}\hat{x}_j - \frac{1}{er}(1-A)\sin Mt\,(\delta_{ai}-\hat{x}_a\hat{x}_i). \tag{3.17}$$

But as we said, a periodicity alone is not enough; we need to "close" the period. For the electric charge, the principle for closing the period is not in classical mechanics. It is provided, at the quantum level, by the Bohr-Sommerfeld quantization condition. In other words, only when we consider electric fluctuations around the monopole and require that they properly "encircle" the internal $U(1)_{EM}$ loop in a closed manner do we get the charge quantization [20], which turns out to be Q=ne with n being an integer.

We must mention one last thing about the basic features of SU(2) monopoles, namely, their relation to Dirac monopoles [18]. So far we have dealt with a smooth, regular so called hedgehog solution, whose asymptotic behavior is given by

$$\hat{\phi}^a \sim x^a/r$$
$$A^a_i \sim \frac{1}{e}\varepsilon_{aij}\frac{x_j}{r}\ . \tag{3.18}$$

Once the existence of such a solution is established, it is often more convenient to go to a unitary (or ableian) gauge in which particle identification will be easier. It is achieved by a singular gauge transformation

$$\begin{cases} U = e^{-i\varphi I_3}e^{i\theta I_2}e^{i\varphi I_3} \\ I_i = \text{SU(2) generators} \end{cases} \tag{3.19}$$

In this gauge, the fields for large r behave like

$$\hat{\phi}^a \sim \delta_{a3}$$
$$A^a_i \sim \delta_{a3}\frac{1}{e}\varepsilon_{i3k}\frac{x_k}{r(r-x_3)}\ , \tag{3.20}$$

i.e., the Higgs field is pointing along the third isospin direction and the monopole potential is precisely of the form of Dirac, including the string. We shall see later that this abelian form naturally arises when we deal with isodoublet fermions in the presence of an SU(2) monopole.

3-2. An SU(5) Monopole

For a monopole to induce a baryon number violation, it must have an ability to couple to a fermion multiplet whose members carry different baryon numbers. In this subsection, we shall discuss the simplest of such circummstances, namely a monopole in SU(5) grand unified theories a là Dokos and Tomaras [21].

Explicitly the generators of the SU(2) subgroup for the monopole, which we shall denote by $SU(2)_M$, are chosen to be

$$\vec{T} = \frac{1}{2}\,\mathrm{diag}\,(0,0,\vec{\tau},0). \tag{3.21}$$

Just like in the case of a pure SU(2) monopole, one wants to write down an ansatz for a static spherically symmetric solution. In the case at band, however, the requirement of spherical symmetry does not suffice to fix the form of the ansatz; because the symmetry group of the problem is much larger than SU(2). there exist many subgroups which are compatible with such a, rather mild, requirement. Nonetheless the strategy is clear. We look for the ansatz which is invariant under the largest possible subgoup Γ of $U(5)=SU(5)\times U(1)$ (the U(1) factor is related to the B-L number), which is compatible with spherical symmetry. In equations,

(A) spherical symmetry

$$\begin{aligned} &[L_i + T_i\,,\ A_j] = i\varepsilon_{ijk}A_k \\ &[L_i + T_i\,,\ A_0] = 0 \\ &[L_i + T_i\,,\ \Phi] = 0 \\ &(L_i + T_i)H = 0 \end{aligned} \tag{3.22}$$

(B) invariance under $\Gamma \subset U(5)$

$$[\Gamma_i, A_\mu] = 0, \quad [\Gamma_i, \Phi] = 0, \quad \Gamma_i H = 0 \tag{3.23}$$

(C) compatibility of (A) and (B)

$$[\Gamma_i,\ L_j + T_j] = 0 \tag{3.24}$$

where $A_\mu = A_\mu^a G^a$, $\Phi = \Phi^a G^a$, $H=(H_\alpha)$ are, respectively the SU(5) gauge fields, the real Higgs fields in the adjoint representation 24 and the complex Higgs fields in the fundamental representation 5. L_i is the angular momentum operator, and T_i, G^a, Γ_i are the generators of $SU(2)_M$, SU(5), and Γ, in that order.

To begin with, consider (3.24). If u is an element of Γ, $[u,\ T_i]=0$ leads to

$$u = \begin{bmatrix} a & b \\ \lambda\mathbb{1} & \\ c & d \end{bmatrix}, \tag{3.25}$$

where the matrices a, b, c and two numbers λ and d must satisfy

$$\begin{cases} ac^\dagger + bd^* = 0\ , & ca^\dagger + b^\dagger d = 0 \\ aa^\dagger + bb^\dagger = \mathbb{1}\ , & cc^\dagger + |d|^2 = 1 \\ |\lambda|^2 = 1 \end{cases} \tag{3.26}$$

The authors of Ref. 21 actually considered a subgroup of this, given by setting b=c=d=0. If we follow their path, u is reduced to the form

$$U = \begin{bmatrix} a & & \\ & e^{\alpha} \mathbb{1} & \\ & & 0 \end{bmatrix} , \qquad a \in U(2) \tag{3.27}$$

i.e., Γ is $U(2)\times U(1)$ or $SU(2)\times U(1)\times U(1)$. The ansatz we shall get is already simple enough for this choice of Γ. The five generators of Γ can be conveniently chosen as

$$\begin{aligned} \vec{\Gamma} &= \tfrac{1}{2}\,\mathrm{diag}\,(\vec{\sigma}, 0, 0, 0) \\ \Gamma_4 &= \tfrac{1}{2\sqrt{2}}\,\mathrm{diag}\,(1, 1, -1, -1, 0) \\ \Gamma_5 &= \tfrac{1}{2}\,\mathrm{diag}\,(1, 1, 0, 0, 0) \end{aligned} \tag{3.28}$$

Now from the remaining requirements (3.22) and (3.23) with Γ_i given by (3.28), one can easily deduce the desired ansatz in the regular gauge:

$$\begin{cases} H_i = 0 \ \text{ for } i=1,2,3,4 , \quad H_5 = \frac{1}{g}h(r) \\ \Phi = \mathrm{diag}\,(\phi_1(r), \phi_1(r), \phi_2(r)\mathbb{1} + \phi_3(r)\vec{\tau}\cdot\hat{r}, -2(\phi_1(r)+\phi_2(r))) \\ A_0 = \mathrm{diag}\,(J_1(r), J_1(r), J_2(r)\mathbb{1} + J(r)\vec{\tau}\cdot\hat{r}, -2(J_1(r)+J_2(r))) \\ A_i = (\hat{r}\times\vec{T})_i \,\frac{1-K(r)}{gr} \\ g = SU(5)\ \text{coupling constant} \end{cases} \tag{3.29}$$

The rest of the work is the same as before; substitute the ansatz into the expression for the energy, minimize that with respect to the radial functions and so on. One thing we must take into account in such a procedure is the boundary conditions at infinity for the Higgs fields. They must approach the prescribed vacuum values which ensure the correct hierarchical breaking pattern at desired scales. In terms of the fields in the ansatz, this corresponds to

$$\begin{cases} \phi_1(r) \to \nu g , \quad \phi_2(r) \to \frac{1}{2}\nu g(-\frac{1}{2}+\varepsilon) \\ \phi_3(r) \to \frac{1}{2}\nu g(\frac{5}{2}-\varepsilon) , \quad h(r) \to gv \\ \nu \sim 10^{14}\,\mathrm{Gev} , \quad \nu\varepsilon \sim v \sim 10^{2}\,\mathrm{Gev} . \end{cases} \tag{3.30}$$

Strictly speaking, no one has checked that a desired monopole-dyon solution exists with the above ansatz and boundary conditions. For the purpose of this talk, we shall be content, as were Dokos and Tomaras, to observe the strong resemblance of (3.29) to the SU(2) ansatz (3.13) and assume that a Julia-Zee type solution exists with the asymptotic behavior $K(r)\to e^{-ar}$, $J(r)\to M+b/r$, $J_1(r)\to O(\frac{1}{r^2})$ as $r\to\infty$. It should be remembered that $r\to\infty$ here really means $1/M_W < r < 1/\Lambda_{QCD}$, i.e., r is in the region where the only unbroken groups are $SU(3)_C \times U(1)_{EM}$ but yet the color force is sufficiently weak so that the semiclassical treatment makes sense.

The magnetic and the electric fields for the configuration above, in the regular gauge, are given by

$$\vec{B} \underset{r\to\infty}{\sim} -\frac{\hat{r}}{gr^2}\,\hat{r}\cdot\vec{T} \quad , \quad \vec{E} \underset{r\to\infty}{\sim} \frac{b\hat{r}}{gr^2}\,\hat{r}\cdot\vec{T} \tag{3.30}$$

To see what charges it possesses we must go to the unitary gauge where $\hat{r}\cdot\vec{T}$ becomes T_3. It is then decomposed into

$$T_3 = -\frac{1}{2}\left[\frac{Q}{e} + \frac{2}{\sqrt{3}}\Lambda_8\right]$$
$$\frac{Q}{e} = \text{diag}\,(-1/3, -1/3, -1/3, 1, 0)$$
$$\Lambda_8 = \frac{1}{2\sqrt{3}}\,\text{diag}\,(1, 1, -2, 0, 0) \qquad (3.31)$$

The dyon carries both color and electromagnetic charges.

At this juncture, let us make one point crystal clear, which is about the way the information of $SU(2)_M$ multiplet structure is reached at points far away from the monopole without being very much suppressed: Needless to say, the $SU(2)_M$ monopole group is spontaneously broken at the grand unification scale. However its U(1) subgroup, generated, in the unitary gauge, by T_3, is unbroken and the static monopole (dyon) field transmits the $SU(2)_M$ multiplet structure out to the asymptotic region. The monopole couples exclusively to $SU(2)_M$ non-singlets, while the ordinary transverse excitations, the gluons and the photons, are blind to such a structure.

How does the monopole actually couple to the fermions? This is readily given by writing out the interaction part

$$g\left[\bar{\xi}\, A_\mu^a T^a \gamma^\mu \xi + A_\mu^a \,\mathrm{Tr}\,(\Psi^\dagger \gamma_0 T^a \gamma^\mu \Psi)\right], \qquad (3.32)$$

where T^a are the $SU(2)_M$ generators and ξ and Ψ are the $\underline{5}_R$ and $\underline{10}_L$ multiplets given by

$$\xi = \begin{bmatrix} d_1 \\ d_2 \\ d_3 \\ e^+ \\ \bar{\nu} \end{bmatrix}_R , \qquad \Psi = \begin{bmatrix} 0 & u_3^c & -u_2^c & -u_1 & -d_1 \\ -u_3^c & 0 & u_1^c & -u_2 & -d_2 \\ u_2^c & -u_1 & 0 & -u_3 & -d_3 \\ u_1 & u_2 & u_3 & 0 & -e^+ \\ d_1 & d_2 & d_3 & e^+ & 0 \end{bmatrix}_L . \qquad (3.33)$$

One then gets the couplings

$$g A_\mu^3 \Big[\overline{(u_2^c, u_1)}_L \frac{\tau_3}{2}\begin{pmatrix} u_2^c \\ u_1 \end{pmatrix}_L + \overline{(-u_1^c, u_2)}_L \frac{\tau_3}{2}\begin{pmatrix} -u_1^c \\ u_2 \end{pmatrix}_L$$
$$+ \overline{(d_3, e^+)}_L \frac{\tau_3}{2}\begin{pmatrix} d_3 \\ e^+ \end{pmatrix}_L + \overline{(d_3, e^+)}_R \frac{\tau_3}{2}\begin{pmatrix} d_3 \\ e^+ \end{pmatrix}_R \Big]. \qquad (3.34)$$

Indeed the members of each multiplet carry distinct baryon numbers and the monopole above is seen to possess a potentiality for causing transitions leading to baryon number non-conservation.

4. SU(2) Doublet Fermions in the Presence of a Monopole (Dyon)

We will now go back to a pure SU(2) monopole (dyon) and put an isodoublet of Dirac fermion in such a field. The wave function of such a fermion is a tensor product

$$\psi_{\alpha i} = (u \otimes \xi)_{\alpha i} , \qquad (4.1)$$

where u_α and ξ_i are, respectively, a Dirac spinor and an isospinor. The Dirac equation then is of the form

$$\left(i\gamma^\mu \otimes \mathbb{1}\,\partial_\mu + \gamma^\mu \otimes \frac{\tau^a}{2} e A_\mu^a - m\,\mathbb{1}\otimes\mathbb{1}\right)(u \otimes \xi) = 0 . \qquad (4.2)$$

What we wish to enphasize hereafter is the relation between (4.2)

and the abelian Dirac eqation we explored in some detail in section 2, their similarity and the difference.

Let us begin with the similarity. For this, we shall stay out of the core region. It is easily checked that in the asymptotic region, the radial component of the isospin $\hat{r}\cdot\vec{\tau}$ is conserved. So it is natural to decompose ξ into eigenstates of $\hat{r}\cdot\vec{\tau}$, which we have actually done in section 2 for $\vec{\tau}$ interpreted as spin. If we recall

$$(\hat{r}\cdot\vec{\tau})\eta_\pm = \pm\eta_\pm$$
$$\eta_+ = \begin{pmatrix} \cos\frac{\theta}{2} \\ e^{i\varphi}\sin\frac{\theta}{2} \end{pmatrix}, \qquad \eta_- = \begin{pmatrix} e^{-i\varphi}\sin\frac{\theta}{2} \\ -\cos\frac{\theta}{2} \end{pmatrix}, \tag{4.3}$$

ψ can be written as

$$\psi = u_-\otimes\eta_+ + u_+\otimes\eta_- , \tag{4.4}$$

where the meaning of the subscrits $\pm$ for u will become self-explanatory shortly. When we substitute (4.4) and the asymptotic form of the dyon field in $A_0=0$ regular gauge into (4.2), after a bit of algebra, we arrive at the following expression:

$$\left\{\left[i\not{\partial} + \tfrac{1}{2}\left(-\frac{(1-\cos\theta)}{r\sin\theta}\right)\vec{\gamma}\cdot\hat{\varphi} + \tfrac{1}{2}\left(-\frac{d}{dr}\left(\frac{Jt}{er}\right)\right)\vec{\gamma}\cdot\hat{r} - m\right]u_-\right\}\otimes\eta_+$$
$$+\left\{\left[i\not{\partial} - \tfrac{1}{2}\left(-\frac{(1-\cos\theta)}{r\sin\theta}\right)\vec{\gamma}\cdot\hat{\varphi} - \tfrac{1}{2}\left(-\frac{d}{dr}\left(\frac{Jt}{er}\right)\right)\vec{\gamma}\cdot\hat{r} - m\right]u_+\right\}\otimes\eta_- = 0 \tag{4.5}$$

Because η_+ and η_- are independent, what we got are two sets of decoupled abelian Dirac equations. Notice the $\pm 1/2$ factors

appearing in (4.5). They are precisely the quantized value for e'g where $e'=\pm\frac{e}{2}$ is the electric charge of the femions. In other words, $u_\mp$ are the wave functions for the charge doublets in the unitary gauge with charges $\pm\frac{e}{2}$. Furthermore each system now must possess an extra spin $-e'g\hat{r}$, which in fact was an isospin $-\frac{\vec{\tau}\cdot\hat{r}}{2}$ in the regular gauge. A spin was created out of an isospin and this is the fourth derivation of the extra angular momentum promised in section 1.

Let us now confine ourselves to the peculiar state with total angular momentum J=0 which will play the main role in the Rubakov's phenomenon. Since this is the state for which the extra angular momentum is anti-parallel with the Dirac spin, we may write

$$u_\pm = \begin{pmatrix} f_\pm(r)\eta_\pm \\ g_\pm(r)\eta_\pm \end{pmatrix}, \quad (\vec{\sigma}\cdot\hat{r})\eta_\pm = \pm\eta_\pm , \tag{4.6}$$

and ψ becomes

$$\psi = \begin{pmatrix} f_-\eta_-\otimes\eta_+ + f_+\eta_+\otimes\eta_- \\ g_-\eta_-\otimes\eta_+ + g_+\eta_+\otimes\eta_- \end{pmatrix}. \tag{4.6}$$

Working out the tensor products, this can also be written as [3]

$$\psi = \frac{1}{2i}\begin{bmatrix} \left((f_+ - f_-) + (f_+ + f_-)\vec{\tau}\cdot\hat{r}\right)\tau_2 \\ \left((g_+ - g_-) + (g_+ + g_-)\vec{\tau}\cdot\hat{r}\right)\tau_2 \end{bmatrix}. \tag{4.7}$$

As should be clear from the preceding discussions, SU(2) Dirac equations are nothing other than the two completely decoupled abelian equations far from the monopole. No new physics, apart

from the phenomena already discussed in Sect. 2, cannot possibly occur for such a system. But now comes the only and the all important difference, the behavior inside the core, or, in the limit of infinitesimal core size, the boundary condition at the origin [3]. Here, all we have to remember is the fact that all the fields vanish sufficiently fast as $r \to 0$ for a non-abelian monopole. This means we can completely forget about the monopole and simply study the free Dirac equation near the origin,

$$(i\gamma^\mu \otimes \mathbb{1}\partial_\mu - m\,\mathbb{1}\otimes\mathbb{1})\,\psi = 0. \tag{4.8}$$

To avoid confusion, we must say that there is a qualification about the previous sentence; we have not completely forgotten about the monopole. The special form (4.7) of ψ, which we shall substitute into the free equation, knows about the monopole. When we do this, we obtain

$$\begin{cases} (i\partial_t - m)(f_+ - f_-) + \frac{2i}{r}(g_+ + g_-) + i\frac{d}{dr}(g_+ + g_-) = 0 \\ (i\partial_t - m)(f_+ + f_-) + i\frac{d}{dr}(g_+ - g_-) = 0 \\ (i\partial_t + m)(g_+ - g_-) + \frac{2i}{r}(f_+ + f_-) + i\frac{d}{dr}(f_+ + f_-) = 0 \\ (i\partial_t + m)(g_+ + g_-) + i\frac{d}{dr}(f_+ - f_-) = 0 \end{cases} \tag{4.9}$$

The parts relevant for our discussion are those with $\frac{2}{r}$ singularity which are multiplied by $g_+ + g_-$ and $f_+ + f_-$. These arose from the operation $\vec{\sigma}\cdot\vec{\nabla}\,(\vec{\sigma}\cdot\hat{r}) = \frac{2}{r}$, i.e., precisely due to the special form of ψ. These singularities must be absent, for

otherwise the solutions for $f_\pm$ and $g_\pm$ will behave like $\sim 1/r^2$ at the origin, a singularity of non-integrable nature. This gives us the desired boundary conditions at the origin

$$\begin{aligned} f_+ + f_-\,|_{r=0} &= 0 \\ g_+ + g_-\,|_{r=0} &= 0 \end{aligned} \tag{4.10}$$

Behold that these conditions connect together the otherwise decoupled wave functions u_- and u_+. This coupling of states with different charges, together with quantum anomaly in r-t plane, will play all the tricks in inducing the Rubakov effect.

In relation to the above boundary conditions, let us ask a question; does the zero energy solution, which we obtained for ableian case, continue to exist? Recall that the zero energy solution was of the form

$$\begin{cases} f = \frac{g}{|g|}\frac{1}{r}F \quad , \quad g = \frac{1}{i}\frac{1}{r}G \\ -G = F \propto e^{-mr} \end{cases} \tag{4.11}$$

Now if we try to satisfy one of the conditions in (4.10), say the one for f, we may do so by choosing $f_- = +\frac{1}{r}F$ and $f_+ = -\frac{1}{r}F$. However in such a case, $g_- = g_+ = -\frac{1}{i}\frac{1}{r}F$ and the boundary condition for g cannot be satisfied. It is easy to convince oneself that no choice of $f_\pm$ and $g_\pm$ compatible with (4.11) cannot simultaneously satisfy (4.10). No zero energy normalizable solution exists.

In fact the above conclusion is valid for the case where the fermion mass term is an SU(2) singlet. For example the mass terms produced by the Weinberg-Salam Higgs field in $\underline{5}$ in SU(5) theory is such a singlet with respect to the $SU(2)_M$ discussed in the previous section. If, instead, the mass term is generated by the SU(2) triplet of Higgs field, the situation is entirely different. In such a case the mass term has the structure $m\, \mathbb{1} \otimes \vec{\tau}\cdot\hat{r}$ and when it operates on the isospin functions $\eta_\pm$, it gives the effective mass $m\, q/|q|$ in the abelian equations for $u_\pm$. This in turn changes the relation between F and G into $G=-\frac{q}{|q|}F$ and the extra sign change provided by $q/|q|$ factor to, say, g_+ makes the boundary condition (4.10) satisfied. This zero energy solution is in fact the one found by Jackiw and Rebbi [22].

This then completes our brief survey of the monopoles in interaction with fermions. We hope the present discussions have layed sufficient ground work and will be useful in understanding further, truly quantum field theoretical phenomena, as exemplified in the Rubakov's effect.

References

References below are basically those which I consulted in preparing for this talk and are by no means complete. For general reviews of monopoles and more references, see, for example, S. Coleman, "Classical Lumps and Their Quantum Descendants", in New Phenomena in Subnuclear Physics, edited by A. Zichichi (Plenum 1977); "The Magnetic Monopole Fifty Years Later", HUTP-82/A032 (1982), and P. Goddard and D. Olive, Rep. Prog. Phys. 41, 1357 (1978).

[1] P.A.M. Dirac, Proc. Roy. Soc. (London) Ser. A, 133, 60 (1931).

[2] J.P. Preskill, Phys. Rev. Lett. 43, 1356 (1979).

[3] V.A. Rubakov, JETP Lett. 33, 644 (1981); Inst. Nucl. Res. Preprint P-0211, Moscow (1981); Nucl. Phys. B203, 311 (1982). See also C.G. Callan, Phys. Rev. D25, 2141 (1982); Princeton preprints (1982).

[4] P.A.M. Dirac, Proc. Roy. Soc. (London) Ser. A, 133, 60 (1931); Phys. Rev. 74, 817 (1948).

[5] T.T. Wu and C.N. Yang, Phys. Rev. D12, 3845 (1975).

[6] For a pedagogical review, see T.Eguchi, P.B. Gilkey and A.J. Hanson, Phys. Rep. 66, 213 (1980).

[7] J. Schwinger, Science 165, 757 (1969).

[8] T.T. Wu and C.N. Yang, Nucl. Phys. B107, 365 (1976).

[9] Y. Kazama, C.N. Yang, and A.S. Goldhaber, Phys. Rev. D15, 2287 (1977),
Y. Kazama and C.N. Yang, Phys. Rev. D15, 2300 (1977),
Y. Kazama, Int. J. Th. Phys. 17, 249 (1978).

[10] A.S. Goldhaber, Phys. Rev. Lett. 36, 1122 (1976).

[11] H.J. Lipkin, W.I. Weisberger, and M. Peshkin, Ann. Phys. (N.Y.) 53, 203 (1969).

[12] Y. Kazama, C.N. Yang, and A.S. Goldhaber, Phys. Rev. D15, 2287 (1977), A.S. Goldhaber, Phys. Rev. D16, 1815 (1977).

[13] S. Adler, Phys. Rev. 177, 2426 (1969), J.S. Bell and R. Jackiw, Nuovo Cim. 51, 47 (1969).

[14] See Ref. 6 for a review.

[15] J. Schwinger, Phys. Rev. 128, 2425 (1981), J.H. Lowenstein and J.A. Swieca, Ann. Phys. (N.Y.) 68, 172 (1971).

[16] G. 't Hooft, Nucl. Phys. B79, 276 (1974), A.M. Polyakov, JETP Lett. 20, 194 (1974).

[17] B. Julia and A. Zee, Phys. Rev. D11, 2227 (1975).

[18] J. Arafune, P.G.O. Freund, and C.J. Goebel, J. Math. Phys. 16, 433 (1975).

[19] M.K. Prasad and C.M. Sommerfield, Phys. Rev. Lett. 35, 760 (1975).

[20] E. Tomboulis and G. Woo, Nucl. Phys. B107, 221 (1976).

[21] C. Dokos and T. Tomaras, Phys. Rev. D21, 2940 (1980).

[22] R. Jackiw and C. Rebbi, Phys. Rev. D13, 3398 (1976).

Figure Captions

Fig. 1. Regions R_a, R_b and the overlap R_{ab} around the monopole.

Fig. 2.(a) Incoming wave with helicity h=-1 for q=eg > 0.
$\vec{p}$ is the momentum, and $\vec{\sigma}$ is the spin vector.
(b) Outgoing wave after the scattering, which now has h=+1.

Fig. 3. Typical behavior of the radial functions J(r), K(r) and H(r) for a dyon solution.

Fig. 1

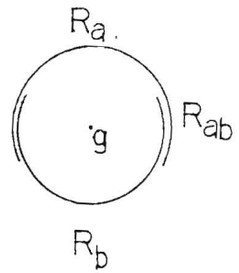

Fig. 2

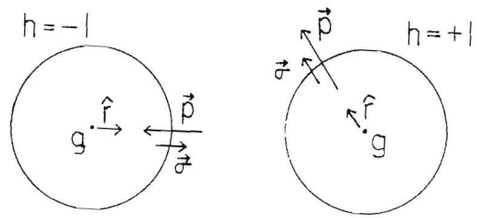

Fig. 3

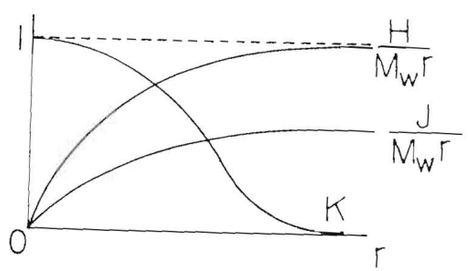

A Simple Picture of Rubakov-Callan Effects

Makoto Kobayashi

KEK

I will present a very intuitive way of understanding the Rubakov-Callan Effects of monopole induced baryon number nonconservation.

We consider the 't Hooft-Polyakov monopole for the SU(2) gauge theory. First let us investigate behavior of SU(2) doublet fermions in the background monopole field. Since the 't Hooft-Polyakov solution is invariant under simultaneous transformations of the spatial rotation and the SU(2) transformation, motion of fermions conserves

$$J = L + S + T \tag{1}$$

where L, S and T are the orbital angular momentum, the spin and the SU(2) spin, respectively. In the following only J = 0 mode is relevant, and we can describe it in the γ_5 diagonal representation as follows

$$\psi = \begin{pmatrix} X_+ \\ X_- \end{pmatrix}, \tag{2}$$

$$X_\pm = \frac{1}{\sqrt{8\pi r^2}} \{q_\pm(r) + p_\pm(r)\, x\cdot\tau\}\tau_2 \ .$$

In the above matrix notation for $X_\pm$, the row vector corresponds to the SU(2) spin. Performing a singular gauge transformation which aligns the background Higgs field into the third axis, we have

$$X_\pm \to X'_\pm = X_\pm g_0^T$$

$$= \frac{1}{\sqrt{8\pi r^2}}\, g_0^{-1} \begin{pmatrix} 0 & -(q_\pm + p_\pm) \\ q_\pm - p_\pm & 0 \end{pmatrix} \tag{3}$$

$$g_0 \hat{x}\cdot\tau\, g_0^{-1} = \tau_3 \tag{4}$$

From eq. (3) we see that charge eigenstates are $q \pm p$. In the following we will denote them as

$$U_\pm = (q_\pm - p_\pm)/\sqrt{2}$$
$$D_\pm = (q_\pm + p_\pm)/\sqrt{2} \tag{5}$$

Since $\hat{x}\cdot\tau$ is singular at r=0, $p_\pm(r=0)$ must vanish. Therefore we have the following boundary condition for $U_\pm$ and $D_\pm$;

$$U_\pm\,(t,\ r=0) = D_\pm\,(t,\ r=0). \tag{6}$$

The Dirac equation for doublet fermions in the background monopole field with the zero core approximation can be written as

$$[i\gamma^\mu(\partial_\mu + A_\mu^{cl}) - m]\psi = 0, \tag{7}$$

where

$$A_\mu^{cl} = \begin{cases} 0 & \mu = 0 \\ \frac{1}{2}\tau^a \varepsilon_{aij}\, x^j/r & \mu = i \end{cases} \tag{8}$$

and

$$m = \frac{m_U+m_D}{2} + \frac{m_U-m_D}{2}\hat{x}\cdot\tau \tag{9}$$

Restricting Eq.(7) to the J=0 mode we have

$$\begin{pmatrix} i\partial_t - i\partial_r & m_U \\ m_U & i\partial_t + i\partial_r \end{pmatrix} \Phi_U = 0$$
$$\begin{pmatrix} i\partial_t + i\partial_r & m_D \\ m_D & i\partial_t - i\partial_r \end{pmatrix} \Phi_D = 0 \tag{10}$$

and the boundary condition at r=0 ;

$$\Phi_U(t,\ r=0) = \Phi_D(t,\ r=0) \tag{11}$$

where

$$\Phi_U \equiv \begin{pmatrix} U_+ \\ U_- \end{pmatrix} \quad \text{and} \quad \Phi_D \equiv \begin{pmatrix} D_+ \\ D_- \end{pmatrix} . \tag{12}$$

Here it is convenient to introduce the following quantity defined for $-\infty < r < \infty$:

$$\Phi(t,\ r) = \begin{cases} \Phi_U(t,\ r) & r \geq 0 \\ \Phi_D(t,\ -r) & r \leq 0 \end{cases} \tag{13}$$

Equation (10) can be rewritten as

$$\begin{pmatrix} i\partial_t - i\partial_r & m(r) \\ m(r) & i\partial_t + i\partial_r \end{pmatrix} \Phi = 0 \qquad -\infty < r < \infty \tag{14}$$

with

$$m(r) = m_D + (m_U - m_D)\,\theta(r) \quad . \tag{15}$$

The boundary condition (11) assures continuity of Φ at r=0.

If we assume $m_U = m_D$ ($\equiv m$), Eq.(14) is nothing but the two dimensional free Dirac equation. Therefore energy eigenstates are simply left and right going plane waves without reflection. The left going solution, for example, describes the following process in the actual space; a U particle comes in and is scattered at the center into an outgoing D particle state. The helicity of the particle is conserved.

In the above process the charge of the fermion is not conserved. This charge should be considered to be transferred to the monopole, so that we can describe it as

$$U^+ + M^0 \rightarrow M^{++} + D^- \tag{16}$$

where M^0 and M^{++} denote the pure monopole and the doubly charged dyon respectively. To describe the above process precisely we have to take into account the behavior of the gauge field as well as the fermion field inside the core region. This is however out of the scope of the present talk. In the following we will consider the effects of the Coulomb interactions in a very intuitive manner.

The static energy of the Coulomb electric field of the dyon is essentially the mass difference of the dyon and the pure monopole. If the kinetic energy of the initial U particle is less than this mass difference, the process (16) is impossible from the energy conservation. However in the region very close to the core the attractive Coulomb energy between D^- and the dyon M^{++} will compensate the mass difference, so that we can consider $M^{++} + D^-$ state there.

Now we can imagine what happens actually. The outgoing D particle is pulled back by the Coulomb field of the dyon and turns the direction of motion. Eventually D falls into the center and becomes the outgoing U particle. Then the charge of the dyon is transferred back to the fermion. Since the Coulomb interaction does not change the spin state, the helicity of the fermion is flipped at the turning point. Therefore the net reaction is

$$U^+ + M^0 \to M^0 + U^+ \tag{17}$$

with the helicity of U^+ being flipped.

Another possible process is a pair production from the electric field between D^- and M^{++}. Suppose that a pair production of $D'\bar{D}'$ takes place, where D' may or may not belong to the same doublet as D. D' falls into the center and becomes U'. Then the reaction is

$$U^+ + M^0 \to M^0 + D^- + \bar{D}'^- + U'^+. \tag{18}$$

In the case of massless fermions, pair production processes must be dominant because massless particles cannot flip the helicity and the reaction (17) is impossible.

Now it should be noted that the above pair production process leads to the baryon number nonconservation in the SU(5) GUT version of the monopole. Suppose that the SU(2) gauge group acts on the third

and fourth components of the quintet of the GUT SU(5) as usual. Then we have two doublets of fermions for the first generation:

$$\begin{bmatrix} e^- \\ \bar{d}_3 \end{bmatrix}, \begin{bmatrix} \bar{u}_2 \\ u_1 \end{bmatrix} \tag{19}$$

Replacing the unprimed and primed doublets in (18) by the first and second doublets in (19) respectively, we have

$$e^- + M^0 \to M^0 + \bar{u}_1 + \bar{u}_2 + \bar{d}_3. \tag{20}$$

Let us estimate the cross section of the baryon number nonconserving processes $\sigma_{\Delta B \neq 0}$ in the massless fermion case. Since the pair production processes are only conceivable processes for the massless fermions and one half of possible pair productions lead to the baryon number non-conservation, $\sigma_{\Delta B \neq 0}$ must be 1/2 of the unitary bound of J = 0 channel:

$$\sigma_{\Delta B \neq 0} = \frac{1}{2}\sigma^{\text{U.B.}}_{J=0} = \frac{2\pi}{E^2} \tag{21}$$

Obviously this is not suppressed by the heavy masses or $\exp(-1/g^2)$ factors. In the massive fermion case the helicity flip processes such as (17) will take place and the calculation of the relative weights of these processes will require more elaborate works.

Monopole Annihilations and the Knee in Cosmic Ray Data*

P. Rotelli† #

National Laboratory for High Energy Physics(KEK)

Oho-machi, Tsukuba-gun, Ibaraki-ken, 305 Japan

* Talk given at the 1st Kamioka Mine Workshop on Proton Decays and Monopoles(October 1982)

† Permanent Address: Dipartimento di Fisica, Universita di Lecce, 73100 Lecce, Italy

Work supported by: Instituto Nazionale di Fisica Nucleare(INFN), Sezione di Bari, Italy.

Abstract

The hypothesis is made that the knee in the integrated primary cosmic ray spectrum is due to the nucleon(antinucleon) decay products of monopole-antimonopole annihilations. The rate of such annihilations is calculated and some speculations on the annihilation scenario are presented.

Great interest has arisen lately on the possible existence in nature of magnetic monopoles. Monopoles have been searched for by physicists since Dirac showed[1] that they could provide a reason for charge quantization, one of the outstanding fundamental problems of our era. More recently Polyakov[2] and independently 't Hooft[3] showed that monopoles exist as solutions of the SO(3) gauge model of Georgi-Glashow and this stimulated much subsequent theoretical work. In particular, it has been shown that monopoles are inherent in grand unified models which, furthermore, predict a monopole mass value of the order of 10^{16} GeV[4]. This continuing interest has recently surged with the reported observation of a monopole candidate by B. Cabrera[5]. However, the upper monopole flux limit of Cabrera is orders of magnitude higher than those set by other experimenters and some indirect considerations[6] such as the number of free monopoles in the Galaxy consistent with the survival of the Galactic magnetic field[7], or the limits set by monopole induced baryon decays[8].

In this paper we wish to add some esoteric speculations concerning possible indirect evidence for the existence of monopoles from cosmic ray data. Before doing so, we wish to point out a series of prejudices upon which our analysis is made, and emphasize the enourmous extrapolation we shall be making from machine energies of $\sim$ 100 GeV to energies of order 10^{16} GeV. If monopoles† exist, then they should be of both types of magnetic charge and some annihilations between monopoles of opposite charge should occur. What can we predict about these annihilations? Do we know the average number of particles produced, the multiplicity distribution or the nature and ratio of the particles produced? I believe the answer is yes, because I believe there is evidence that annihilations

† In what follows we shall consider only pure magnetic monopoles for simplicity, without any electric charge i.e. we do not consider dyons.

display some universal features in these properties. The data available on particle annihilation is limited to $\sqrt{s} \lesssim 4$GeV for $\bar{p}p$ ($\sqrt{s} \lesssim 16$GeV if total $\bar{p}p$-pp differences are considered) and $\sqrt{s} \lesssim 33$GeV for e^+e^- annihilations. Nevertheless, these two processes, so different in the properties of the incoming particles, exhibit surprising similarities. Most notably they share a common, characteristically narrow, KNO curve and have comparable growth rates in average multiplicity. In particular, both sets of average multiplicity can be fitted with a power growth rate i.e. $\langle n \rangle \sim s^{\delta}$, with δ compatible with 0.28. This last observation is very biased, it stems from the fact that recently[9] A.D'Innocenzo and I have shown that a simple two-particle branching model with only two-body decays reproduces the KNO curve seen in annihilations and furthermore predicts just this value of δ.

There is another potential source of information on annihilation processes, that provided by the study of the central region of any particle-particle interaction if, as some believe[10], the particles created there are produced in a generalized annihilation process. While only a small fraction of available energy flows on average to the central region, this source of information on annihilation by-passes the problem of rapidly decreasing cross-sections for bona-fide annihilation channels.

Now let us make the enourmous extrapolation that we warned of earlier. Let us assume that in any monopole-antimonopole annihilation the same KNO multiplicity structure and (of more importance for this work) the same average multiplicity growth rate occurs. If monopoles have 10^{16}GeV of mass, then the energy available in their annihilation is $2\ 10^{16}$GeV. A reasonable fit to the total average multiplicity $\langle n \rangle$ in known annihilations is $3s^{.28}$, so the predicted total number of particles created would be $\langle n \rangle_{monopole} = 4\ 10^9$. The average energy of each particle would therefore be $\langle E \rangle = 5\ 10^6$GeV $= 5\ 10^{15}$eV. This follows from the identity $\langle E \rangle \langle n \rangle = \sqrt{s}$. Most of the particles created decay, but the protons(antiprotons)

survive and contribute to the primary cosmic ray flux. We can also estimate from present data that of the order of 10% of the particle output should be in the form of nucleon-antinucleon.

Thus an immediate question poses itself - Is there any peculiar effect in the primary cosmic ray data at $\sim 5\ 10^{15}$eV? The strict answer to this question is no. But there is something in the measured integrated primary cosmic ray flux at an energy close enough to maintain our interest. There is the so called "knee" or "bump" at $\sim 10^{15}$eV(see fig. 1). Let us consider this knee and separate it phenomenologically from its background. At an order of magnitude above or below the knee the integrated flux I is well fitted by the standard power law form $KE^{-\gamma}$, except that the values of K and γ are different in the two regions. We can readily fit both by the functional form:

$$I_b = (E^{\gamma_1}/K_1 + E^{\gamma_2}/K_2)^{-1} \qquad (1)$$

where the subscript b stands for background and $\gamma_2 > \gamma_1$, so that for $E \gg 10^{15}$eV I_b behaves like $K_2 E^{-\gamma_2}$, while for $E \ll 10^{15}$eV it behaves as $K_1 E^{-\gamma_1}$. A good fit to the compilation of Hillas[11] is given by †,

$$\gamma_1 = 1.69 \qquad 1/K_1 = 3\ 10^{-20}\ m^{+2} s^{+1} sr^{+1}$$

$$\gamma_2 = 2.03 \qquad 1/K_2 = 2.2\ 10^{-25} m^{+2} s^{+1} sr^{+1} \qquad (2)$$

(with E in eV)

† It should be noted that Hillas has shifted downwards the extensive air shower data from Chacaltaya(squares) by a factor of 1.5 in order to elliminate disaccordance between the various data points.

The total integrated flux in the region 10^{18}eV > E > 10^{11}eV can then be expressed as,

$$I(E) = I_b(E) + I_k(E) \tag{3}$$

where the subscript k stands for knee. For I_k we choose the functional form:

$$I_k(E) = Ae^{-\alpha E} \tag{4}$$

This form can be justified, in part, by the fact that just such a spectrum is seen in measured annihilation processes and the integration of an exponential gives an exponential with the same exponent. However, storage of the cosmic ray particles in the galaxy should modify this form. Our real justification for (3) is that it is a convenient phenomenological form from which we can readily read off the desired information. Indeed A is the total integrated flux rate of the knee, while $1/\alpha$ is the average energy <E>. A good fit to the compilation of Hillas is given by,

$$A = 6.6\ 10^{-6} m^{-2} s^{-1} sr^{-1}$$

$$\alpha = 1.53\ 10^{-15} eV^{-1} \tag{5}$$

It should be noted that the data in fig. 1 is plotted on an $E^{1.5}I(E)$ versus E basis and so the curve shown is our fit to I multiplied by $E^{1.5}$. From (4) we deduce that,

$$F_k^{2\pi} = 4\ 10^{-9}\ cm^{-2} s^{-1}$$

$$\langle E \rangle_k = 6.5\ 10^5 GeV \tag{6}$$

where $F_k^{2\pi}$ is the 2π flux rate of the knee. From $\langle E \rangle_k$ we can determine† either a) the monopole mass M (if the average multiplicity is assumed), or b) the average annihilation multiplicity (if the monopole mass is assumed).

a) With $\langle n \rangle = 3s^{.28}$ → $M = 10^{14}$GeV (7)

b) With $M = 10^{16}$GeV → $\langle n \rangle = 3.1\ 10^{10}$ → $\langle n \rangle = 2.5\ s^{.31}$ (8)

where the last deduction in b) used $\langle n \rangle = 16$ at $\sqrt{s} = 20$, a value consistent with the results of e^+e^- annihilation[12]. Since grand unified theories suggest the order of magnitude of the monopole mass given in b), we shall henceforth in this analysis assume the multiplicity growth rate $s^{.31}$ and abandone our prefered value for δ(case a). We recall that power rates for particle production and growth rates as high as $s^{1/3}$ are predicted in thermodynamical models[13].

Before proceeding in our analysis we wish to observe that alternative average multiplicity growth rates yield the following corresponding mass values,

a') $\langle n_{ch} \rangle = -4.56 + 2.63 \ln s$ → $M = 4.5\ 10^7$ GeV (9)

a'') $\langle n_{ch} \rangle = 2.24 + 0.007 \exp[2.33\sqrt{\ln(s/0.04)}]$ → $M = 7\ 10^{10}$GeV (10)

Both examples are fits to the e^+e^- data, and for each we have assumed $\langle n \rangle = 3/2 \langle n_{ch} \rangle$. The functional form in (10) is a prediction of planar perturbative QCD (but with the numerical factors treated as free parameters).

---

† We ignore, for simplicity, the acceleration undergone by the nucleons during storage. This effect should not increase $\langle E \rangle_k$ by more than 50%. All our results must be considered as order of magnitude estimates.

Obviously neither is compatible with the mass scale for monopoles predicted by grand unified models.

Now returning to case b) with $M = 10^{16}$ Gev and $\langle n \rangle = 2.5\ s^{.31}$, we have that,

$$\langle n \rangle \simeq 3\ 10^{10} \quad \text{and} \quad \langle n_N \rangle = 3\ 10^{9} \tag{11}$$

where $\langle n_N \rangle$ is the average number of nucleons(antinucleons) in each annihilation. Using the value of $F_k^{2\pi}$ in (6) and the relationship $F_k^{2\pi} = \frac{1}{4} \rho_N V = 1/4\ \rho_N c$, where ρ_N is the density of nucleons(antinucleons) in the Galaxy which constitute the knee, we find

$$\rho_N = 5.5\ 10^{-19}\ cm^{-3} \tag{12}$$

With the storage time in the galaxy plus halo given by $\tau = 3\ 10^{15}$s and a galaxy plus halo volume[14] $V = 3\ 10^{68} cm^3$, we can calculate the rate R_N of nucleon production needed to saturate the knee flux:

$$R_N = \frac{N}{\tau} V = 5.5\ 10^{34} s^{-1} \tag{13}$$

And since each annihilation produces $3\ 10^9$ nucleons this implies a galactic monopole annihilation rate of,

$$\text{Rate of annihilations} \simeq 2\ 10^{25} s^{-1} \tag{14}$$

Thus the number of monopoles annihilating per second would be $4\ 10^{25}$. An estimate of the number of monopoles in the galaxy(plus halo) can then be made, in the usual way, by calculating the number that have annihilated since the birth of the galaxy assuming a time independent annihilation rate given by (14).

$$\text{No of monopoles in galaxy plus halo} \simeq 10^{43} \tag{15}$$

To put this last number in perspective, we note that the Cabrera flux

value, if uniform throughout the galaxy and halo(and if $\beta_M = 10^{-3}$), would imply 10^{52} monopoles. So our estimate is nine orders of magnitude below the Cabrera limit and well within most other published upper limits.

What is the possible annihilation scenario? Many authors dismiss monopole annihilations as insignificant. One of the reasons is that monopoles are so massive that they are dynamically impervious to the presence of another monopole not withstanding the strong magnetic force between them. Consequently monopole capture, let alone annihilation, is a highly improbable phenomena. To bypass this difficulty we shall assume the monopoles are already(in sufficient number) in bound dipole states. This could be an inherence from the early history of the Universe or, more problematically, a consequence of monopoles binding gravitationally to stars, since in this latter case high densities and low relative velocities between monopoles enhance dipole formation. As an aside, we note that magnetic dipoles would not be subject to acceleration out of the galaxy(unlike free monopoles) and are thus not subject to the limits on free monopoles set by the existence of a galactic magnetic field.

Let us consider a couple of example of these dipoles which we shall treat classically(fig. 2). From the Dirac quantization condition the minimum value for the magnitude of the magnetic charge $|g| = 3.29\ 10^{-8}$ maxwells. Consider a dipole formed from two monopoles with magnetic charges $\pm|g|$. If the seperation L between the monopoles(treated as point particles) is say $2\ 10^{-5}$cm, then the magnetic field strength that each monopole experiences is $B \simeq 10^2$gauss. Such a dipole is stable everywhere except perhaps within stars. Its orbital velocity(in its center of mass frame) is $u = 4\ 10^{-2} cm\ s^{-1}$ and it radiates energy at the rate given by the classical formula $P = 2 \times \frac{2}{3} \frac{g^2}{c^3} (\dot{u})^2$ in which g replaces the electric charge. If we denote by T the time such a dipole takes to radiate away sufficient energy to reduce its seperation by just 1%, we find $T = 10^{12} \times$ Age of Universe. The reason one obtains this huge number is that

$(\dot{u})^2 \propto 1/M^2$ and M is 10^{16} GeV. Such a dipole is practically a stable particle.

The situation is very different for dipoles separated by two fermi, $L = 2\ 10^{-13}$cm. In this case $B = 10^{18}$ gauss(!) and $T = 2\ 10^{5}$s. Furthermore at these distances the fermionic condensates of the monopoles mix and may even annihilate, triggering the total annihilation of the dipole. These condensates play an essential role in monopole induced baryon decay. Certainly below this value of L we cannot continue to use classical arguments.

The problem of finding a mechanism for annihilation thus reduces to explaining how a dipole of dimension 10^{-5}cm say, shrinks to one of a few fermi. The only possibility that we can conceive is that this occurs when the dipole is orbiting the outer layers of a star. In the presence of a plasma a dipole can lose energy by the interaction with the plasma. There are several ways to see this, but one is to note that a rotating dipole produces an electromotive force on any charged particle in its vicinity. For example, an electron initially at rest in the dipole center of mass frame will be accelerated by the varying magnetic field of the rotating monopoles and the energy it gains can only come at the expense of the dipole. As a consequence of this scenario, annihilations would only occur for dipoles gravitationally bound to stars.†

How can our hypothesis be tested? The simplest test is the identification of the particle nature of cosmic rays in the knee. We predict that these are protons-antiprotons in equal numbers. Elsewhere in the cosmic ray spectrum upper limits to the antiproton content of $< 10^{-4}$ have been recorded. Such a test is also essential for the most popular

† Since somewhat less than half of annihilation products would penetrate the star and be lost to the cosmic ray flux our annihilation rate should be increased by up to a factor of two.

interpretation of the knee _ that it consists of iron nucleii which have undergone a particular acceleration process. There is another test which depends upon our annihilation scenario. If annihilations occur around stars, then some annihilations should be occuring around the sun. Now we can set an upper limit on this number from the limit on the asymmetry and the diurnal variations of cosmic rays in the knee region. We find that the number of annihilations around the sun cannot exceed $10^{6}s^{-1}$. This means that the sun cannot be a typical source of annihilations (otherwise the galactic annihilation rate would be $< 10^{17}s^{-1}$). This is not without precedent, since it has long been known that the sun is a poor source of cosmic rays in general and of energetic cosmic rays in particular ($E > 10$ GeV) by several orders in magnitude. However, some annihilations should occur and a particular signature of such events would be the detection of neutrons(antineutrons) in the primary knee flux. These particles being highly relativistic, live long enough to reach the earth almost without attenuation.

Finally, we conclude on a historical note. The idea that annihilations of one sort or another might contribute to the cosmic ray flux dates back to 1942 when F.A. Millikan, V.M. Neher and W.H. Pickering[15] suggested that nuclear annihilations could explain the various knees originally seen in cosmic ray data. As the data improved these knees dissapeared (and now only the one we have been considering in this work exists and refuses to go away). A few years later O. Klein[16] considered the consequences of the annihilation between matter galaxies and anti-matter galaxies. These ideas have not born great fruit, we can only hope that our version is a little more successful.

The author wishes to thank the theory group at KEK and Steve Olsen for patient and helpful discussions. He also wishes to take this opportunity of thanking KEK for the hospitality afforded to him during his stay in Japan.

References

1. P.A.M. Dirac, Proc. Roy. Soc. 133 (1931) 60.
2. A. Polyakov, Pis'ma Eksp. Teor. Fig. 20 (1974) 430 (JETP Lett. 20 (1974) 194)
3. G. 't Hooft, Nucl. Phys. B79 (1974) 276, ibid, B105 (1976) 538
4. M. Daniel, G. Lazarides and Q. Shafi, Nucl. Phys. B170 (1980) 156
   C.P. Dokos and T.N. Tomaras, Phys. Rev. D21 (1980) 2940
5. B. Cabrera, Phys. Rev. Lett. 48 (1982) 1378
6. See for example: J. Ellis, D.V. Nanopoulos and K.A. Olive, Phys. Lett. 116B (1982) 127 G. Giacomelli, "Experimental Status of monopoles" Univ. of Bologna preprint IFUB 82-26, and references therein.
7. E.N. Parker, Astrophys. J. 160 (1970) 383
   S.A. Bludman and M.A. Ruderman, Phys. Rev. Lett. 36 (1976) 840
   G. Lazarides, Q. Shafi and T.F. Walsh, Phys. Lett. 100B (1981) 21
   M.S. Turner, E.N. Parker and T.J. Bogdan, "Magnetic monopoles and the Survival of Galactic Magnetic Fields", Enrico Fermi Institute Preprint No. 82-18.
8. C.G. Callan Phys. Rev. D25 (1982) 2141
   V.A. Rubakov, Pis'ma Zh. Eksp. Teor. Fig. 33 (1981) 658 (JETP Lett. 33 (1981) 644)
   F. Wilczek, Phys. Rev. Lett. 48 (1982) 1146
   E. W. Kolb, S.A. Colgate and J.A. Harvey, Phys. Rev. Lett. 49 (1982) 1373
   S. Dimopoulos, J. Preskill and F. Wilczek, Phys. Lett. 119B (1982) 320
   L. Bracci and G. Fiorentini, "Monopolic atoms and monopole catalysis of proton decay" IFUP TH 82-18 (1982)
9. A. D'Innocenzo and P. Rotelli, Lett-Nuovo Cimento 35 (1982) 65
10. A. D'Innocenzo, G. Ingrosso and P. Rotelli, Nuovo Cimento A25 (1979) 393; Nuovo Cimento A55 (1980) 417; Lett. Nuovo Cimento 27 (1980) 457; Proceeding of the V European Symposium on Nucleon-Antinucleon Interactions, Bressanone, Italy (June 1980)
11. A.M. Hillas in "Cosmic Rays and Particle Physics-1978" Ed, T.K. Gaiser. AIP Conference Proceedings No. 49, Particles and Fields Subseries No. 16, P. 373
12. See for example, L. Criegee and G. Knies, Phys. Reports 83 (1982) 152
13. P. Rotelli, Phys. Rev. 182 (1969) 1622
14. S. Hayakawa "Cosmic Ray Physics" John Willy and Sons
15. R.A. Millikan, V.M. Neher and W.H. Pickering, Phys. Rev. 61 (1942) 397
16. O. Klein, ArkivMat, Astronom. Fys. 31A (1944) No.14

Figure Captions

Fig. 1 The primary(integrated)cosmic ray spectrum multiplied by $E^{1.5}$ versus $\log_{10}E$.

This compilation is that of A.M. Hillas. Solid circles-proton satellite calorimeter results. Open circles, air shower calorimeter results. Open squares, air shower data from Chacaltaya reduced by a factor of 1.5.

Fig. 2 A magnetic dipole formed from pure monopoles. L is the seperation distance and u the orbital speed in the center of mass frame.

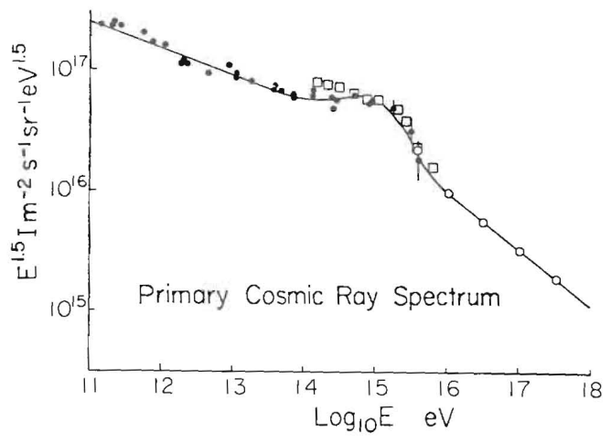

Fig. 1

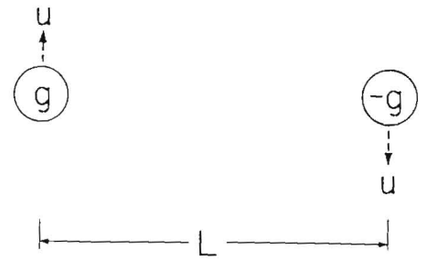

Fig. 2

KOBE-82-07

Search for Magnetically Trapped Monopoles with a SQUID Fluxmeter

Takeo Ebisu and Tadashi Watanabe

Department of Physics, Faculty of Science
Kobe University
Nada-ku, Kobe 657, Japan

December, 1982

Abstract

We propose to search for superheavy magnetic monopoles with a SQUID-fluxmeter, which may be trapped in old ferromagnetic materials on the earth.

A prototype version of the SQUID-detector made up has shown satisfying stability for continuous running of more than 50 hours. By using a larger-scale detector of this type under construction, we intend to perform three kinds of experiments (i) a search for monopoles in iron magnetic sands of 200 Kg, (ii) in grate-bars of 200 Kg if the re-trap is possible and (iii) in iron ores in the sintering process for 150 hours.

Since the present experimental limits on slow monopoles are very high, the substantial improvement is possible with the experiments proposed here.

§1. Introduction

The problem of detecting very massive magnetic monopoles ($10^{15} \sim 10^{17}$ GeV/c^2) suggested by Grand Unified Theoreis has attracted considerable attention since Cabrera found one candidate event.[1] From the stand point of view of cosmology and particle physics, it is very important to obtain the monopole flux or to lower the limits of it.

In this report we would like to discuss a search for monopoles which might be trapped magnetically in materials on the earth.[2] Appreciable concentrations of trapped monopoles are expected in old ferromagnetic ores, albeit the very poor abundance in the cosmic ray flux. It is not practicable to wait for incident monopoles because of the difficulty of too long-term operation of the SQUID-fluxmeter and the small size of our detector.

The principle of our experiment is the following: When ferromagnetic materials are heated above their Curie point, the superheavy GUTs monopoles will be released and diffuse downward. We can detect them by using a SQUID-fluxmeter.[3]

We have made up a prototype version of a SQUID-search coil system, which will be discussed in detail in §2. Next, in §3 the stability of the detector is examined for more than 50 hours with and/or without trial samples. In §4 we propose three kinds of experiments with a larger-scale detector, which should substantially lower the present experimental limits on the monopole flux at the earth.

§2. Experimentals

We have made up a prototype version of a superconducting SQUID-search coil. The outline is shown in Fig. 1. Samples are heated above their Curie point in a furnace placed strictly above the search coil.

Furnace Furnace is built of firebrick in which nichrome wire is filled. It is possible to heat samples to a temperature above 1000°C, higher than the Curie point of iron, 770°C. The distance between the furnace and the search coil is 130 cm. The effect of the geomagnetic field on released monopoles is negligible for this distance.

Search Coil Depending on the size of immediately available Dewar system, the diameter of search coil was determined to be 30 mm.*) Search coil is composed of four-turns of niobium wire wound on a glass tube 30 mm in diameter. All parts are shielded with a superconducting lead foil closed at the bottom.

---

*) It is not useful to increase the number of turns regardless of matching to the SQUID. A few turns are proper for a search coil of 0.005 inch wire, a few centimeters in diameter. We are now constructing another SQUID-detector with a search coil 80 mm in diameter.

SQUID A model SQE-102 system with SP-probe by S.H.E. Corp. is used. Final voltage output of noise is 2 mVp-p when the time constant is one second.

Magnetic Shield At first only the superconducting shield was made.*) It was assured that noise is not created by moving a small magnet in the exterior region of glass Dewar. But due to the trapped geomagnetic field inside the shield, minute vibrations of search coil can create appreciable noise signals. The SQUID, the flux transformer and the associated wiring were set up as regidly as possible. A Mumetal cylinder closed at the bottom is set at room temperature surrounding the whole system, that reduces the Earth's magnetic field to a few milligauss. Then very stable performance of the SQUID detector was obtained.

Calibration The detector sensitivity has been calibrated in the following way. We have measured the SQUID response to a known magnetic flux produced by a calibration solenoid coil, which flux corresponds to that of the monopole passing through the search coil. The voltage output of the SQUID was 20.6 mV. This value

---

*) Magnetic shield is essential to handle a SQUID. The term of magnetic shield bears a double meaning in this case. One is magnetic shield in itself, the other is to make a low field region. In order to attain good magnetic shield, it is most feasible to use superconducting materials.

is understood to be the smaller one because the search coil is positioned close to superconducting shield and experiences a larger magnetic flux for the real monopole than that of the calibration solenoid coil. On the other hand we obtain 41 mV as the voltage output for Dirac's monopole by calculating the self-inductance of the superconducting circuit. We can conclude that the voltage output of the SQUID stands between 20.6 mV and 41 mV.

§3. Results

Several permanent magnets available at our laboratory were studied as trial samples. The total weight of magnets was 700 grm. We have also operated the detector for 50 hours successfully to obtain the stability for a long period of time.

In Fig. 2 are reproduced the recorder trace which shows the continuous running of 50 hours without sample heating and several hours running under the operation of the furnace. The width of the trace corresponds to the noise of 2 mV mentioned before. The disturbance at midway in Fig. 2(a) was caused by the vibration on liquid nitrogen transfer. Signals due to the real monopole should be a shift from the baseline of the trace by about 20 times of the noise level. The direction of shift depends on the sign of the monopole charge.

We cannot see any significant deflection in the recorder trace.

§4. Future Plans

The iron ore is one of the most favourable materials for trapping of magnetic monopoles. We intend to carry out three different experiments by courtesy of Kobe Steel, Ltd.. The first is the heating experiment of the iron grate-bars which are parts of a conveyor running through a sintering furnace. The sintering furnace processes 1.8×10^6 tons of ore annually. Monopoles may be released from iron ores in the sintering process and will be re-trapped in grate-bars if possible someway. Grate-bars used day and night for two years have been already supplied by Kobe Steel. Its total weight is 200 Kg.

For our second experiment, the similar way of measuring on the iron magnetic sand of 200 Kg is being planned, which is also provided by the company. The third plan is the performance of the experiment in the yard of Kobe Steel. The detector placed below the sintering furnace will wait for released monopoles from the heated ores for 150 hours. We are going to start these experiments as soon as the construction of a larger search coil 80 mm in diameter is completed.

We wish to thank K. Yaskawa for granting the use of Mumetal cylinder and K. Yamagata for many stimulating and helpful discussions. We are also grateful to KOBE STEEL, LTD. for their cooperation.

References

(1) B. Cabrera, Phys. Rev. Lett. 48, 1378 (1982).

(2) E. Goto, J. Phys. Soc. Japan 13, 1413 (1958);
C. Kittel and A. Manoliu, Phys. Rev. B15, 333 (1977).

(3) See, for example, O. V. Lounasmaa, Experimental Principles and Methods Below 1 K (Academic Press, London and New York, 1974);
M. Tinkham, Introduction to Superconductivity (McGraw-Hill, 1975).

Figure Captions

Fig. 1. Schematic drawing of the SQUID-detector. The figures stand for the size in mm.

Fig. 2. Recorder traces. (a) shows typical disturbances. Drift is observed at the initial stage of operation. Another disturbance is also observed on liquid nitrogen transfer. (b) is an example of the trace on heating a sample magnet. (c) is a part of the trace on continuous running of 50 hours without sample heated.

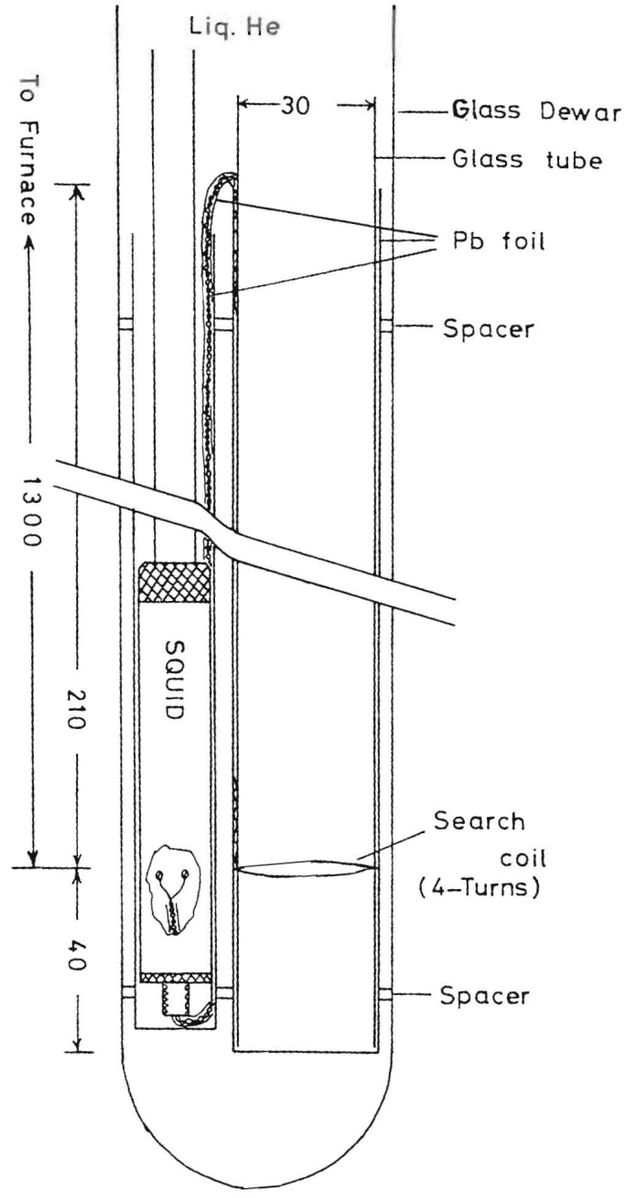

Fig.1.

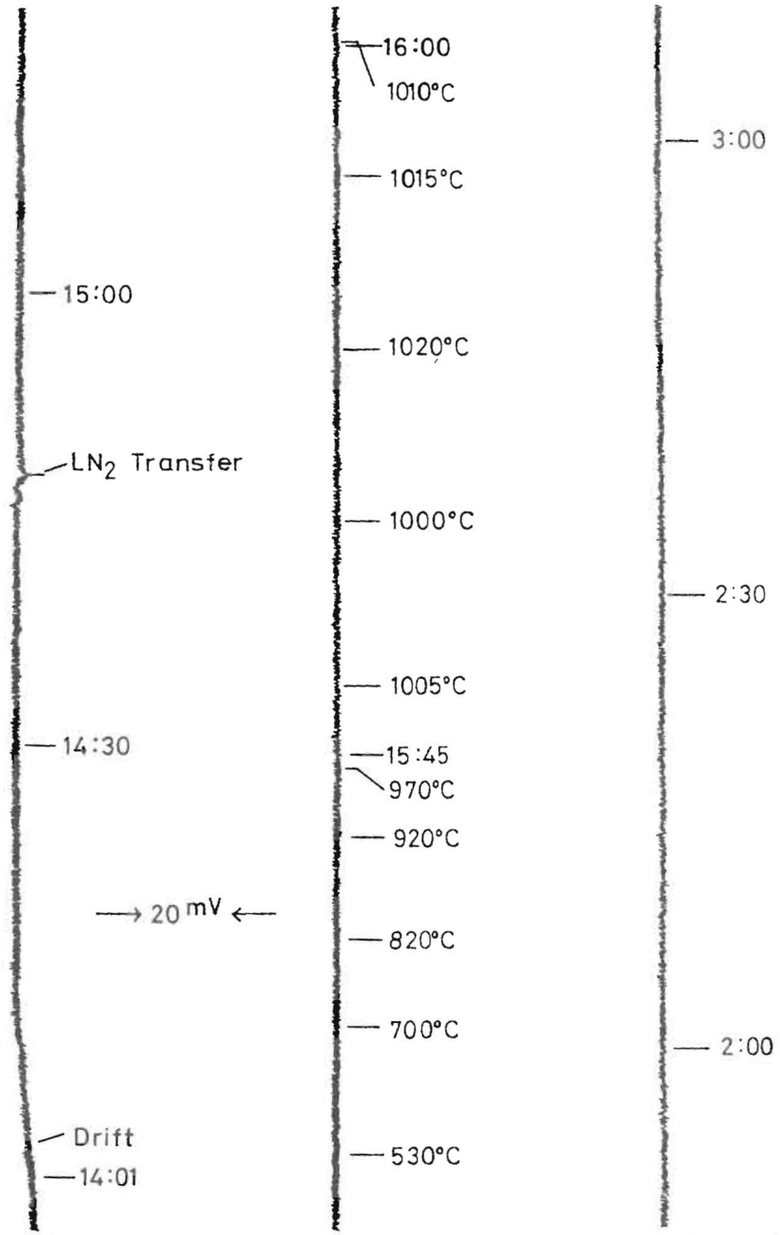

Fig. 2(a)

Fig. 2(b)

Fig. 2(c)

A SEARCH FOR SLOWLY MOVING MAGNETIC MONOPOLES*

Fumiyoshi Kajino

Institute for Cosmic Ray Research
University of Tokyo
Midori-cho, Tanashi-shi
Tokyo, 188 Japan

ABSTRACT

A search for slowly moving magnetic monopoles is being performed using scintillation counters and proportional chambers which are situated on the ground at sea level. An energy threshold is set at 1/20 minimum ionization. An upper limit of 2.57×10^{-11} $cm^{-2}sr^{-1}sec^{-1}$ for the flux of magnetically charged particle is set at the velocities between $1.0\times10^{-4}c$ and $1.0\times10^{-2}c$, with 90% confidence level.

Introduction

Existence of magnetic monopoles was first suggested by Dirac[1] in 1931, but this theory could not predict the mass of the magnetic monopoles. The mass of the magnetic monopoles was first predicted by 't Hooft[2] and Polyakov[3] in 1974. The monopole mass m_g is expressed by the formula, $m_g = Cm_w/\alpha \simeq 10^4$ GeV, where C is a numerical coefficient of an order 1, m_w is a typical vector boson mass $\sim 10^2$ GeV, and α is the gauge coupling constant. In case that this concept is applied to the George-Glashow's SU(5) grand unified theory[4](GUT), the mass is expressed as $m_g = Cm_x/\alpha \sim 10^{16}$ GeV, where m_x is the mass of X bosons which induce the transition from quarks to leptons.

---

* This work is being performed by members of the MUTRON collaboration: T. Kitamura, Y. Ohashi, A. Okada, K. Mitsui, S. Matsuno, I. Nakamura, T. Aoki, Y. Yuan (ICRR); S. Ozaki, S. Higashi, T. Takahashi (Osaka City University).

The masses predicted by GUTs are so heavy that neither accelerators nor cosmic rays can produce magnetic monopoles through interactions. If they are truly in existence, they must be created at a period of birth of the Universe according to the standard Big Bang model[5]. Fig.1 shows the velocities of the magnetic monopoles as a function of their masses[6]. They are accelerated in various magnetic fields such as terrestrial, solar and galactic magnetic fields. GUT monopoles with the mass of $\sim 10^{16}$ GeV are estimated to be accelerated by the galactic magnetic fields up to a velocity about $10^{-2}c$ by taking account of Goto's[7] and Lazarides's[8] models. In order to keep the galactic magnetic fields intact, they cannot be reduced faster than the time-scale to generate the fields on the basis of the Dynamo theory. This leads to the Perker's limit of the flux of the monopoles of about $10^{-16}cm^{-2}sr^{-1}sec^{-1}$.

If the monopoles are being trapped in the solar system, their velocity will be about $10^{-4}c$ which is the escape velocity from the system and the velocity of the earth in it. Thus it is important to search magnetic monopoles with velocities between $10^{-4}c$ and $10^{-2}c$.

Recently, it was pointed out by Rubakov[9] and others[10,11] that the monopoles will induce baryon decays. Possible decay modes are predicted to be $p,n \rightarrow e^{+}$ + pions in the minimal SU(5) GUT. A mean free path of the moving magnetic monopoles to induce the baryon decay will be less than an order of strong interactions[11].

Experimental Apparatus

Fig.2 shows the experimental apparatus to search magnetic monopoles. This apparatus consists of 6 layers of scintillation counters, 9 layers of proportional chambers and 14 layers of iron absorbers. Each layer of the scintillation counters consists of 19 scintillators, each size of which is 240cm×20cm ×1cm. Each scintillation counter has two photomultiplier tubes (PMT) attached at the ends through light guides. SCSN 20 scintillators and R594 PMTs are used. Each layer of proportional chambers consists of 4 chambers, each effective volume of which is 246cm×92cm×2cm. Mixed gas of 90% argon and 10% CH_4 flows inside. Thickness of each iron absorber is 12 cm for inner 12 layers and 1 cm for outer 2 layers. Even if the Rubakov type interactions are induced by the moving magnetic monopoles, the detector can detect monopoles, because as the sufficiently thick iron layers can absorb decay particles so the time sequence of each layer does not been prevented by such decay particles. The detector is situated on the ground at sea level in Tokyo.

A block diagram of a data aquisition system is shown in Fig.3. The average value of the high voltage supplied to each PMT is about 1500 V. Gains of the PMTs are about 5×10^{5}. Gains of amplifiers are set at 50 and discriminator levels are set at 50 mV which corresponds to 1/20 minimum ionization energy loss. Two signals of the PMTs on each scintillation counters are coincided with each other.

Fast Time to Digital Converter (TDC) has 6 inputs of stop signals, each of which is generated by OR signal of the scinti-

llation counters of each layer. Its time resolution is 0.5ns/count, and its full scale is 510 ns. Slow TDCs have 60 ch inputs of stop signals, each of which is generated by OR signals of two of the scintillation counters. Each of their time resolutions is 50 ns/count and each channel consists of 16 bits scaler. The coincidenced discriminator outputs from 114 scintillation counters are registered in Input Buffers. Eight analog outputs from PMTs are fed into the summing amplifier. Its output is fed into each of Analog to Digital Converters (ADC).

Each of 36 proportional chambers has linear amplifier and logarithmic amplifier. The output signals from linear amplifiers are discriminated at 1/20 of minimum ionization and discriminator outputs go to 36 inputs of TDCs. Each of their time resolutions is 50 ns/count and each channel consists of 16 bits scaler. Pulse heights of logarithmic amplifiers are registered in 36 ADCs.

A principle diagram of a trigger method is shown in Fig.4. Trigger signals are generated using the signals from respective layers of the scintillation counters. A signal from the first layer generates a gate signal for the second layer. If a signal from the second layer comes in the duration of the gate, next gate signal for the third layer is generated. The sequential process continues up to the 6th layer. Thus the trigger signal is generated by the successive delayed coincidence of six layers, and it is possible to trigger for particles which pass through the detector from opposite direction.

The area-solid-angle product for the detector is 5.49×10^{4} $cm^{2}sr$. This value must be doubled for the heavy magnetic monopoles predicted by GUTs because they could penetrate the earth.

Energy Loss of Magnetic Monopoles

Ionization energy losses of magnetic monopoles at low velocities for carbon (scintillator) and argon were calculated by Ritson[12] using Thomas-Fermi statistical model of atomic wave functions, which are shown in Fig.5. The energy threshold of our detector is set at 1/20 the minimum ionization energy loss. Thus the velocities greater than $\sim 1.3\times10^{-4}c$ for the scintillation counters and $\sim 3.5\times10^{-4}c$ for the proportional chambers can be measured with our detector according to this model. If the Rubakov type interactions occur, the energy loss is large enough to detect the monopoles even at low velocities less than $\sim 10^{-4}c$.

Results

The apparatus is being run. Data of about 19 days in live time are analized only using scintillation counters. No candidate for the magnetic monopole is obtained.

Thus we can set an upper limit of $2.57\times10^{-11}cm^{-2}sr^{-1}sec^{-1}$ for the flux of magnetic monopoles at the velocities between $1.0\times10^{-4}c$ and $1.0\times10^{-2}c$, with 90% confidence level.

Comparison with Other Results

Our result for the upper limit flux of magnetic monopoles is shown in Fig.6 with other results[11,13,14].

J.D. Ullman have reported the results of upper limit for slowly moving particles at velocities between $3.3\times10^{-4}c \sim 1.2\times10^{-3}c$. Proportional counters were used for his experiment and the energy threshold was set at twice the muon ionization loss peak. So his experiment may be excluded for magnetic monopoles search by the Ritson's calculation.

References

1. P.A.M. Dirac, Proc. Roy. Soc. 133, 60 (1931);
   Phys. Rev. 74, 817 (1948).
2. G. 't Hooft, Nucl. Phys. B79, 276 (1974).
3. A. Polyakov, JETP Lett. 20, 194 (1974).
4. H. Georgi and S.L. Glashow, Phys. Rev. Lett. 32, 438 (1974).
5. For example, s. Weinberg, Gravitation and Cosmology,
   John Wiley & Sons (1971).
6. F. Kajino, Uchūsen Kenkyū, 26 No.2, 79 (1982).
7. E. Goto, Progress of Theor. Phys. 30, 700 (1963).
8. G. Lazarides et al., Ref. TH. 3008-CERN (1980).
9. V.A. Rubakov, Zh. Eksp. Teor. Fiz. 33, 658 (1981)
   (JETP Letters 33, 644 (1981);
   USSR Academy of Sciences Institute for Nuclear Research
   Preprints, P-0204, 0211 (1981);
   Nucl. Phys. B203, 311 (1982).
10. C.G. Callan, Princeton Univ. Preprints "Disappering Dyons"
    and "Dyon-Fermion Dynamics" (1982).
11. J. Ellis et al., Ref. TH. 3323-CERN (1982).
12. D.M. Ritson, SLAC-PUB-2950 (1980).
13. T. Mashimo, Uchūsen Kenkyū 26 No.2, 56 (1982).
14. R. Bonarelli et al., Phys. Lett. 112B, 100 (1982).

Figure Captions

Fig.1: Velocities of magnetic monopoles which are accelerated by various magnetic fields, as a function of masses.

Fig.2: Schematic view of monopole detector.

Fig.3: Block diagram of data aquisition system.

Fig.4: Principle diagram of trigger method.

Fig.5: Ratio of ionization energy loss to minimum ionization of magnetic monopoles in carbon (scintillator) and argon, as a function of velocity β. The energy threshold of our detector is also shown.

Fig.6: Compilation of experimental upper limits on the flux of magnetic monopoles as a function of velocity β.

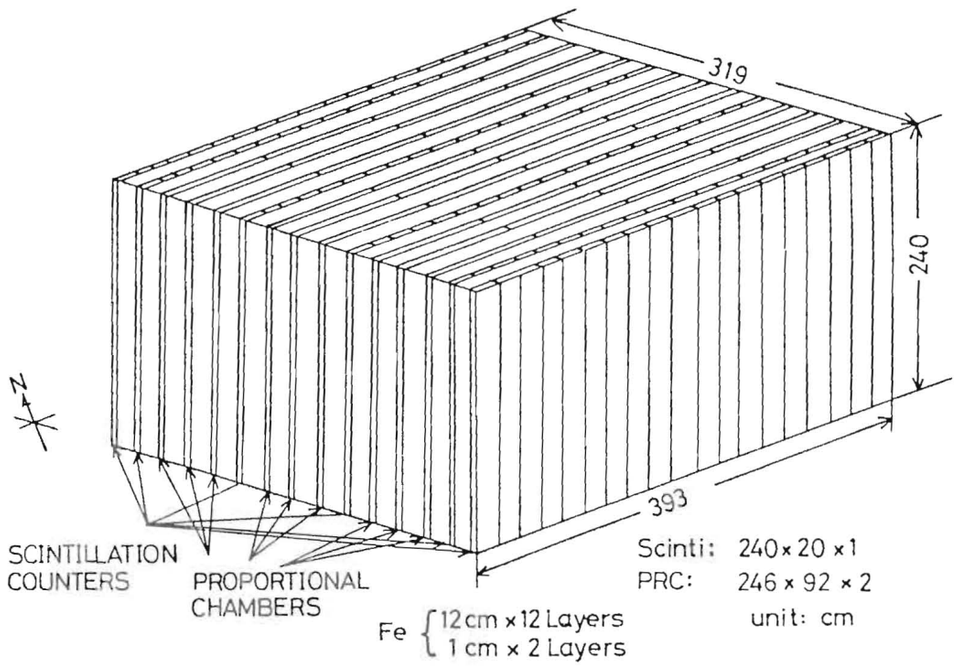
319
240
393
N
SCINTILLATION COUNTERS
PROPORTIONAL CHAMBERS
Fe {12 cm × 12 Layers
1 cm × 2 Layers
Scinti: 240 × 20 × 1
PRC: 246 × 92 × 2
unit: cm

Fig. 2

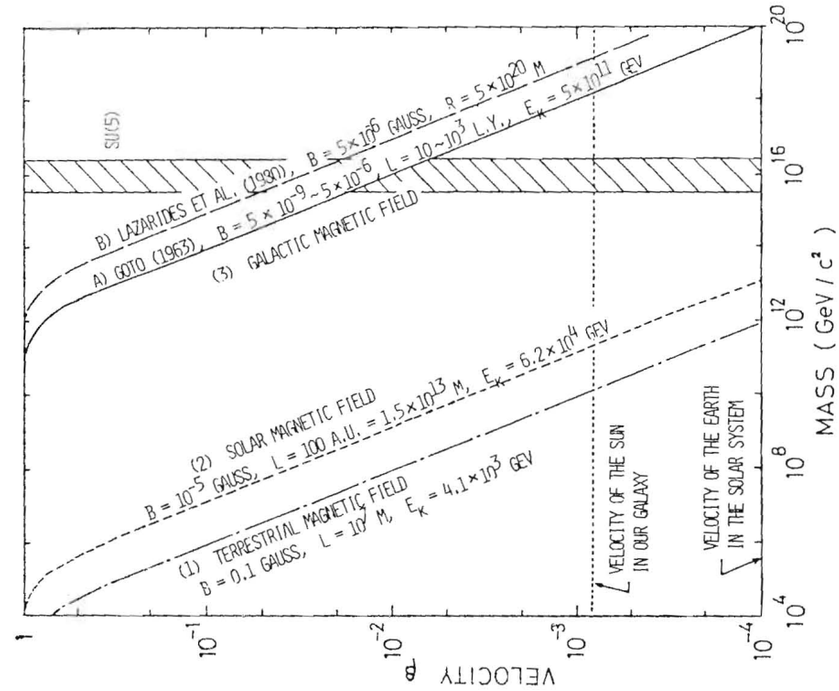
SU(5)
B) LAZARIDES ET AL., (1980), B = 5×10^6 GAUSS, R = 5×10^20 M
A) GOTO (1963), B = 5 × 10^-9 ~ 5 × 10^-6, L = 10 ~ 10^3 L.Y., E* = 5×10^11 GEV
(3) GALACTIC MAGNETIC FIELD
(2) SOLAR MAGNETIC FIELD
B = 10^-5 GAUSS, L = 100 A.U. = 1.5×10^13 M, E* = 6.2×10^4 GEV
(1) TERRESTRIAL MAGNETIC FIELD
B = 0.1 GAUSS, L = 10^7 M, E* = 4.1×10^3 GEV
VELOCITY OF THE SUN IN OUR GALAXY
VELOCITY OF THE EARTH IN THE SOLAR SYSTEM
MASS (GeV / c^2)
VELOCITY β

Fig. 1

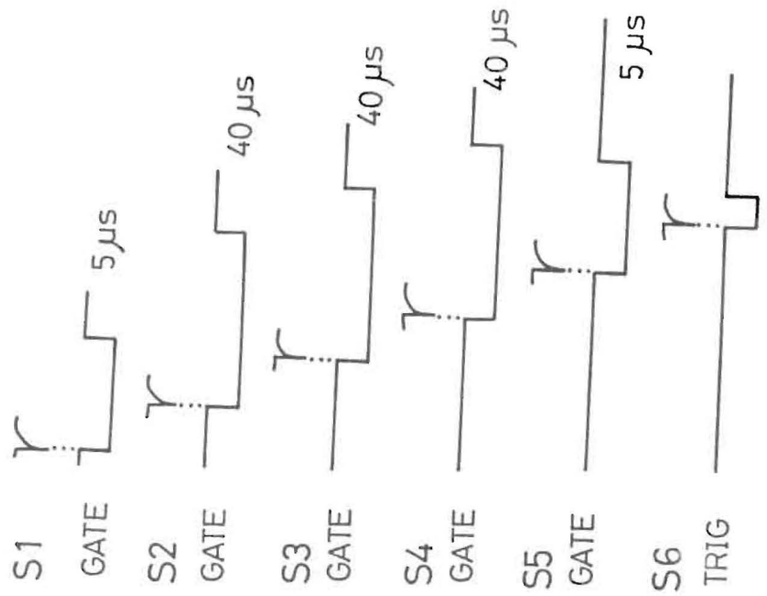
S1
GATE
5 µs
S2
GATE
40 µs
S3
GATE
40 µs
S4
GATE
40 µs
S5
GATE
5 µs
S6
TRIG

Fig. 4

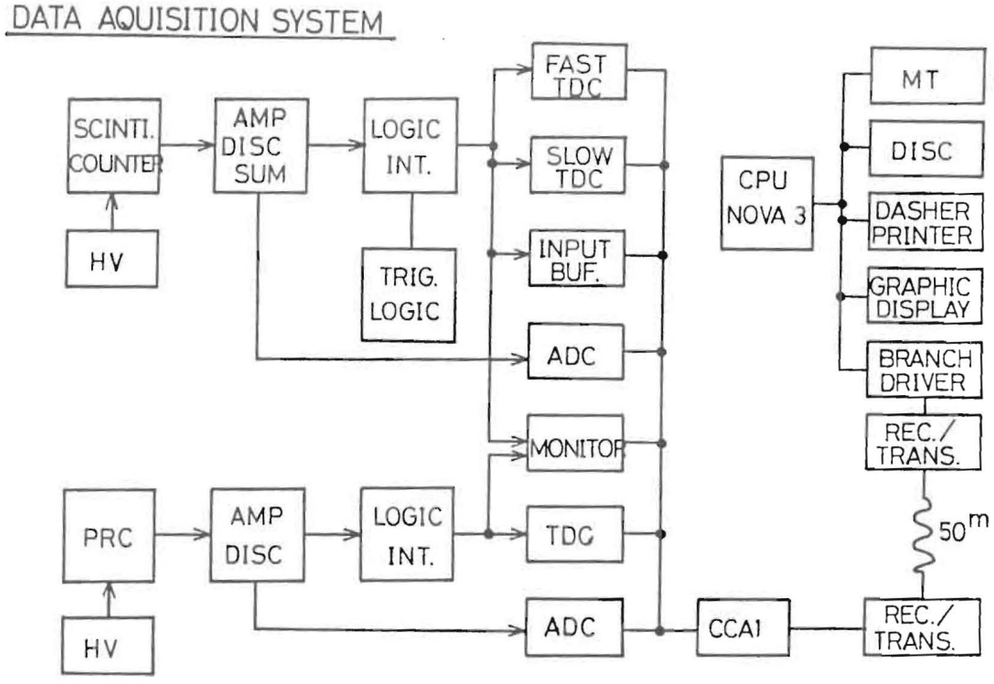
DATA AQUISITION SYSTEM
SCINTI. COUNTER
HV
AMP DISC SUM
LOGIC INT.
TRIG. LOGIC
FAST TDC
SLOW TDC
INPUT BUF.
ADC
MONITOR
TDC
ADC
PRC
HV
AMP DISC
LOGIC INT.
CPU NOVA 3
MT
DISC
DASHER PRINTER
GRAPHIC DISPLAY
BRANCH DRIVER
REC./ TRANS.
50m
CCA1
REC./ TRANS.

Fig. 3

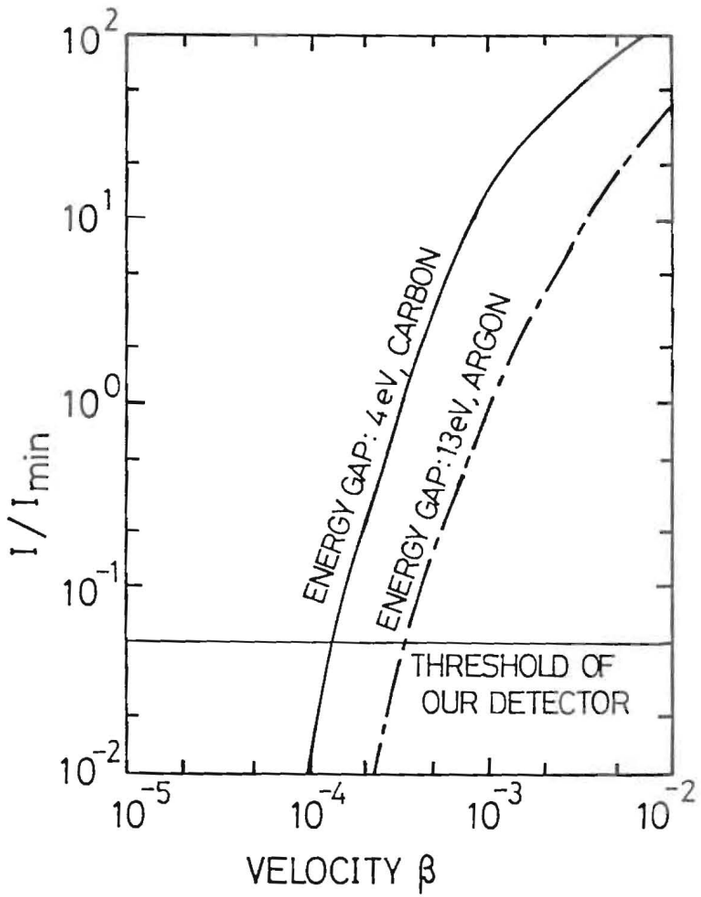
10^2
10^1
10^0
10^{-1}
10^{-2}
I / I min
ENERGY GAP: 4 eV, CARBON
ENERGY GAP: 13eV, ARGON
THRESHOLD OF
OUR DETECTOR
10^{-5}
10^{-4}
10^{-3}
10^{-2}
VELOCITY β

Fig. 5

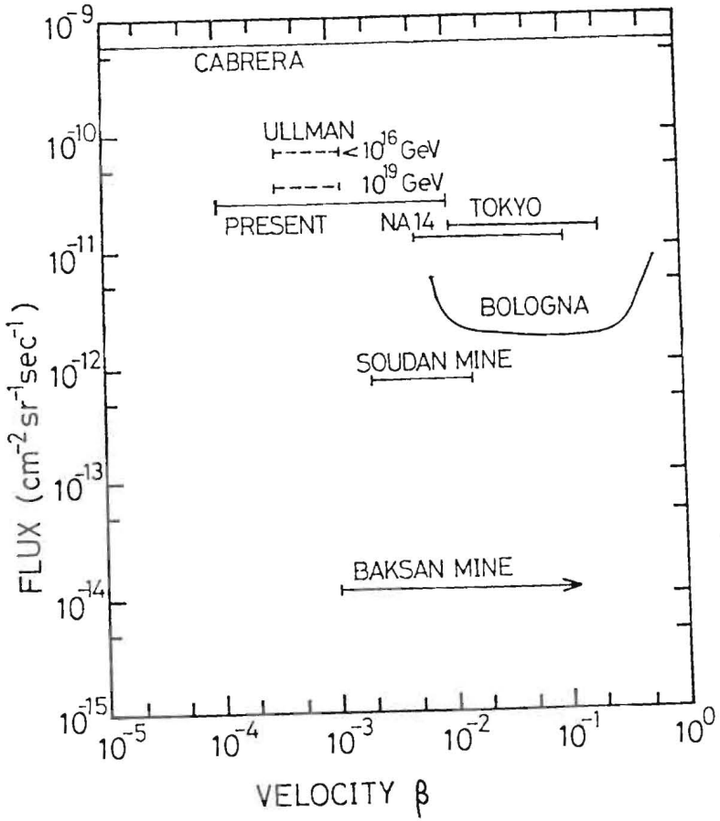
10^{-9}
10^{-10}
10^{-11}
10^{-12}
10^{-13}
10^{-14}
10^{-15}
FLUX (cm^{-2} sr^{-1} sec^{-1})
CABRERA
ULLMAN
$< 10^{16}$ GeV
10^{19} GeV
PRESENT
NA 14
TOKYO
BOLOGNA
SOUDAN MINE
BAKSAN MINE
10^{-5}
10^{-4}
10^{-3}
10^{-2}
10^{-1}
10^{0}
VELOCITY β

Fig. 6

SEARCH FOR SLOW MAGNETIC MONOPOLES IN COSMIC RAYS

S.HIGASHI, S.OZAKI and T.TAKAHASHI
Physics Department, Osaka City University, Sugimoto,
Sumiyoshiku, Osaka, Japan
and
K.TSUJI
Physics Department, Kinki University, Higashi-Osaka,
Osaka, Japan

The super heavy magnetic monopoles have been searched in the cosmic rays with the detector which is designed to discriminate the pulses from the proportional counters at 1/20 of the pulses induced by the minimum-ionizing particles. The upper limit of the flux is $2.1\times10^{-12}/cm^2sr$ sec for the monopoles having $\beta = 1\times10^{-3}$ to 4×10^{-3}.

Since the grand unified theories [1-3] predict the existence of the magnetic monopoles which may have a mass of the order of 10^{16} GeV/c^2, numerous experiments [4-8] have been carried out to find these particles in the primary cosmic rays. They were supposed to be created at the time of so called big bang and have been survived untill now with interacting on the matter or the field in the universe. Consequently their velocities [9-11] are expected to distribute widely at rather small value of $\beta \sim 10^{-2}$ to 10^{-4} where β is the ratio of a particle velocity to the speed of light. The values of β estimated are depending, of course, on the astrophysical arguments, such as how they are interacting with the surrounding matter or accelerated by the galactic magnetic field and so on. In some case, the regeneration of the galactic field may limit the velocities of the monopoles and also the flux of these particles. One of the basic idea to detect the monopoles on which the previous searches have been designed to distinguish them from the other kinds of the particles, is the heavy ionization of the monopoles in a matter due to the magnetic charge carried by them. This is true when these particles have the velocities close to that of light. However if the astrophysical arguments described above is correct, the values of β of the monopoles incident to the earth will be as small as $\sim10^{-2}$ to 10^{-4} and these speeds are similar to or less than that of the electrons moving around inside the atoms. In these cases there seems no reason to allow the extension of the theoretical formula for the ionization loss

[12] in a matter by the monopoles obtained at $\beta \sim 1$ to the case of β as low as 10^{-2} or less. So a couple of theoretical calculations have been carried out to compute the ionization loss for these small values of β, although these calculations are still preliminary results. For instance, according to K. Hayashi's calculation [13] the ionization loss by the monopoles is given by the formula of $\sim(100\beta)^3$ GeV/cm in water approximately. This will give less than 1 MeV/cm at β less than 10^{-3} which is almost 1/10 of the energy loss by the minimum-ionizing particles. This forced us to set the bias to discriminate the output pulses from the detector as low as possible, preferably less than 1/20 of that corresponding to the minimum-ionizing particles in order to operate the detector without lossing any candidate of the monopoles. According to S.P.Ahlen et al [14] , the ionization loss is approximately 20 MeV/g cm^{-2} in ~~Si~~ Silicon at $\beta \sim 10^{-3}$, which is rather large ionization. Table 1 shows the list of the experiments which have been performed recently to search the superheavy monopoles in the cosmic rays. From the standpoint of the ionization loss in the detector they, except one, seems to us to use rather high bias voltage to detect the monopoles.

The estimations of the monopole flux incident to the earth from the outer space are widely distributed from a few to the order of 10^4 or more per year per square kilometer depending on the model used. From the experimental results so far obtained, only the upper limits have been given on the monopole fluxes of the order of $10^{-10} \sim 10^{-12}/cm^2$sr sec,

except one which is performed by using the superconducting coil to detect the monopoles and he found one event giving the flux $6.1 \times 10^{-10}/cm^2$sr sec [5]. So for designing the apparatus for the monopole hunting, the effective area of the detector is also the other factor to be considered. In this experiment the array of the proportional counters are used to have wider area of the detection.

The apparatus consists of five layers of the proportional counters, the distance from the top to bottom layer being three meters as shown in Fig. 1. Each layer has 12 counters, $5 \times 10 cm^2$ and 500 cm long. One counter has two sense wires and a ground wire. A gas mixture of 90 % Ar and 10 % CH_4 is overflowed. All of the counters are operated with a common 2300 volt power supply which is still in the plateau region at the relation of the counting rate versus the applied voltage but almost 300 volt higher than the starting point of the plateau. Usually the gain of the proportional counters as the function of the applied voltage V is expressed by a exponential law $\exp(\alpha \times V)$ where $\alpha = 0.01$. So if the bias voltage of discriminator is set for the pulses due to the passages of the minimum-ionizing particles at 2000 volts, then at the 2300 working volts the pulses corresponding to the one twentieth of the minimum-ionizing particles could pass through the discrimination level. The output pulses from each counter are fed into his own one shot multivibrator which make a square pulse of 10 μs long and a delayed signal at the end of the square pulse. The output pulses are also fed to the trigger circuit

to make a master pulse, which is a sort of a successive delayed coincidence. With this circuit one can be sure that the time sequences of the pulses which generate the master pulses are delayed monotonously from top to bottom or from bottom to top layer. The master pulse starts the 20 MHz clock generator and clock signals are fed to the 8-bit scaler. Secondly, the delayed signals from each channel initiate to load the datum of the scaler to 8-bit shift register of corresponding channel. Time informations stored to these shift registers will be recorded on a paper tape.

Since the apparatus has been operated at sea level, a veto pulse is necessary to prevent the triggering of the circuits by the passage of the single muons in the cosmic rays. In the case of the proportional counters which are used in this experiment, the drift velocity of the electrons in the gas will be 1 mm/ 20 ns. In our geometry the drift length is 2.5 cm. So the time jitter of the pulses induced by a single particle among the counters will have at most 500 ns. Thus the veto pulse which may take out the contribution of the single muons from the data has been generated by the 4-fold coincidence among the counters of the first to fourth layer, with the time resulution of 1 μs. With this circuit the fastest particle which can be detected with the set up is 3 m/1 μs or $\beta = 10^{-2}$ in the case of vertical incidence, since the master pulses can be produced only when the time difference between the top layer and the bottom is longer than 1 μs. Slowest particle is 3 m/10 μs which is limited by the length

of the square pulses 10 μs. Beside these conditions, the fluctuation of the drift time of the electrons or the reading error of the system makes wider the range of the velocity of the monopoles to be detected. Unfortunately the counter array cannot allow to determine the arrival direction of the incident particles in the two dimensions. So the value of the β computed is evaluated with the assumption of the vertical incidence of the particles in the direction parallel to the counter axis.

After 9 months running of the apparatus with the monopole triggering where almost all of the events due to the single muons were rejected by means of the veto pulses, 40300 events have been recorded. On these events, the following three requirements are applied to select the candidates for a monopole trajectory. First one is that at least one of the counters at the fifth layer which is located at the middle of the array must be hit within the proper timing and total number of the counters hit in one event is less than 8. Then to go to the next step, all of the combinations of the counters hit has been made with a condition of taking out one counter from each layer from the first to fifth. Second requirement is a geometrical condition that a straight line has to be able to draw through the inside of the counters selected. For this purpose the least square method is applied to the positions of the sense wires of the counters. Then D(L) which is the root mean square deviation of the wire positions from the straight line obtained has been computed and this value must

be less than 2.2 cm to classify the track as the monopole candidates. The above requirement for locating all of the selected counters on a straight line, D(L) less 2.2 cm, has been determined from the results of analyzing the events which are generated artificially on the assumption that a muon pass through the counter array. The third one is the condition for the timing informations of the output pulses of these counters. The least square method is applied also to the timing data by assuming that the arrival times of the pulses have a linear relation to the positions of the counter layers. Then the inclination of the straight line obtained could be the inverse of the velocities with which the particle passed through the array and the root mean square deviation $D(1/\beta)$ on the timing data are also computed to test the correctness of the straightness assumption on them. The limit of the value of $D(1/\beta)$ have been computed also for the events produced artificially, in which the particles pass straightly through the counter array with all possible combinations of the incident direction and position, satisfying the requirements to generate the master pulses and the electrons ejected along the pass of the particles drift to the sense wire with the velocity of 1 mm/20 ns. From the distribution of the $D(1/\beta)$ thus obtained, one can conclude that the value of $D(1/\beta)$ should be less than 200 ns if the data are generated by the passage of a single particle. Following these analyses, the tracks which satisfy the above conditions $D(L) < 2.2$ cm and $D(1/\beta) < 200$ ns, are classified as the monopole candidates. If one event has more

than one track satisfying the conditions, the one having the smallest $D(1/\beta)$ will be registered as the candidate. The distribution of the values of $1/\beta$ of these candidates is shown in Fig. 2 for $1/\beta$ larger than 100. The tracks having $1/\beta$ less 150 could be considered the one due to the incident muons since in some case it is possible to make such velocity by the delay of the arrival time to the sense wires with some fluctuations of the drift velocity, emission of knock on electron by the incoming particles or the reading error. The other feature of the $1/\beta$ distribution is that no track has been found to have $1/\beta$ larger than 250. This makes it possible to set the upper limit of the flux of the magnetic monopoles in the cosmic rays at 90 % confidence level as 2.1×10^{-12}/cm^{2}sr sec for the monopoles for β less than 4×10^{-3}, since the aperture of the counter array is 2.3 m^{2}sr and the time of the observation is 231×10^5 sec. In the range of $1/\beta$ between 150 and 250, there are 38 tracks found, which is similar to the number of the tracks expected from the accidental coincidences among the counters of the five layers satisfying the above requirements. At present the estimation of the accidental coincidence is so rough that it does not mean to reject the possibility to find the true track due to the magnetic monopoles in the events after a fine analysis.

Table 1 shows the fluxes of the magnetic monopoles in the cosmic rays observed by our experiment and the others performed by the method similar to ours. Our detector constructed by the proportional counters has the merit that it

Table 1

Searches for slow monopoles

	Acceptance in m^2 sr	Time in 10^5 sec	$< 1/\beta <$	Detector	dE/dx min.	Flux (cm^2 sr sec)$^{-1}$
J.D.Ullman	0.95x2	48	860 to 3000	PR Counter	2	$2.5x10^{-11}$
B.Cabrera	0.0126	130	----	SQUID Coil	----	$6.1x10^{-10}$
R.Bonarelli et al	5.0x2	108	1.7 to 140	Scintil.	25	$2x10^{-12}$
J.K.Sokolowski et al	4.1	4.8	100 to 3300	Scintil.	0.01	$1.2x10^{-10}$
T.Mashimo et al	1.1	137	10 to 100	Scintil.	1.2	$1.5x10^{-11}$
S.Higashi et al	2.3x2	231	250 to 1000	PR Counter	0.05	$2.1x10^{-12}$

is easy to operate them with low discrimination level for the output pulses from the counters as low as 1/20 of that corresponding to the minimum-ionizing particles without any increase of the background counts. Also it is easy to have large area of the detector with negligibly small dependence of the pulse height on the spatial position. However, it is necessary to measure the inclination of the particle trajectory in order to improve velocity information. It is planned to add two layers which serve position data along 5 m long sense wires and pulse height data. At present, the upper limit of the monopole flux in the cosmic rays at 90 % confidence level has been concluded to be $2.1x10^{-12}/cm^2$ sr sec in the velocity range of $1x10^{-3}$ to $4x10^{-3}$.

As we described earlier, the proportional counters used in the experiment can be treated as the drift chambers with almost constant drift velocity. Thus the timing informations could be transfered to the distances of the trajectories of the particles from the sense wires at each layer. Then it is possible to increase the accuracy on the geometrical condition, which check the straightness of the positions of the particle trajectories at the five layers, to reject the spurious events and also we may have better timing informations of the arrival of the particles at each plane of the counters. These analyses on the data so far obtained are going on now which may give us the better results on the existence of the monopoles in the cosmic rays.

References

[1] H.Georgi and S.L.Glashow, Phys.Rev.Lett. 32 (1974) 438.

[2] H.Georgi, H.R.Quinn and S.Weinberg, Phys.Rev.Lett. 33 (1974) 451.

[3] A.Buras, J.Ellis et al., Nucl.Phys. B135 (1978) 166.

[4] J.D.Ullman, Phys.Rev.Lett. 47 (1981) 289.

[5] B.Cabrera, Phys.Rev.Lett. 48 (1982) 1378.

[6] R.Bonarelli, P.Capiluppi et al., Phys.Letters 112B (1982) 100.

[7] J.K.Sokolowski and L.R.Sulak, private communication June 17 (1982).

[8] T.Mashimo et al., J.Phys.Soc.Jpn. 51 (1982) 3067.

[9] P.J.E.Peebles, Physical Cosmology, Princton Univ.Press.

[10] G.Lazarides et al., Phys.Letters 100B (1981) 21.

[11] P.Langacker, 1981 Int.Symp.on Lepton and Photon Interactions.

[12] S.P.Ahlen, Phys.Rev. D17 (1978) 229.

[13] K.Hayashi, Nuovo Cim.Lett. 34 (1982) 10 and see his references.

[14] S.P.Ahlen and K.Kinoshita, preprint to be published in Phys.Rev.D (1982).

Figure Captions

Fig. 1. Schematic diagram of apparatus.

Fig. 2. $1/\beta$ distribution of the monopole candidates.

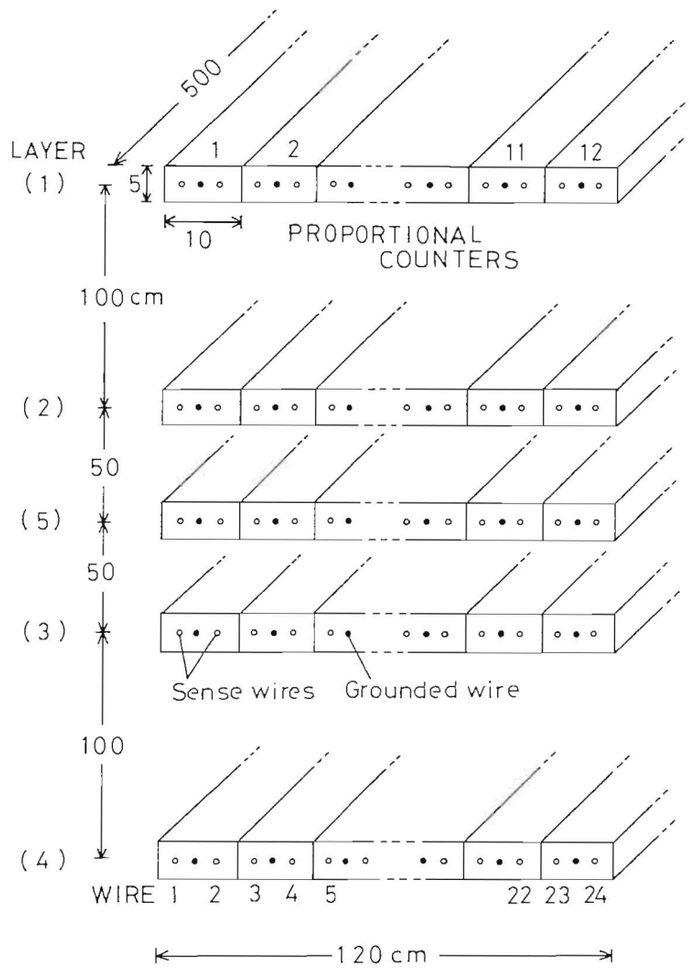
500
LAYER
(1)
5
1
2
11
12
10
PROPORTIONAL
COUNTERS
100 cm
(2)
50
(5)
50
(3)
Sense wires
Grounded wire
100
(4)
WIRE 1 2 3 4 5
22 23 24
120 cm

Fig. 1

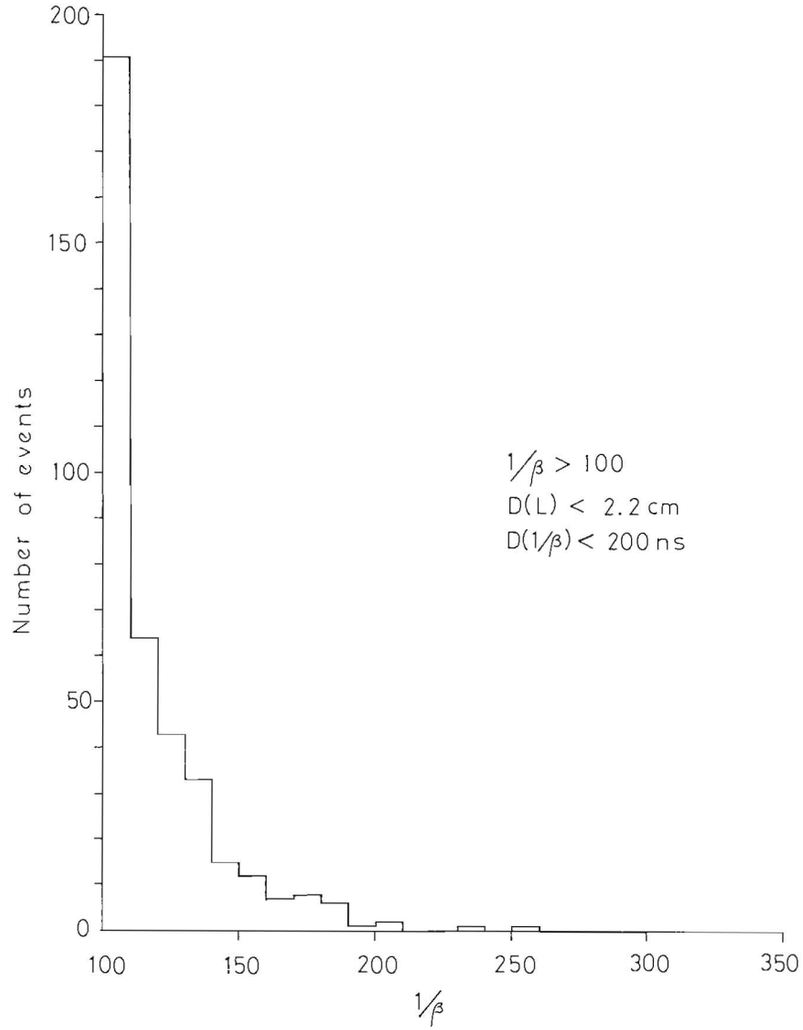
200
150
100
50
0
Number of events
100
150
200
250
300
350
1/β
1/β > 100
D(L) < 2.2 cm
D(1/β) < 200 ns

Fig. 2

PROTON DECAY EXPERIMENT AT KOLAR GOLD FIELD.

S.MIYAKE

Institute for Cosmic Ray Research, University of Tokyo.

N.ITO, S.KAWAKAMI, Y.HAYASHI and N.HIRAOKA.

Osaka City University.

M.G.K.MENON, B.V.SREEKANTAN, V.S.NARASIMHAM, M.R.KRISHNASWAMY and N.K.MONDAL.

Tata Institute of Fundamental Research.

1. Introduction

Proton Decay experiment at K.G.F. has been in operation since November 1980 at the depth of 7,600 m.w.e of standard rock. The detector comprises a stack of iron plates and proportional counters in 34 horizontal layers in orthogonal conditions. Fig.1 shows the both view of the detector. The absorbers are of a uniform thickness of 12 mm except those between layers 1,2 and 32,33. The proportional counters are formed from hollow iron pipes of square cross section of 10 x 10 cm^2. The volume of detector is 4 m (width) x 6 m (depth) x 3.7 m (height) and total weight 140 tons. Fig.2 shows the pulse height distribution of proportional counter exposed to natural radio activity. First sharp peak corresponds to characteristic X ray (6.4 KeV) of Fe and second broad one to the ionisation loss by Compton electrons within the gas of counter. These shape is very useful for calibration and monitor of detector in deep underground. Each counter pulse height (4.5 mV corrresponds to single particle) is independently amplified (gain 80, decay time constant 10 μsec.) and the pulse height is converted to width using discriminators (level 100 mV). The ionisation is measured in terms of the equivalent number of minimum ionising particles. The trigger is employed both with a 5 layer coincidence in any of 11 consecutive layers and tracks crossing any 2 in 3 consecutive layers. Counting rate of counter is about 10 / sec on average and spurious counter is about 0.25 / trigger.

The resolution of detector is

$\Delta\theta = \Delta\varphi \leq 3^\circ$, $\Delta N / N \simeq 0.3$ for N = 1 - 100 particles.

Layer efficiency = 97.5 %, Chance rate ≃ 20 / day

Event rate (cosmic ray muon) ≃ 1.9 / day.

By this detector, we can study

(1) Muon physics; Angular distribution, Intensity, Energy Spectrum, Multiple Muons, ----

(2) Neutrino Physics ; Flux, New particle (heavy mass 2 - 3 GeV, long life 10^{-8} - 10^{-9} sec, decays mainly into 3 body,etc) produces by neutrino interactions and anomalous cascade (high energy contents, depth independent, double centered in energy flow, ---)

(3) Proton decay, Magnetic monopole and idetification of electron neutrino and muon neutrino through secondary products etc,---)

2. Experimental Data.

During the live time of 560 days, 1045 events have been recorded and these have been classified into various categories as shown in Table.

Category of events	Observed No.	Expected No.
Atmospheric muons ($\theta \leq 55^\circ$)	979	~980
Parallel muons ($N_\mu \geq 2$)	12	
Neutrino interactions in rock ($\theta > 55^\circ$)	29	~ 28
Neutrino interactions inside detector	11	~ 16
(a) Multiprong events	5	
(b) Single tracks penetrating the top layer including stopping atmospheric muons.	5	
(c) Single tracks penetrating sides or bottom layers	6	
Kolar events	2	
Nucleon decay candidates.	7	

Fig.3 shows angular distribution of atmospheric muons and muons produced by neutrino interactions within rock. These are in good agreement with the expected values. Within 1.5 years operation, neutrino events produced inthe

rock is 29 (expected 28) . On the other hand, expected number of events in detector is about 16 are compared with single tracks terminated in the detector (stop or generated by neutrinos) of 11 events and multiprong of 5 events. Out of them 3 events can be expected as stopping muons and 2 events ascribe to neutrino induced muons coming from rock. Except these, remaining 7 events can not be explained as normal figure by the pattern configuration and pulse height. Here we discuss only fully confined events strongly indicative of nucleon decay.

3. Fully confined events.

Nucleon Decay Candidate No.587 (10 - 11 - 1981) Fig.4

The pattern of event is electromagnetic cascades. The zenith angle is about 58°. The total range of shower is about 20 radiation length and total number of particles is 42.6 and estimated energy is 980 MeV with an uncertainty of 20 %. This event could be due to a neutrino interaction or proton decay ($P \rightarrow e^{+} + \pi^{\circ}$). The neutrino interaction could occur at 19th layers through one of the two processes.

$\nu_e(\tilde{\nu}_e) + Z \rightarrow e^{-}(e^{+}) + Z'$ (Charged current) estimated rate 0.3/1.5 yrs.

$\nu(\tilde{\nu}) + Z \rightarrow \nu(\tilde{\nu}) + \pi^{\circ} + Z'$ (Neutral current) " 0.3/1.5 yrs.

In case of about 1 GeV cascade, normally shower could not path through materials 20 r.l. and shower maximum should come around 2 - 3 r.l instead of 6 - 7 r.l. These features are more easily understood if the event is composed of separate showers oriented back to back. From the configuration of event, a plausible interpretationis proton decay in layer 15 to $P \rightarrow e^{+} + \pi^{\circ}$. with energy of U_e = 500 MeV and $U_{\pi^{\circ}}$ = 500 MeV.

Nucleon Decay Candidate No.867 (28 - 4 - 1982) Fig.5

This event has the following features ;

(1) A kink at the point B (or B') with deflection angle of 37° (57°)

(2) Normal ionisation along the path BC.

(3) Increased ionisation at the end point A.

These feature suggest the creation of a particle at the point C' which

slowed down to point A with a scatter along its path at the point B (B').

The only background is from neutrino interactions of the type

$\nu(\tilde{\nu}) + Z \rightarrow \nu(\tilde{\nu}) + \pi^{ch} + Z'$ (interaction at C) .

$\nu_\mu(\tilde{\nu}_\mu) + Z \rightarrow \mu^{\mp} + \pi^{ch} + Z'$ (" at B)

Estimated rate $< 0.15/1.5$ yrs.

From pulse height information, this event can be interpreted as $P \rightarrow \tilde{\nu} + \pi^{+}$ with $E_{\pi} \simeq 435$ MeV. It is possible to explain this event as $P \rightarrow \tilde{\nu} + K^{+}$ $\hookrightarrow \mu^{+} + \nu$ but in this case background will be lower by another factor of 10.

Nucleon Decay Candidate No.877 (7 - 5 - 1982) Fig.6

This event has the following features

(1) BC a non showering particle, pion or muon.

(2) A shower like along AB.

(3) A kink at the point B of angle $23^{\circ} \pm 5^{\circ}$

This event could be generated by any of the following processes.

(a) $\nu_\mu(\tilde{\nu}_\mu) + Z \rightarrow \mu^{-}(\mu^{+}) + \pi^{\circ} + Z'$ (interaction at B)

(b) $\nu_e(\tilde{\nu}_e) + Z \rightarrow e^{-}(e^{+}) + \pi^{ch} + Z'$ (" at A or B)

(c) $\nu(\tilde{\nu}) + Z \rightarrow \nu(\tilde{\nu}) + \pi^{ch} + Z'$ (" at C and charge exchange at B)

Total expected rate of neutrino background $< 0.1/1.5$ yrs . This event could be interpreted as $N \rightarrow e^{+} + \pi^{-}$ U_e = 400 Mev, U_{π} = 450 Mev.

For the confined events, we adopt a total weight of 60 tons in the central volume of the detector and obtain the life time of bound nucleons

$$\tau_N \simeq \frac{3.6 \times 10^{31} \times 1.5 \times 0.5}{3} = 9 \times 10^{30} \text{ yrs.}$$

If we take 7 candidate events and with 100 tons of fiducial weight, we estimate $\tau_N = 6.5 \times 10^{30}$ yrs.

We have another two confined events with energy of about 270 MeV and 700 MeV. These one can be interpreted as neutrino interactions within our detector from the configuration of events.

4. Short track events.

In addition to the above confined events, we have observed some confined short track events. The general feature of these events are;

(1) There are no straight and fully ionizing tracks traversing $\gtrsim 6$ layers.

(2) Most of the tracks have gaps along their path suggestive of soft component (e,γ). In general there is a kink (scatter) along the path.

(3) The visible energy of these tracks is $\lesssim 200$ MeV estimated from the ionisation and the range of the tracks.

A few examples of these events is shown in Fig.7.

An important point is whether they are

(a) Low energy neutrino events with $E_\nu \lesssim 300$ MeV. or

(b) Some other phenomena such as nucleon decay modes suggested by Pati-Salam (1973) where $P \dashrightarrow 3\nu + \pi^+$, $3\nu + \pi^+ + \pi^+ + \pi^-$, $2\nu + e^+ + \pi^\circ$ --- $N \dashrightarrow 3\nu + \pi^\circ$, $3\nu + \pi^+ + \pi^- + \pi^\circ$, ---- etc are dominant with a mean pion energy of about 250 MeV. It is almost impossible to explain by chance coincidence to fire 6 layer 6 counters. The shape seems quite different from the type expected from GUTs model. It is not well known as to low energy neutrino flux, but high frequency occurence of phenomena could not explain. We have indicated here only the general features of the short track events with a view to emphasise the need to look for such examples in the more elaborate detectors planned for proton decay experiments.

Refereces

1. M.R.Krishnaswamy ,et.al Phys. Lett 106B (1981) 339

2. M.R.Krishnaswamy, et.al Phys. Lett 115B (1982)349.

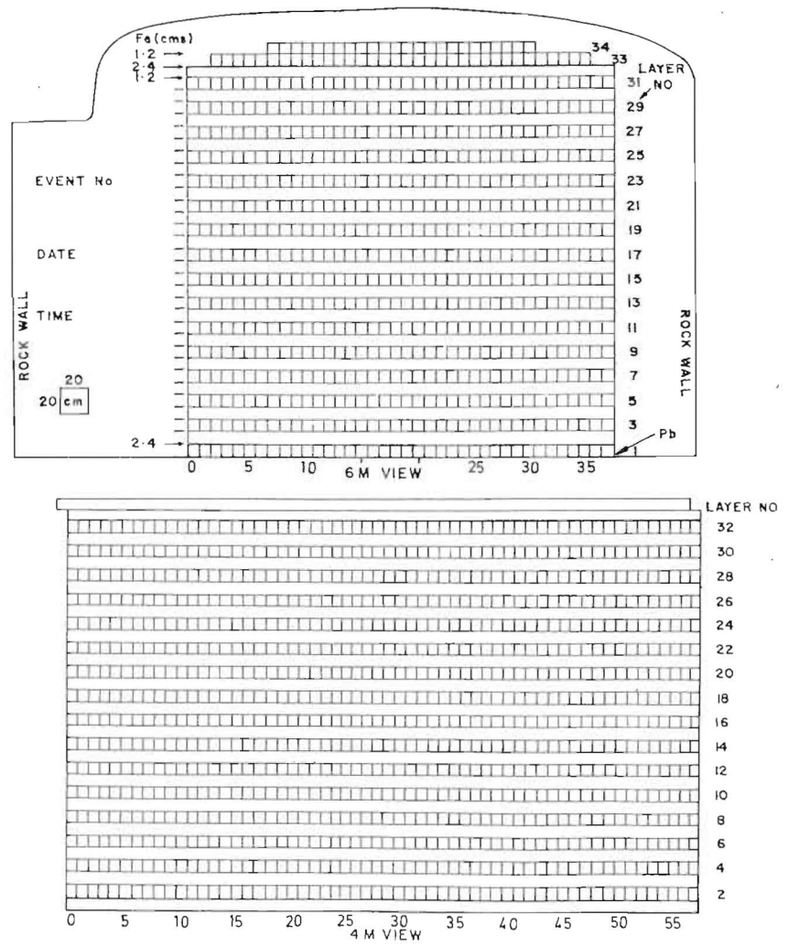

Fig.1 Both View of the Proton Decay Detector.

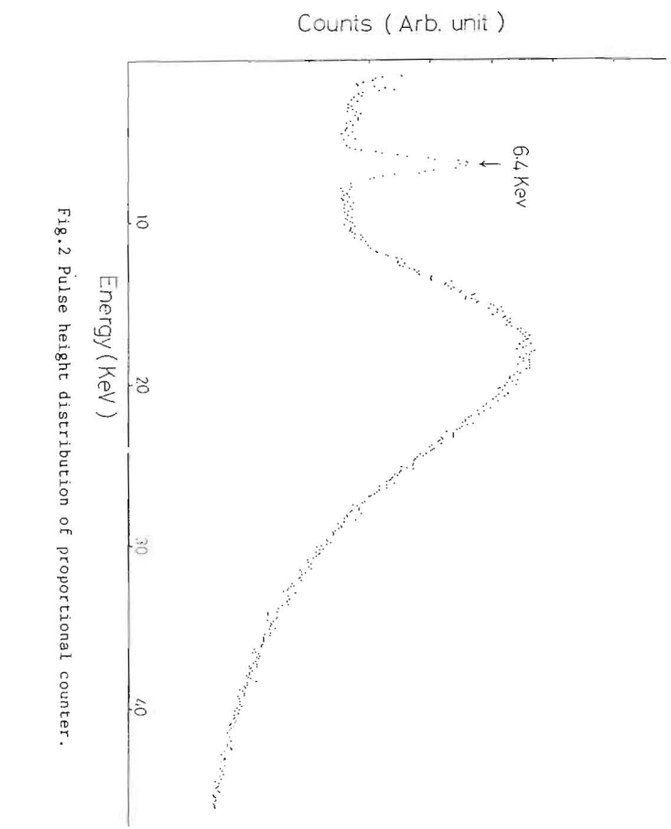

Fig.2 Pulse height distribution of proportional counter.

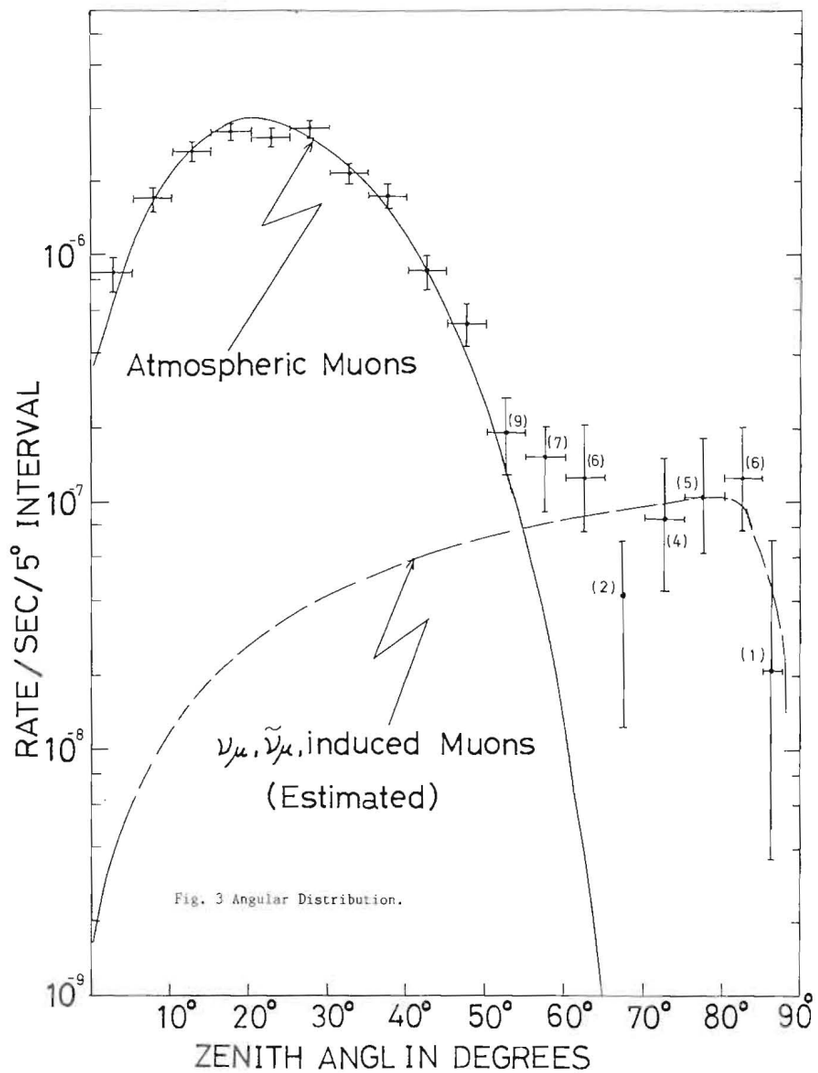

Fig. 3 Angular Distribution.

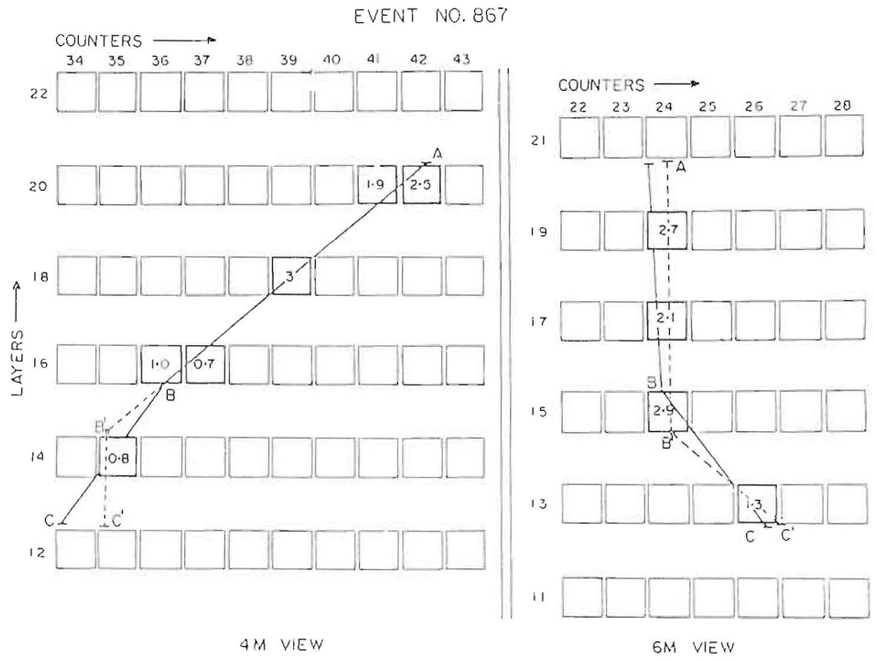

Fig.5 Nucleon Decay Candidate. $P \rightarrow \tilde{\nu} + \pi^+$ or $P \rightarrow \tilde{\mu} + K^+$

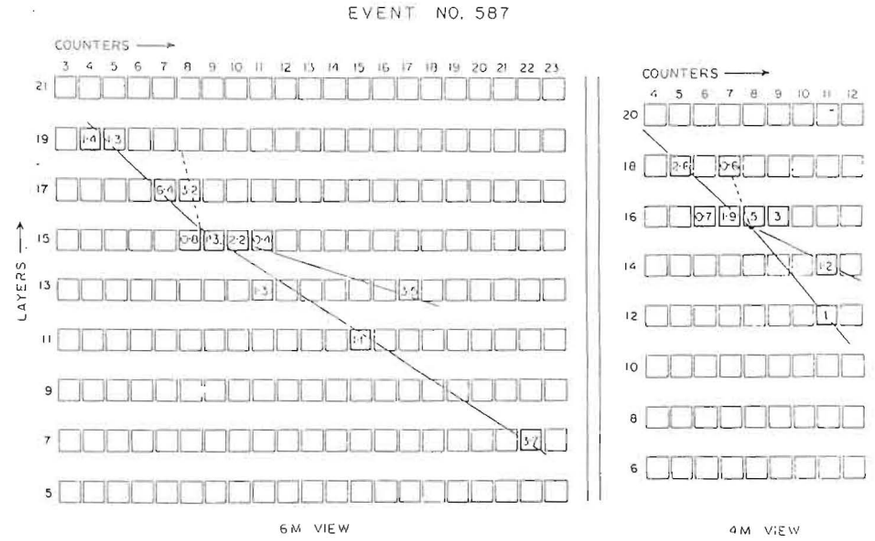

Fig.4 Nucleon Decay Candidate. $P \rightarrow e^+ + \pi^\circ$

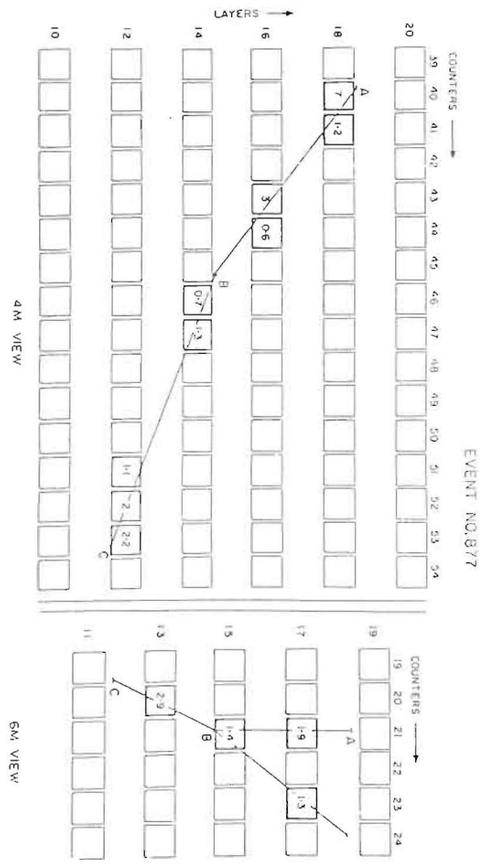

Fig.6 Nucleon Decay Candidate. $N \rightarrow e^{+} + \pi^{-}$

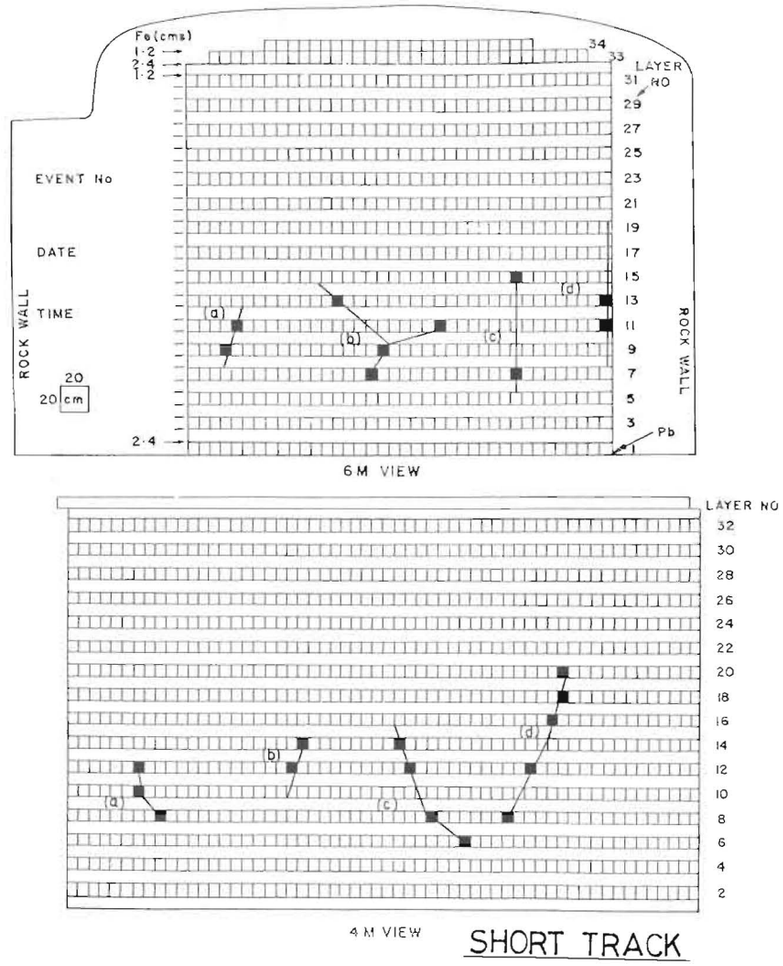

Fig.7 Short Track Event.

SEARCH FOR MONOPOLES BY MEANS OF ARTIFICIAL GRAVITATION

Hajimé Yoshiki

The search for the magnetic monopoles whether in cosmic ray or on earth seems to depend on experimenters' personal views of the matter today. One of the features of the monopole predicted by Grand Unification Theories is that it has an exceedingly heavy mass of the order of 10^{15}-10^{17} Gev/c^2 or 2 to 200 ngrams.

This peculiar feature of the monopole, apart from its monopolarity, motivates us to look for such particles among matters in the presence of gravity. In fact a field of 1 Tesla exerts on a unit monopole a force of 2 ev/Å or 20 Gev/m, whereas a unit monopole of mass of 10^{16} Gev/c^2 will be pulled toward the center of the earth by the gravitational force of 1 Gev/m on the earth's surface only. If a monopole at rest is accelerated by the earth's gravitation by 100 Å on the surface of the earth, the common binding force can not bring it at rest anymore which is in the order of 10 ev/Å.

Separating a monopole from a bulky matter, whether as an isolated object, or as a system composed of monopole and ordinary substances bound by electromagnetism, is another problem experimenters to

decide. The latter is more attractive because there are chances for the experimenters to handle the system in the laboratory (e.g. keeping it in a jar(!) after taking a photo of B-field emanating from the monopole using techniques like electron holography(!)[1]). For instance one can think of a particle of γ-hematite(Fe_2O_3) which is a spicular powder of 0.1 μm in length weighing about 10^{-16} gram which is 10^8 times lighter than the monopole. Proper choice of liquid (like liquid helium whose surface tension is 0.1 dyne/cm at 4.2 K) would separate a γ-hematite particle with monopole from those without monopole by floating the powder on the liquid[2]. γ-hematite is widely used for, for instance, magnetic tapes. This type of approach however is limited by its low processing speed if the abundance of the monopole is as predicted by theorists, although it excels in retaining the sample if once discovered.

If however the monopole is allowed to leave the laboratory after detecting it, a number of schemes are conceivable. One of such, as proposed by Wisconsin group[3], is to detect the object directly under a sintering plant which sinters small sized iron ore into larger pieces more suitable for blast furnaces in steel mills. When the iron ore is heated above Curie temperature in the sintering plant the monopole or the system thereof should begin to diffuse downward by

gravity and after about 1 to 1000 seconds reach the iron boundary, to start a free fall toward a Cabrera type detector placed below. One of the largest sintering plants in Japan is 5 m wide , 120 m long and able to process 22,000tons of iron ore maximum per day. The sintering plant is ordinarily four storied and the first floor is normally left spacious enough to render various services and is able to accommodate such detectors. Japan possesses about 50 of such plants. If the area of Cabrera coil[4] is $300cm^2$, the monopole search is done effectively for one ton of ore per day per plant per detector. Each detector cost about 10^7 yen with two fold coincidence Cabrera coils. Japan is one of the largest steel producing countries and one can access to the varieties of iron ore of the world very readily. The land is small and the supply of liquid helium is easily done. Thus the Wisconsin type monopole search is also feasible in Japan.

However we propose here another quite interesting way of search: artificial gravity, or decelerating the sample at the rate of $10g_o$ to $1000g_o$, where g_o is the acceleration of the gravity on earth's surface (9.8 m/sec^2). Since the electromagnetic binding is in the order of 10 ev/Å and this is about 10 to 1000 times stronger than the gravitational pull on the monopole, by exerting such deceleration properly on sample for a

certain length of time, the monopole will be turn off the system and start a free fall. In Fig 1, we show an example of such system. The decelerator is constructed out of 1) a table which holds the sample up to 200 kg, 2) a pneumatic device which accelerates the sample preliminarily downward, 3)pads which stop the falling table and decelerate the sample and 4) seismic balance which disperses the shock received by the pads. It can deliver the deceleration of $10g_o$ to $1000g_o$ to the sample by changing the pads. The length of action time is inversely proportional to the deceleration determined by the nature of the pads and enough to accelerate the monopole up to 0.2 to 20Gev seen from the sample's system. Repetition rate is 10 to 20 sec per cycle. It can thus process at least 300 tons of sample a day. First of attractive features of this scheme is that by monitoring the arrival time and the direction of the monopole the background is kept negligible. Second is that if once the monopoles be detected in a good deal of numbers, one may try to determine its mass through threshold by changing the pads.

Although the system itself costs about $2x10^7$ yen, if one try to sample millions of tons of iron ore over the period of years in future, the problem will be how to put each portion of the sample (about 100kg) on the detector's table every cycle day and night. This

requires knowledges of ore transportation, robot technology and so on. However a preliminary experiment in the order of 100 tons can be done in the laboratory.

As a remark to choosing sample ore, it should be noted that not only pyrogenetic ore, but also any ore which experienced strong shocks more than $10g_o$ such as blasting, centrifugal crushing and so on should be avoided before it is sent to detecting system.

References

1) Tonomura,A. et al. Phys.Rev.Let.48(1982)1443: B-field image will look like a half moon when the monopole charge is the smallest.

2) Combinatin of a magnetic field of 1 Tesla and frothed water is anoth possibility. We assume that the hematite holds monopoles.

3) Cline,D. et al. "A New Experimental Technique to Search for Relic Magnetic Monopoles" 1982, Madison, Wisconsin.

4) The above group claims $1m^2$.

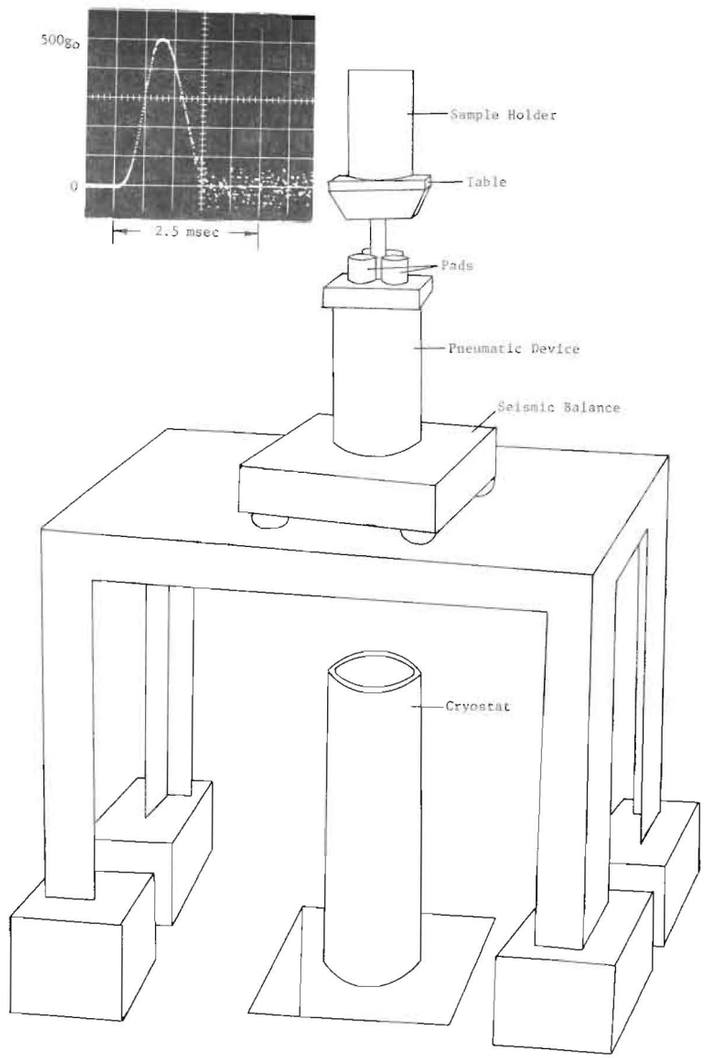

Fig. 1

Grand Unification mass scale and proton life time in SO(10) model

Noboru YAMAMOTO

Dept. of Physics, Osaka Univ.
Toyonaka, Japan

Abstract

We study super heavy gauge boson mass threshold effect and derive formulas for grand unification mass scale and the Weinberg angle in SO(10) GUT. Proton life time is estimated by the obtained formula. Relation with the formula derived by L. Hall is also discussed.

§1. Introduction

To analyze mass threshold effect in grand unified theory, two different methods has been used. One method is the renormalization group equation in mass dependent renormalization scheme[1]. And the other is a method of effective lagrangian[2]. The former method was used by T. Goldman and D.A. Ross[1] to estimate a grand unification mass scale in the SU(5) GUT model taking into account the effect of gauge boson mass threshold. T. Matsuki, Y. Hara and the present author in the previous works[3] studied the SO(10) model in detail using the method of Goldman and Ross. In this method, it is impossible to solve renormalization equations analytically, and we must use the numerical solutions of equations.

On the other hand, L. Hall[4] discussed the unification mass scale using the effective lagrangian introduced by S. Weinberg[2]. He found "matching function corrections" for effective coupling constant. The effective lagrangian is got by integrating out the super heavy field. Gauge fixing for super heavy gauge bosons and for the other gauge bosons are needed separately. This makes the effective gauge theory intransparent.

In this paper we will derive the formula in mass dependent renormalization scheme. This formula corresponds to the "matching function" of L. Hall. The formula is derived in §2. We also estimate the unification mass scale and proton life time in the SO(10) GUT in §3. §4 is devoted to summary and discussions.

§2. Renormalization group

In this section we follow the renormalization scheme used by T. Goldman and D.A. Ross[1]. Renormalization group equation in this method has a form,

$$\mu \frac{\partial \alpha_i(\mu)}{\partial \mu} = \sum_j \beta_{ij}(\mu, M_i, M_j, m_f, m_H)\,\alpha_i \alpha_j , \quad (2.1)$$

where $\alpha_i = g_i^2/4\pi$ are coupling constants, β_{ij} mass dependent β-functions, and M_i, m_f and m_H masses of gauge bosons, fermions and of Higgs particles, respectively. Index i runs from 1 to 8 for the SO(10) model[3].

The β-functions up to one-loop approximation were given in Ref. 3 for the SO(10) model. They are rather involved to write down here. In Ref. 3, we were forced to solve Eq.(2.1) by numerical computation because of the entanglement of the eight equations. However analysis performed by them shows that we may substitute all coupling constants α_j's in the i-th β-function β_i by one coupling constent α_i. This approximation simplifies Eq.(2.1) considerably, and we get approximate solutions of Eq.(2.1) as,

$$\frac{1}{\alpha_i(Q^2)} - \frac{1}{\alpha_i(Q_0^2)} = \sum_{r_j^G \subset R^G} T_2^{(i)}(r_j^G) \times V(Q^2, M^2, Q_0^2) + \sum_{r_j^h \subset R^h} T_2^{(i)}(r_j^h)\, S_2(Q^2, Q_0^2, M^2) + \sum_{r_j^f \subset R^f} T_2^{(i)}(r_j^f)\, S_3(Q^2, Q_0^2, M^2) , \quad (2.2)$$

where functions V, S_2 and S_3 are defined in Appendix. $T_2^{(i)}(r)$ are indeces of r in terms of subgroup G_i, and $r_j^G(r_j^h, r_j^f)$ are components of direct sum decomposition of $R^G(R^h, R^f)$. R^G, R^h and R^f are representation of gauge boson, Higgs scalar, and fermions, respectively.

To get a "matching function" type formula, we consider the case $Q^2 \to \infty$, $Q_0^2 \to 0$. In this limit, functions V, S_2 and S_3 have simple forms,

$$V(Q^2, Q_0^2, M^2) = \frac{-11}{12\pi}\left\{\log\frac{Q^2}{M^2} - 3.25\cdots\right\} ,$$
$$S_2(Q^2, Q_0^2, m^2) = \frac{1}{24\pi}\left\{\log(Q^2/m^2) - 8/3\right\} ,$$
$$S_3(Q^2, Q_0^2, m^2) = \frac{2}{12\pi}\left\{\log(Q^2/m^2) - 5/3\right\} . \quad (2.3)$$

In the limit $Q^2 \to \infty$ the condition

$$\alpha_i^{-1}(Q^2) - \alpha_j^{-1}(Q^2) \to 0 \quad (2.4)$$

must be satistied in GUT. In this limit, Eq.(2.2) becomes

$$\alpha^{-1}(Q^2) - \alpha_i^{-1}(Q_0^2) = \beta_{\text{asymptotic}} \cdot \log(Q^2/Q_0^2) + \sum_{r_j^G \subset R^G} T_2^{(i)}(r_j^G)\frac{(-11)}{12\pi}\left\{\log\frac{Q_0^2}{M_j^2} - 3.25\right\} + \sum_{r_j^h \subset R^h} T_2^{(i)}(r_j^h)\frac{1}{24\pi}\left\{\log(Q_0^2/m_h^2) - 8/3\right\} + \sum_{r_j^f \subset R^f} T_2^{(i)}(r_j^f)\frac{2}{12\pi}\left\{\log(Q_0^2/m_f^2) - 5/3\right\} , \quad (2.5)$$

for $Q^2 \gg M_i^2 \gg Q_0^2$.

The formula written above corresponds to the matching function derived by L. Hall[4]. The constant terms in Eq.(2.5) represents mass threshold effects. Numerical values of these terms are different from that of Hall's matching function. Difference of renormalization scheme may explain this discrepancy. Whereas Hall used the $\overline{MS}$-scheme. We have used the momentum subtraction scheme. The applicability of Eq.(2.5) is restricted in the region $Q^2 >> M_i^2 >> Q_0^2$, while Eq.(2.4) has no such a limitation. A useful formula for unification scale interms of α_{em} and α_s can be derived from Eq.(2.5) as follows.

The electromagnetic coupling constant α_{em} is related to α_1 and α_2 as

$$\alpha_{em}^{-1} = \frac{5}{3}\alpha_1^{-1} + \alpha_2^{-1} . \qquad (2.6)$$

Consider the combination $\alpha_{em}^{-1} - \frac{8}{3}\alpha_s^{-1}$. In the limit $Q^2 \to \infty$, this combination must vanish because of Eq.(2.4) and (2.6), namely

$$\alpha_{em}^{-1}(Q^2) - \frac{8}{3}\alpha_s^{-1}(Q^2) \to 0 \quad \text{as} \quad Q^2 \to \infty . \qquad (2.7)$$

For the SO(10) model, Eq.(3.7) implies that

$$\log(M_X^2/m_W^2) = \frac{4\pi}{21}\left[\alpha_{em}^{-1}(2m_W) - \frac{8}{3}\alpha_s^{-1}(2m_W)\right] - 2.097 + \frac{1}{3}\log(M_E^2/M_G^2) + \frac{1}{21}\log(m_W^2/m_{Higgs}^2) + \frac{1}{63}\log(m_W^2/m_{10}^2) . \qquad (2.8)$$

Here M_E and M_G are masses of gauge bonsons characterizing the SO(10) model, m_{Higgs} is a mass of Higgs scalar of which goldstone mode translated into longitudinal mode of X(Y) boson, and m_{10} is mass of coloured Higgs scalar.

We also get the formula for the Weinberg angle $\sin^2\theta_W(2m_W)$, as

$$\sin^2\theta_W(2m_W) = \frac{1}{6} + \alpha_{em}(2m_W)\left[\frac{5}{9}\alpha_s^{-1}(2m_W) - 0.1302 + \frac{1}{4\pi}\left\{\frac{7}{6}\log\left(\frac{M_E^2}{M_F^2}\right) + \frac{17}{2}\log\left(\frac{M_E^2}{M_G^2}\right) + \frac{1}{9}\log\left(\frac{m_{Higgs}^2}{m_W^2}\right)\right\}\right] . \qquad (2.9)$$

In Eq.(2.8), we can see that the mass threshold effect of heavy gauge boson make unification mass scale 2.85 times smaller than mass scale predicted in θ-function approximation.

§3. Unification mass scale and proton life time

The values of $\alpha_{em}(2m_W)$ and $\alpha_s(2m_W)$ should be determined from experimental value. Renormalization group analysis including two-loop effect tells us that "two-loop corrected" coupling constant are

$$\alpha_{em}^{-1}(2m_W) = 128.5 ,$$

are

$$\alpha_s^{-1}(2m_W) = 9.5 , \ 8.6 , \ 7.7 , \qquad (3.1)$$

for $\Lambda_{\overline{MS}} = 0.1, 0.2$ and 0.3 Gev respectively[1,3].

Putting it into Eq.(2.8) and (2.9), we get,

$$\log(M_X^2/m_W^2) \simeq \log(2.7\times10^{12})^2 + \frac{1}{3}\log\left(\frac{M_E^2}{M_G^2}\right) + \frac{1}{21}\log\left(10^{15}\text{Gev}/m_{Higgs}\right)^2 + \frac{1}{63}\log\left(10^{15}\text{Gev}/m_{10}\right)^2 , \quad (3.2)$$

and

$$\sin^2\theta_W(2m_W) = \Big[0.215 + 6\times10^{-4}\Big\{\frac{17}{6}\log(M_E^2/M^2) + \frac{7}{2}\log(M_E^2/M_G^2) + \frac{1}{9}\log(m_{Higgs}/10^{15}\text{GeV})^2\Big\} + \alpha_{em}(2m_W)\cdot\Delta\alpha_2^{-1}\Big] \Big/ \Big\{1+\alpha_{em}(2m_W)\cdot\{\Delta\alpha^{-1} \quad \alpha_2^{-1}\}\Big\} , \quad (3.3)$$

for $\Lambda_{\overline{MS}} = 0.2$ Ge V . In the derivation of Eq.(3.3) from Eq.(2.9), we have taken into account w-boson mass threshold effect and two-loop effect in desert region. $\Delta\alpha_1^{-1}$ and $\Delta\alpha_2^{-1}$ in Eq.(3.3) due to two-loop effect and given by

$$\Delta\alpha_1^{-1} = \frac{1}{4\pi}\Big\{-\frac{190}{123}\log(1-\frac{41}{24\pi}\log(M_X^2/m_W^2)\alpha_1) + \frac{18}{19}\log(1+\frac{19}{24\pi}\alpha_2\cdot\log(M_X^2/m_W^2))$$

$$+\frac{44}{21}\log(1+\frac{17}{4\pi}\alpha_3\cdot\log(M_X^2/m_W^2))\Big\} ,$$

$$\Delta\alpha_2^{-1} = \frac{1}{4\pi}\Big\{-\frac{6}{41}\log(1-\frac{41}{24\pi}\alpha_1\log(M_X^2/m_W^2)) + \frac{217}{19}\log(1+\frac{19}{24\pi}\alpha_2\log(M_X^2/m_W^2)) + \frac{26}{17}\log(1+\frac{17}{4\pi}\alpha_3\log(M_X^2/m_W^2))\Big\} . \quad (3.4)$$

Proton life time τ_P in SO(10) model is given by [3.5]

$$1/\tau_P = \sum_i 16\pi\frac{\alpha_x(2M_X)^2}{M_X^4}\left(\frac{k_i E_{Mi} E_{li}}{M_P}\right)\left[F_N(9k_i^2/16)\right]^2 \times |A|^2 \times W_i \times |\psi(0)|^2 . \quad (3.5)$$

Here A is a factor due to renormalization effect of operator.

For F_N, a hadron structure function we take as[6]

$$F_N(P) = \left[1 + P^2/0.71\,(\text{GeV})^2\right]^{-2} . \quad (3.6)$$

A squared value of proton wave function at the origin $|\psi(0)|^2$ is determined from non-leptonic hyperondecay[7],

$$|\psi(0)|^2 \simeq 1.0 \times 10^{-2}\ (\text{GeV})^3 , \quad (3.7)$$

SU(6) weight factors w_i and the phase factors, $(k_i E_{Mi} E_{li}/M_P)$ are calculated for each two-body decay mode. In the calculation of w_i we have adopted the recoil model of Kane and Karl[5].

The value of coupling constant $\alpha_x(2M_X)$ is estimated from

eq.(2.2). Eq.(3.2) is used for the estimation of the value of M_X, of course. The parameter M_E/M_G in Eq.(3.2) depends on patterns of symmetry breaking. Here we consider two cases. In one case (case A), the SO(10) breaks to $G_S = SU_C(3) \times SU_L(2) \times U_Y(1)$ through SU(5). In the other cace (case B) the SO(10) symmetry breaks to G_S via $SU(4) \times SU_L(2) \times SU_R(2)$. The important point is that the value of M_E/M_G is less than unity for case A while greater than unity for case B. The case that $M_E/M_G = 1$ corresponds to the SU(5) limit.

The life time τ_p is summarized in the Figure. As we can read from the Figure, the SU(5) limit values of τ_p and $\sin^2\theta_W$ are

$$\sin^2\theta_W = 0.220\ ,\ 0.216\ ,\ 0.214\ , \tag{3.8}$$

$$\tau_p(\text{years}) = 1.26\times10^{28},\ 2.2\times10^{29},\ 1.2\times10^{30} \tag{3.9}$$

for $\Lambda_{\overline{MS}} = 0.1, 0.2$ and 0.3 Gev, respectively. Proton life time τ_p in case A (case B) is smaller (larger) than this SU(5) limit value for any possible choice of v.e.v. of super heavy Higgs scalars.

Recent analysis gives the values of $\sin^2\theta_W$ and $\Lambda_{\overline{MS}}$ as[8]

$$\sin^2\theta_W = 0.229 \pm 0.01 \quad (p=1 \text{ fixed}), \tag{3.10}$$

and

$$\Lambda_{\overline{MS}} = 0.16\ {}^{+0.10}_{-0.08}\ \text{GeV}\ . \tag{3.11}$$

The allowed rarge of τ_p are

$$7.5\times10^{27} \le \tau_p(\text{years}) \le 5.3\times10^{29} \quad \text{for } \Lambda_{\overline{MS}} \cong 0.1\,\text{GeV},$$

$$3.0\times10^{29} \le \tau_p(\text{years}) \le 2.3\times10^{31} \quad \text{for } \Lambda_{\overline{MS}} = 0.2\,\text{GeV},$$

$$2.4\times10^{30} \le \tau_p(\text{years}) \le 2.1\times10^{32} \quad \text{for } \Lambda_{\overline{MS}} = 0.3\,\text{GeV}$$

§4. Summary and discussion

We discussed unification mass scale and proton life time using the formula derived in §2. Result for proton life time is

$$3.0\times10^{29}\ \text{years} \leq \tau_p \leq 2.3\times10^{31}\ \text{years}, \tag{4.1}$$

for $\Lambda_{\overline{MS}}=0.2\,\text{GeV}$, $m_{10}=m_{\text{Higgs}}=10^{15}\,\text{GeV}$ and $\sin^2\theta_w=0.229\pm0.01$

In this paper, we have neglected renormalization effects of gauge parameters and running mass. D.A. Ross and T. Goldman disscussed this effects and concluded that it causes ± 5% uncertainty in τ_p.

Uncertainties of Higgs masses also make the value of τ_p more indefinite. Taking into account these uncertainties altogether.

We estimate as

$$\tau_p = 2.6\times(8.8)^{\pm1}\times(6.5)^{\pm1}\times10^{30}\ \text{years}, \tag{4.1}'$$

for $10^{12}\,\text{GeV} \leq m_{\text{Higgs}}, m_{10} \leq 10^{18}\,\text{GeV}$, $\Lambda_{\overline{MS}}=0.2\,\text{GeV}$, and $\sin^2\theta_w=0.229\pm0.01$.

For the values of $m_{10} \lesssim 10^{12}\,\text{GeV}$, proton decay mediated by coloured Higgs is comparable with that mediated by gauge boson. Eq.(4.1)' cannot use in this case.

K.G.F. group reports their result of experiment[9] on proton decay as

$$\tau_p = (6-7.5)\times10^{30}\ \text{years}. \tag{4.2}$$

Mont blanc group also reports[10]

$$\tau_p = (0.8-1.6)\times10^{31}\ \text{years} \tag{4.3}$$

These result is compatible with our results.

Acknowledgements

The author would like to thank Professor Akio Hosoya for careful reading manuscript. Numerical computation was performed in the computation centre at Osaka University.

References

(1) D.A. Ross, Nucl. Phys. B140 (1978), 1.
T. Goldman and D.A. Ross, Nucl. Phys. B171 (1980), 273,
Phys. Lett. 84B (1979), 208.

(2) S. Weinberg, Phys. Lett. 91B (1980), 51.

(3) T. Matsuki and N. Yamamoto, proton life time in an SO(10) grand unified theory, KEK-TH-38, (1981).
Y. Hara, T. Matsuki and N. Yamamoto, Prog. Theor. Phys. 68 (1982), 652.

(4) L. Hall, Nucl. Phys. B178 (1981), 75.

(5) G. Kane and G. Karl, Phys. Rev. D22 (1980), 273.
J. Ellis, M. Gaillard, D. Nanopoulos and S. Rudaz, Nucl. Phys. B176 (1980) 61.

(6) Y. Hara, Prog. Theor. Phys. 68 (1982), 642.

(7) Y. Hara and K. Hikosaka, Prog Theor. Phys. 66 (1981), 2206.

(8) A.J. Buras, "Proceeding of the 1981 International Symposium on Lepton and Photon Interactions at High Energy, Bonn, Germany, August 1981."
J.E. Kim, P. Langacker, M. Levine and H.H. Williams, Rev. Mod. Phys. 53 (1981), 211.

(9) M.R. Krishnaswany et al., Phys. Lett. 115B (1982), 349.

(10) G. Battistoni et al., Phys. Lett. 118B (1982), 461.

Appendix

The functions V, S_2 and S_3 are mass dependent β-functions coming from gauge boson, Higgs scalar and fermions, respectively. They are calculated as[3],

$$V(Q^2, Q_0^2=0, M^2) = \int_0^1 dx (2+8\cdot x-8x^2) \log\left[\frac{M^2}{M^2+Q^2\cdot x(1-x)}\right]$$
$$-\int_0^1 dx \int_{-x}^{x} dy \left\{ 6 \log\left[\frac{4x\cdot M^2-(3x^2-4x+y^2)Q^2}{4x M^2}\right]\right.$$
$$-2\log\left[\frac{4(1-x)M^2-(3x^2-4x+y^2)Q^2}{4(1-x)M^2}\right]$$
$$+2\,\frac{(x^2+y^2+2x-4)Q^2}{4(1-x)M^2-(3x^2-4x+y^2)Q^2}$$
$$\left.-2\,\frac{(5x^2+x+y^2)Q^2}{4xM^2-(3x^2-4x+y^2)Q^2}\right\}, \quad \text{(A.1)}$$

$$S_2(Q^2, M^2) = \int_0^1 dx\,(1-2x)^2 \log\left[\frac{x(1-x)Q^2+M^2}{M^2}\right], \quad \text{(A.2)}$$

and

$$S_3(Q^2, M^2) = \int_0^1 dx \cdot 4x(1-x) \log\left[\frac{x(1-x)Q^2+M^2}{M^2}\right]. \quad \text{(A.3)}$$

Figure Caption

Values of the Weinberg angle, $\sin^2\theta_w$ and proton life time τ_p predicted by Eqs. (3.3) and (3.5) are plotted for $\Lambda_{\overline{MS}} = 0.1, 0.2$ and 0.3 GeV. Dotted and dashed lines corresponds to case B. The regions bounded by two solid lines are allowed for case A.

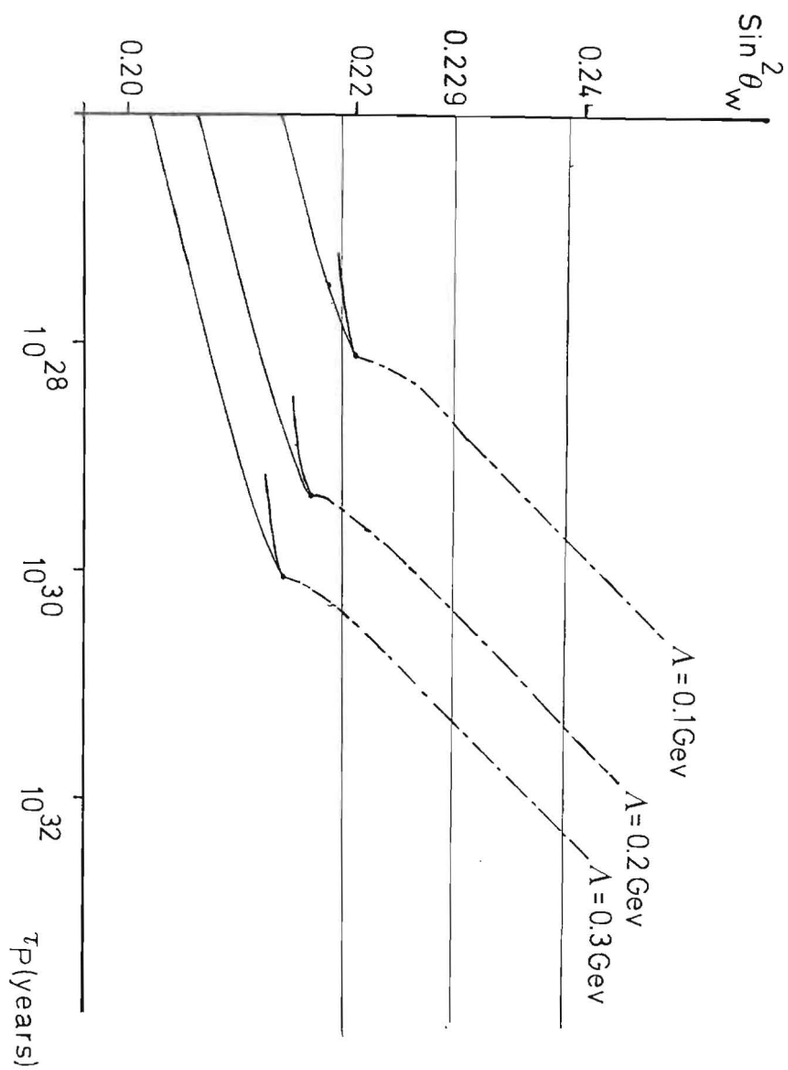

MEASUREMENT OF THE MASS OF THE ELECTRON NEUTRINO USING ELECTRON CAPTURE IN ^{163}Ho

Shinjiro Yasumi

KEK

Today I would like to talk about a measurement of the mass of the electron neutrino using electron capture in ^{163}Ho. This experiment is now being done by the following collaboration; KEK: S. Yasumi, G. Rajasekaran, M. Ando, F. Ochiai, H. Ikeda, T. Ohta and P. M. Stefan; Osaka University: M. Maruyama; T.I.T.: N. Hashimoto; Tohoku University: M. Fujioka, K. Ishii, T. Shinozuka, K. Sera, T. Omori, G. Izawa, M. Yagi and K. Masumoto; University of Tsukuba: K. Shima; Kyoto University: Y. Inagaki.

Finally I am going to make a short review on present status of these studies (m_{ν_e} measurement using electron capture in the nucleus) in the world, together with our future plans.

§1. Introduction

To determine the mass of the (anti) electron neutrino, measurements of the β-ray spectrum of tritium have long been studied so far[1,2,3].

A. De Rújula[4] of CERN proposed a new way to measure the electron neutrino mass using the radiative electron capture decay process of the nucleus. This method is essentially based on the three body phase space as same as in the case of the tritium β-ray measurement, however, it is claimed this approach has a great advantage that complicated atomic and molecular interplays hardly exist in this case[4]. One problem to be solved seems to be a statistics. For some nuclide, however, one can

expect the resonant enhancement in IBEC (Internal Bremsstrahlung in Electron Capture)[5,4]. CERN group is doing experiments[6,7,8] based on this proposal[4].

Bennett et al.[9,10] are trying to use non-radiative electron capture to evaluate the electron neutrino mass.

We are doing an experiment[11] to determine the electron neutrino mass using electron capture in ^{163}Ho. At the beginning of the present study there were only contradictory data[4,12] on the Q-value and half life of ^{163}Ho which are closely relevant to the neutrino mass measurement, then we tried to estimate these two quantities from the intensities of M X-rays from ^{163}Ho and the total number of ^{163}Ho in the source.

§2. Preparation of the ^{163}Ho sources

Holmium - 163 nuclei were produced with the ^{164}Dy (p, 2n) reaction. An irradiation on a ^{164}Dy metal target* with 20 MeV protons was made for 24.1 hours with an average current of 100 μA using the AVF cyclotron of the Cyclotron and Radioisotope Center, Tohoku University. The energy of incident protons (20 MeV) and the thickness of the ^{164}Dy metal target were chosen so as to effectively integrate a large area under the (p, 2n) excitation curve, which was calculated using the code ALICE 81[13].

After the irradiation, elaborate chemical separation processes[14] were followed. Finally four ^{163}Ho sources were prepared by electroplating onto a nickel foil in a 0.5 M ammonium lactate solution. Each source is 3 mm in diameter. An example of the γ-ray spectrum from one of the ^{163}Ho sources is given in Fig. 1, showing that, except ^{88}Y, the contaminant radioisotopes were completely removed from the source. Among four

* We are indebted to Mr. I. Sugai of the Institute for Neclear Study, University of Tokyo, for preparing the ^{164}Dy metal plates.

sources, source No. 3 was the most intense and was used for the photon spectrum measurement, while the others were used subsidiarily.

§3. Total number of ^{163}Ho atoms in the source

We estimated the total number of ^{163}Ho atoms in source No. 3 using the PIXE (Particle Induced X-ray Emission) method in the following way: Another ^{163}Ho source (No. 4) whose intensity of M X-rays was already measured, and a reference holmium foil whose dimensions are the same as the ^{163}Ho source and whose weight is known, were irradiated with 38 MeV protons under the same beam condition. The Ho K X-ray spectra from these two samples are shown in Fig. 2. By comparing the Ho K X-ray intensities of these two samples, and using the ratio of M X-ray intensities of the two ^{163}Ho sources (No. 3 and No. 4), the total weight of ^{163}Ho atoms in source No. 3 was estimated to be (2.37 ± 0.70) μg. Thus, we concluded that the total number of ^{163}Ho atoms in the source is (0.88 ± 0.26) × 10^{16}.

§4. Photon spectrum measurement

The photon spectrum from the ^{163}Ho source (No. 3) was measured with a Si(Li) detector* having a beryllium window 0.3 mil thick. The geometry of the Si(Li) detector was carefully measured with a traveling microscope and several radioactive sources[15]. The thickness of the gold layer on the surface of the silicon crystal was also measured by counting Au-L_α X-rays activated with Rb-K_α X-rays[16]. The measurements were performed both in an air atmosphere and in vacuum. In the latter, the ^{163}Ho source was placed in a vacuum box surrounding the Si(Li) detector as

* purchased from EG & G ORTEC

shown in Fig. 3. Both measurements are in good agreement with each other within experimental uncertainties. A spectrum thus obtained in vacuum, is shown in Fig. 3. After corrections for the detection efficiency, the solid angle and the self-absorption factor for X-rays within the source itself, intensities of the Dy M X-rays emitted from the source were determined as indicated in Table 1.

Using the total number of ^{163}Ho atoms in the source (§3), we can get the M X-ray intensities per atom per 4π steradians for each X-ray peak, as given in the last column of Table 1.

§5. Q-value and the half life of ^{163}Ho

Summing up the M X-ray intensities in the last column of Table 1, we obtain the total intensity of M X-rays per atom of (4.7 ± 1.5) × 10^{-15} photons per 4π steradians per second. If we assume that the average M-fluorescence yield for the dysprosium atom is 0.98%[17], the partial M-capture half life of ^{163}Ho is estimated to be $T^M_{1/2}$ = (4.5 ± 1.5) × 10^4 y. This is in good agreement with CERN's value[7] of (4.0 ± 1.2) × 10^4 y. It should be noted that this agreement is remarkable, considering that these two values were determined under rather different experimental procedures.

Using the value of $T^M_{1/2}$, a useful relation between the Q-value of ^{163}Ho and the mass of the electron neutrino can be deduced as follows: At first we evaluate the nuclear matrix element relevant to the transition ^{163}Ho → ^{163}Dy. Following the CERN group[8], we estimate it to be 5.1% in terms of the log ft value, by taking into account the experimental log ft value of ^{161}Ho and the ratio of the pairing correction factors for ^{161}Ho and ^{163}Ho. From $T^M_{1/2}$ and the matrix element thus obtained, a relation between the Q-value and m_{ν_e} was obtained as shown

in Fig. 4. In this relation, the following data are used: The M_1 and M_2 electron binding energies in dysprosium are 2.047 keV and 1.841 keV, respectively. Electronic wave functions at the origin are calculated by Mann and Waber[18]. Exchange and overlap correction factors are tabulated in a review article by Bambynek et al.[19].

From Fig. 4 we get Q = 2.45 ± 0.08 keV for $m_{\nu_e} = 0$. If we use the upper limit of the Q-value measured by the CERN group[7], we get an upper limit on the mass of the electron neutrino of 1.25 keV. If we adopt 2.45 keV as the Q-value of ^{163}Ho, the half life is estimated to be $(6 \pm 2) \times 10^3$ y.

§6. Feasibility of the electron neutrino mass measurement using an IBEC spectrum in ^{163}Ho

Now we proceed to evaluate the intensity of a part of an internal bremsstrahlung spectrum, G, which is really relevant to the determination of the mass of the electron neutrino;

$$G \equiv \int_{k_{max}-m_{\nu_e}}^{k_{max}} \left(\frac{d\omega}{dk}\right)_{I.B.} dk \quad .$$

It seems convenient that G is defined in terms of its ratio to the total decay rate, as same as in the case of tritium β-ray spectrum. G may be called a figure of merit of the experiment[4].

Using Q-value as determined in this experiment, G values were calculated in the following:

$G = 5 \times 10^{-11}$ for $4\,P_{3/2}$,

and

$G = 8 \times 10^{-11}$ for $5\,P_{1/2,\,3/2}$,

where Q = 2.45 keV is used and m_{ν_e} is assumed to be 50 eV.

These figures suggest that the IBEC approach to estimate the electron neutrino mass is almost hopeless, unless some considerable innovations can be achieved.

§7. Short review of the studies in the world and our future plans

Summarized in Table 2 is the present status of the studies aiming at the electron neutrino mass determination (not including measurements on the mass of the anti electron neutrino). Here I am not going to describe each in detail. Readers who would like to know about it, are invited to refer the original papers.

I 'd like to add a few comments: (1) No one has succeeded in determining the electron neutrino mass from IBEC in ^{163}Ho. (2) Far from that, no one has observed an IBEC in ^{163}Ho. (We are now working on it). (3) If Q-value of ^{163}Ho is determined independently, such a m_{ν_e} vs Q - relation as Fig. 4 combined with the Q-value gives m_{ν_e}. This approach has already been taken by the CERN group. For it, CERN group[6,7,8] measured the Q-value of ^{163}Ho using two nuclear reactions related to it.

We are now trying to improve the m_{ν_e} vs Q - relation (Fig. 4) by reducing experimental uncertainties both in the PIXE measurement and in the M X-ray measurement. Using an improved relation together with Q-value which we are going to measure using a nuclear reaction different from CERN's, it is expected to obtain a new result on m_{ν_e} in the near future.

On the other hand, we are planning an experiment which hopefully reduces atomic physics uncertainties on dysprosium atom using a monochromatic X-ray from the 2.5 GeV Electron Storage Ring in our "Photon Factory" (Synchrotron Radiation Facility in KEK). If this will be achieved, such a non-radiative electron capture approach as Bennett et al.[9,10] may be brought to life.

References

1) K.E. Bergkvist: Nucl. Phys., B39(1972) 317.

2) V.A. Lubimov et al.: Phys. Lett., 94B(1980) 266.

3) J.J. Simpson: Phys. Rev., D23(1981) 649.

4) A. De Rújula: Nucl. Phys., B188(1981) 414.

5) R.J. Glauber and P.C. Martin: Phys. Rev., 104(1956) 158.

6) J.U. Andersen et al.: CERN/PSCC/82-7, April 1, 1982.

7) J.U. Andersen et al.: Phys. Lett., 113B(1982) 72.

8) B. Jonson et al.: CERN-EP/82-142, 7 September 1982.

9) C.L. Bennett et al.: Phys. Lett., 107B(1981) 19.

10) C.L. Bennett: Proc. 17th Rencontre de Moriond Les Arcs-Savoie-France, March 14-26, 1982, p. 413.

11) S. Yasumi et al.: KEK Preprint 82-25, November 1982, E; also, to be published in Physics Letters B.

12) C.M. Lederer and V.S. Shirley: Table of Isotopes, 7th Edition, John Wiley and Sons (1978).

13) M. Blan: Private communication (1981); see also, Ann. Rev. Nucl. Sci., 25(1975) 123.

14) S. Yasumi et al.: Proc. Int. Conf. Neutrino '82, 14-19 June, 1982, Balatonfüred, Hungary, Vol. 1, p. 59.

15) K. Shima: Nucl. Instrum. Meth., 165(1979) 21.

16) K. Shima et al.: J. Appl. Phys., 51(1981) 846.

17) W. Bambynek et al.: Rev. Mod. Phys., 44(1972) 716.

18) J. B. Mann and J.T. Waber: At. Data., 5(1973) 201.

19) W. Bambynek et al.: Rev. Mod. Phys., 49(1977) 77.

20) A. De Rújula and M. Lusignoli: Ref. TH. 3300-CERN, 12 May 1982.

21) A. De Rújula and M. Lusignoli: Ref. TH. 3377-CERN, 2 August 1982.

22) A. De Rújula: Ref. TH. 3322-CERN, 7 June 1982.

23) A. De Rújula and M. Lusignoli: Ref. TH. 3444-CERN, 15 October 1982.

24) E. Beck and H. Daniel: Z. Phys., 216(1968) 229.

Table 1. Intensity of Dy M X-rays from ^{163}Ho atom

X-ray	$e^{-\mu_{Be}\ell_{Be}}$	$e^{-\mu_{Au}\ell_{Au}}$	$e^{-\mu_{Si}\ell_{Si}}$	As	Intensity (photons per sec.)	Intensity (photons per atom per sec.) $\times 10^{16}$
$M_1O_{2,3}$	0.90 ±0.02	0.96 ±0.01	0.93 ±0.01	0.92	0.75 ±0.14	0.86 ±0.31
M_2N_4 $M_1N_{2,3}$	0.85 ±0.02	0.94 ±0.01	0.99 ±0.01	0.90	5.94 ±0.80	6.79 ±2.24
$M_3N_{4,5}$	0.78 ±0.02	0.92 ±0.01	0.99 ±0.01	0.87	4.29 ±0.74	4.90 ±1.67
M_3O_3 $M_5N_{6,7}$ $M_2O_{2,3}$ M_4N_6	0.67 ±0.02	0.88 ±0.01	0.98 ±0.01	0.95	27.4 ±3.3	31.3 ±10.0
M_4N_2 M_5N_3	0.42 ±0.04	0.82 ±0.01	0.96 ±0.01	0.92	3.18 ±0.87	3.63 ±1.45

Remarks:
(1) "As" denotes the correction factor for the self-absorption of the source.
(2) Escape correction factors are 0.98 for $M_1O_{2,3}$ and unity for the others.

Table 2. Present status of the electron neutrino mass measurements

Photon and/or Electron	Proposal	Experiment	Detector or method	Result and Comment
Photon (Singles)		CERN[6,7,8]	Prop. counter	$T^{M}_{1/2}=4.0\times10^{4}$y, Q=2.58keV $T_{1/2}=7\times10^{3}$y, $m_{\nu_e}\leq1.3$ keV, N^{e}_{tot} by RBS+FC
		Princeton et al.[9]	Si	Q>2.1 keV
		KEK-TOHOKU[11] et al.	Si	$T^{M}_{1/2}=4.5\times10^{4}$y, Q=2.45keV $T_{1/2}=6\times10^{3}$y, $m_{\nu_e}\leq1.25$ keV, N^{e}_{tot} by PIXE
Electrons (Singles)		CERN[6,7,8]	MWPC Prop. counter	This measurement was done together with the experiment in the uppermost line in this table by CERN group[6,7,8].
	De Rújula[23]			
Photon-Electron (Coin.)	De Rújula[4]	CERN[6] (planning)	New device[6]	
Photon-Photon (Coin.)		CERN[6,8,22] (^{193}Pt)	Ge+($^{Si}_{NaI}$) (Coin.)	Validity of IBEC theory has been proved. $m_{\nu_e}<500$ eV from IBEC.
Electron-Electron (Coin.)	De Rújula[20] (EEEC)			
Photon+Electron (Calorimetric)	De Rújula[21]	CERN (planning)	Implantation (?)	
		KEK-TOHOKU et al. (thinking)		

Remarks:

(1) In the case where it is not specified, an electron capturing nuclide used in an experiment is ^{163}Ho.
(2) Princeton group estimated the half life of ^{163}Ho to be about 7000 years by measuring the build-up rate of ^{163}Dy from their ^{163}Ho source[10].
(3) A m_{ν_e} measurement using a positron emitter was done by Beck and Daniel, who oblained an upper limit of m_{ν_e} of 4.1 keV[24].
(4) The following abbreviations are used in the Table;

Prop. counter	:	Proportional counter,
MWPC	:	Multiwire proportional chamber,
Ge	:	Intrinsic germanium solid detector,
NaI	:	Sodium iodide crystal,
N_{tot}	:	Total number of ^{163}Ho in a source,
RBS	:	Rutherford back scattering,
FC	:	Faraday cup in a mass separator,
Coin.	:	Coincidence,
Si	:	Si(Li)-SSD.

Figure captions

Fig. 1 Gamma ray spectrum of a ^{163}Ho source (No.3). NB indicates natural background radiations, and CPS means counts per second.

Fig. 2 PIXE measurement of the total number of ^{163}Ho atoms in source No.4 in comparison with that of a reference Ho foil. The total count of the $K_{\alpha_1} + K_{\alpha_2}$ intensity of source No.4 indicated in the figure is the result of a least-squares fit using the shape of combined $K_{\alpha_1} + K_{\alpha_2}$ peak of the reference Ho foil assuming a quadratic background. The chi-squares divided by the number of degrees of freedom is also indicated. It is noted that the present result is consistent with the count obtained by an analysis assuming independent intensities of K_{α_1} and K_{α_2} peaks.

Fig. 3 Photon spectrum from ^{163}Ho measured in vacuum. The setup of the measurement is also shown in the figure. Measured effective area and nominal thickness of the Si(Li) detector are 10.5 ± 0.6 mm^2 and 4.28 mm, respectively. Source-detector distance was 9.87 ± 0.10 mm.

Fig. 4 A relation between the Q-value of ^{163}Ho and the mass of the electron neutrino. The hatched region corresponds to the experimental uncertainty. An upper limit on the Q-value measured in CERN [7] indicated in the figure is 3.30 keV, which corresponds to m_{ν_e} of 1.25 keV. For $m_{\nu_e} = 0$, the curve gives Q = 2.45 ± 0.08 keV. The electron binding energy in the M_1 shell of Dy atom, 2.047 keV, is also shown.

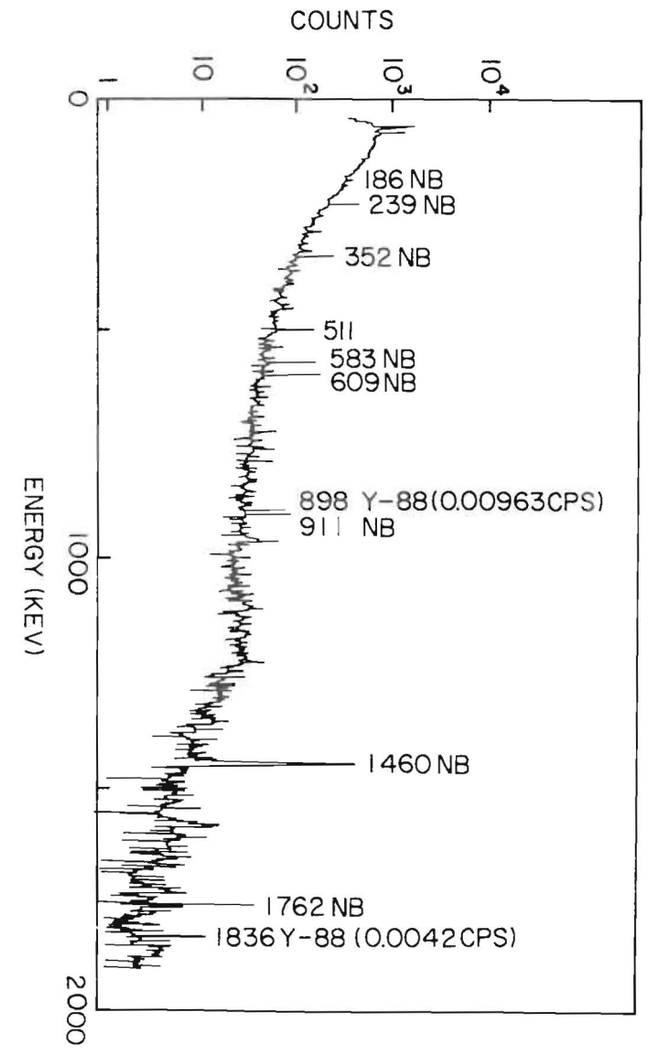

Fig. 1

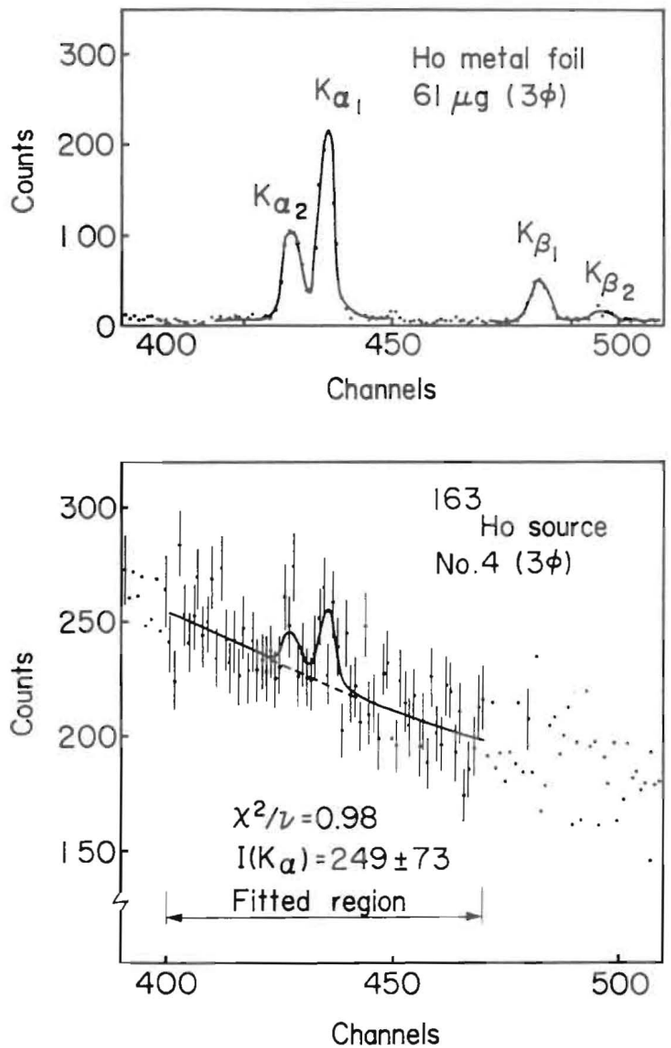
Ho metal foil
61 μg (3φ)
Kα1
Kα2
Kβ1
Kβ2
Counts
Channels
163
Ho source
No.4 (3φ)
χ²/ν=0.98
I(Kα)=249±73
Fitted region

Fig. 2

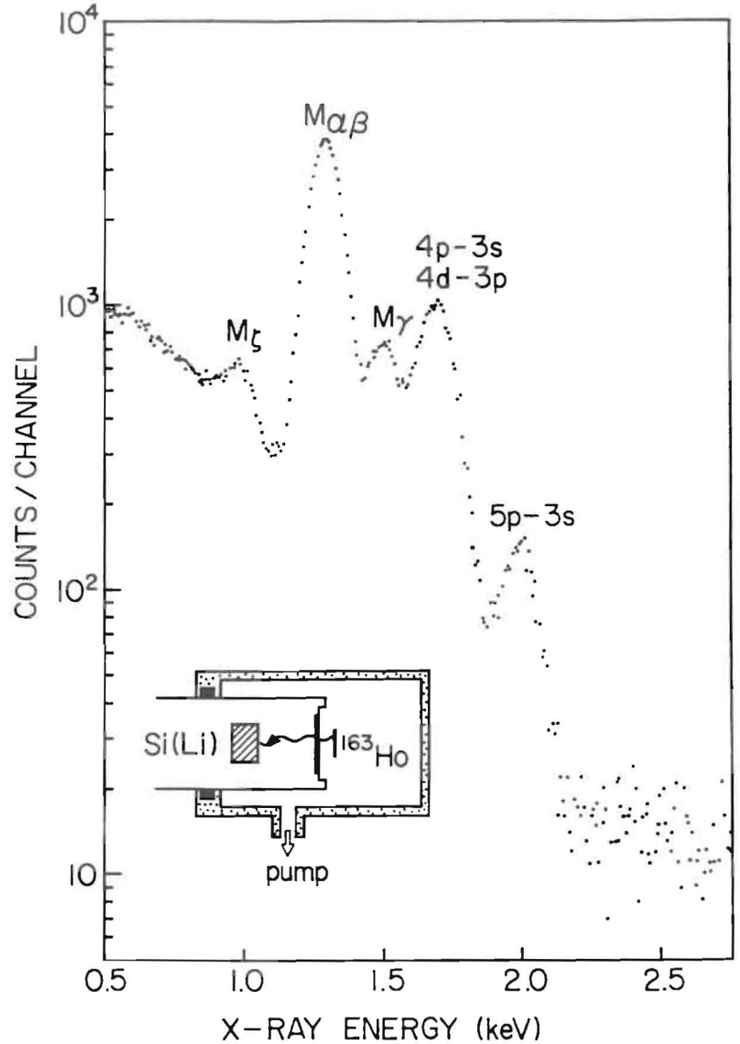
Mαβ
4p-3s
4d-3p
Mγ
Mζ
5p-3s
Si(Li)
163Ho
pump
COUNTS / CHANNEL
X-RAY ENERGY (keV)

Fig. 3

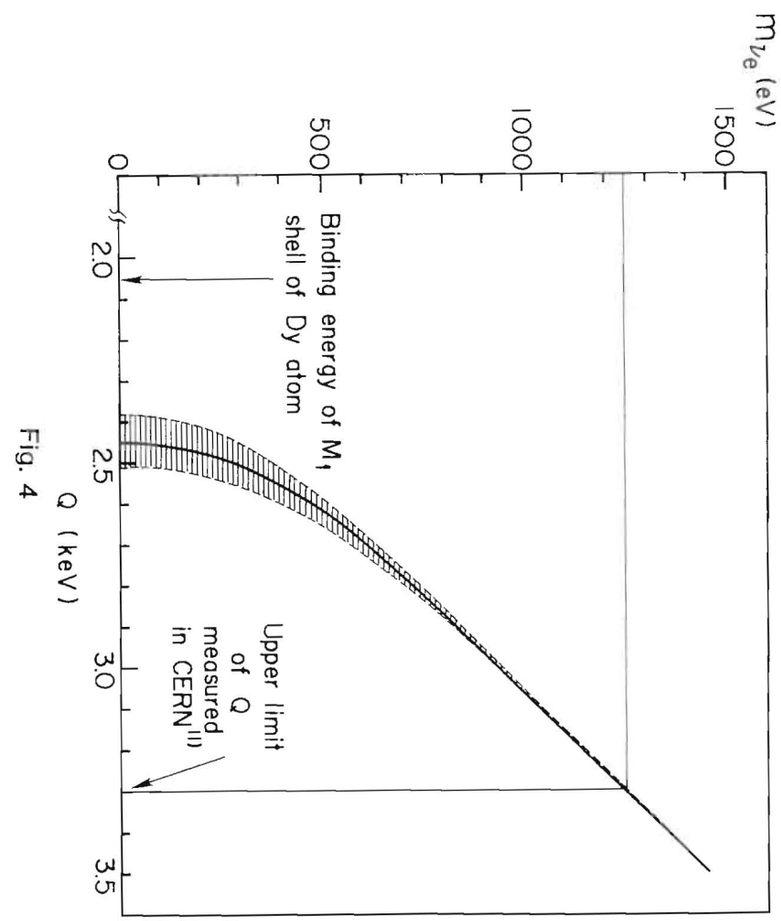

Fig. 4

Neutrino Oscillation*

Osaka University Y. Nagashima

Outline of Talk

1. Introduction
2. Present Status
3. Expected Results in the Near Future
4. How far can we go ?

1. Introduction

Within the frame work of the standard Glashow-Weinberg-Salam SU(2)×U(1) theory of electroweak interaction, all neutrinos are assumed to have zero mass. Here the absence of righthanded neutrinos and strict conservation of lepton number were the two necessary conditions. The advent of grand unified theories have made it more plausible to have massive neutrinos because of quark-lepton mixing and its resultant lepton number nonconservation. There are also cosmological arguments in favor of massive neutrinos.

Oscillations[1] can take place when not all the neutrinos are mass degenerate and when transitions exist between different species of neutrinos. Different species can either mean different lepton number or different flavor. The mixing between ν_e and $\bar{\nu}_e$, ν_μ and $\bar{\nu}_\mu$ are known[2] to be less than 3×10^{-4} from absence of nuclear double beta decay and production

---

* Invited talk at Conference on Monopoles and Grand Unified Theories held at Kamioka in Gifu, October 18-20, 1982

of μ^+ by high energy ν_μ's. In the following we only discuss oscillations by flavor mixing.

When neutrino mass eigenstates $|\nu_i\rangle$, i=1, 2··· are non-degenerate, they generally differ from flavor eigenstates $|\nu_\alpha\rangle$, α=e, μ, τ···· of the weak interaction. The latter are expressed in terms of the former as

$$|\nu_\alpha\rangle = \sum_i U_{\alpha i}|\nu_i\rangle \tag{1}$$

without much loss of generality, we can confine ourselves to the case of two neutrinos. Then

$$|\nu_e\rangle = \cos\alpha|\nu_1\rangle + \sin\alpha|\nu_2\rangle \tag{2a}$$

$$|\nu_\mu\rangle = -\sin\alpha|\nu_1\rangle + \cos\alpha|\nu_2\rangle \tag{2b}$$

Time evolution of mass eigenstates is described by

$$|\nu_i(t)\rangle = |\nu_i(0)\rangle\exp(-iE_it) \tag{3a}$$

$$E_i = \sqrt{p^2+m_i^2} \simeq p+\frac{m_i^2}{2p} \tag{3b}$$

Simple algebra gives

$$P(\nu_\mu\to\nu_e) = |\langle\nu_e(0)|\nu_\mu(t)\rangle|^2$$

$$= \frac{1}{2}\sin^2 2\alpha[1-\cos(E_1-E_2)t] \tag{5a}$$

$$(E_1-E_2)t \simeq \frac{m_1^2-m_2^2}{2}\cdot\frac{t}{E_\nu} \simeq 2\pi\frac{L}{\lambda} \tag{5b}$$

where L=ct is the distance the neutrino travelled and the oscillation length λ is defined by

$$\lambda = \frac{4\pi\hbar E_\nu}{(m_1^2-m_2^2)c^3} = 2.5\,\frac{E_\nu(\text{MeV})}{\delta m^2(eV^2)}\ \text{in m} \tag{5c}$$

Consequently we obtain

$$P(\nu_\mu\to\nu_e) = \sin^2 2\alpha\cdot\sin^2\left(\frac{1.27\delta m^2 L}{E_\nu}\right) \tag{6a}$$

$$P(\nu_\mu\to\nu_\mu) = 1-P(\nu_\mu\to\nu_e) \tag{6b}$$

To illustrate the magnitude of λ, we give a few examples for $\delta m^2 \simeq 1eV^2$

$$\lambda = \begin{cases} 10\ \text{m} : E_\nu = 4\ \text{MeV} \\ 100\ \text{m} : E_\nu = 400\ \text{MeV} \\ 1000\ \text{m} : E_\nu = 4\ \text{GeV} \end{cases} \tag{7}$$

From the above description we see two distinct types of experiment exist, the so called appearance type where we measure $P(\nu_\alpha\to\nu_\beta)$ and disappearance or survival type where we measure $P(\nu_\alpha\to\nu_\alpha)$. The former is in principle more accurate because we detect appearance of a characteristic signal which did not exist originally. However, in terms of physics interpretation, the latter is more general because in principle we are able to detect the oscillation effect regardless of mixing scheme mentioned previously or number of neutrino types. It is also more difficult to do because we are measuring a small difference from unity in case of small oscillation effect.

In extracting meaningful results we distinguish three different regions of L.

(1) Long wave or low mass limit: $L<<\lambda$

In this region eq. (6a) is approximated by

$$P(\nu_\mu \to \nu_e) = \sin^2 2\alpha \cdot (1.27 \frac{\delta m^2 L}{E_\nu})^2 \quad (8a)$$

or

$$\sin 2\alpha \cdot \delta m^2 = \frac{1}{1.27} \frac{E_\nu}{L} P(\nu_\mu \to \nu_e)^{\frac{1}{2}} \quad (8b)$$

If no oscillations are observed, we only obtain a combined upper limit on the mixing angle and mass difference

$$\sin 2\alpha \cdot \delta m^2 < \frac{1}{1.27} \frac{E_\nu}{L} \sqrt{\epsilon} \quad (9)$$

where ϵ is the experimental error. From the expression (9) one observes an obvious advantage of low energy neutrino facilities.

(2) Optimum oscillation region: $L \approx \lambda$

Here we observe $P(\nu_\mu \to \nu_e)$ varying as a function of either distance L or energy E_ν. $P(\nu_\mu \to \nu_\mu)$ will also be reduced from unity considerably.

(3) Short wave or large δm^2 limit: $L \gg \lambda$

Here the neutrino oscillates violently and only the time average of the oscillation is observed.

Consequently

$$P(\nu_\mu \to \nu_e) = \frac{1}{2}\sin^2 2\alpha \leq \frac{1}{2} \quad (10a)$$

$$P(\nu_\mu \to \nu_\mu) = 1 - \frac{1}{2}\sin^2 2\alpha \geq \frac{1}{2} \quad (10b)$$

If there are no observable effects, we again obtain an upper limit

$$\sin^2 2\alpha < 2\epsilon \quad (11)$$

From the eq. 10, 11 we see the determination of the mixing

angle does not depend explicitly on the neutrino energy or the distance and hence they are not critical factors in determining accurate values of $\sin^2 2\alpha$.

If there are N>2 types of neutrinos, the oscillation pattern becomes more complex, but the essential features of the above discussions are maintained with slight modification of 10a, b to

$$P(\nu_\alpha \to \nu_\beta) \leq \frac{1}{N} \quad (12a)$$

$$P(\nu_\alpha \to \nu_\alpha) \geq \frac{1}{N} \quad (12b)$$

The situation is illustrated pictorially in Fig. 1.

There are several hints[2],[3] on possible existence of oscillations, none of them, however, are conclusive.

2. Present status

The best limit in δm^2 exists in the disappearance experiment $\bar{\nu}_e \to x$. A recent reactor experiment[4] at Gösgen using liquid scintillators and He^3 multi-wire proportional chambers measured the reaction

$$\bar{\nu}_e + p \to e^+ + n \quad (13)$$

and compared with the expected $\bar{\nu}_e$ spectrum obtained from the measurement of β-spectrum. The data are taken in L/E_ν range from 5 to 15 m/MeV. No oscillation effects were observed and the limits are

$$(\bar{\nu}_e \to \bar{\nu}_e) \qquad \delta m^2 < 0.016 \text{ eV}^2 \quad (14)$$
$$\sin^2 2\alpha < 0.7$$

The results are presented in Fig. 2. Also shown is the positive result claimed by Reines et al[5], together with Soni-Silverman's analysis of combined reactor data prior to the present result. The two experiments seem incompatible to each other.

When we overview accelerator experiments, the appearance reaction $(\bar{\nu})_\mu \to (\bar{\nu})_e$ is the most repeated process of all. The current best limit is given by BNL-Col. group[7]

$$(\nu_\mu \to \nu_e) \qquad \delta m^2 < .6 \text{ eV}^2 \qquad (15)$$
$$\sin^2 2\alpha < .006$$

done at FNAL using 15' bubble chamber. Limits of other reactions are

$$\bar{\nu}_\mu \to \bar{\nu}_e \qquad \delta m^2 < .91^{(8)} \qquad (16)$$
$$\sin^2 2\alpha < .01^{(9)}$$

$$\nu_e \to \nu_e \qquad \delta m^2 < 2.5^{(7)(10)} \qquad (17)$$
$$\sin^2 2\alpha < 0.7$$

$$\nu_\mu \to \nu_\tau \qquad \delta m^2 < 3.0^{(11)} \qquad (18)$$
$$\sin^2 2\alpha < 0.013$$

$$\bar{\nu}_\mu \to \bar{\nu}_\tau \qquad \delta m^2 < 2.2^{(12)} \qquad (19)$$
$$\sin^2 2\alpha < 0.044$$

CFRR group at FNAL reported[13] consistently higher ν and $\bar{\nu}$ total cross sections than those from other groups and also from their own old data. Their results could be interpreted as the oscillation effects, however the same data were used to derive limits on $\bar{\nu}_\mu \to x$ assuming no oscillation.

$$(\bar{\nu}_\mu \to \bar{\nu}_\mu) \qquad \sin^2 2\alpha < 0.1 \qquad (20)$$
$$\delta m^2 = 25\text{-}250 \text{ eV}^2$$

In summary, although there had been some indications of possible neutrino oscillations, subsequent experimental results at reactors and accelerators have not confirmed them.

3. Results expected in the near future

3-1) E775(BNL-Brown-KEK-OSAKA-PENN.-SUNY-TOKYO(INS)

Using a narrow band beam at BNL and the existing E734 detector which was originally constructed and used to measure $(\bar{\nu})_\mu e \to (\bar{\nu})_\mu e$ scattering, we plan to look for signatures

$$\nu_e + n \to e^- + P \qquad (21)$$
$$\nu_\mu + n \to \mu^- + P$$

to measure appearance reaction $\nu_\mu \to \nu_e$. The detector consists of 128 modules of liquid scintillator and proportional drift tubes (PDT) followed by a gamma catcher consisting of lead-scintillator sandwiches. The detector mass is 200 tons altogether, containing over 90 % active volume. It measures the electron energy with ~ 15 % resolution and has a capability of separating π rays from electrons and of identifying various topologies of background reactions. The critical limit in experimental error comes from the ν_e contamination in the dominant ν_μ beam, estimated to be $\sim 5\times10^{-4}$. The detector is located at L=110 m and the optimum neutrino energy to measure the mixing angle

limit is estimated ~ 7 GeV/c. It is scheduled to run in late fall in 1982. The expected limit is

$$(\nu_\mu \to \nu_e) \qquad \sin^2 2\alpha \lesssim 1.3\times 10^{-3} \tag{22}$$

3-2) E776 (BNL-COL-ILL-JH-NRL)

They plan to build a new detector of 175 fiducial tons at the site 850 m downstream of E775. The signatures are electromagnetic showers and muon tracks. Using the narrow band beam they expect to obtain

$$(\nu_\mu \to \nu_e) \qquad \delta m^2 \lesssim 0.3 \text{ eV}^2 \tag{23}$$
$$\sin^2 2\alpha \lesssim 0.2$$

3-3) Phase II of E775 and E776 (Not approved yet)

E775 plans to split existing detector into two and take one half to 850 m downstream of the present location (Fig. 3). Measuring the ν_μ fluxes at two different locations $L=L_1$ and L_2 with wide band beam, the ratio R becomes

$$R \equiv \frac{N_\mu(L_1)}{N_\mu(L_2)} = 1-K(E_\nu)\sin^2 2\alpha \tag{24a}$$

$$K(E_\nu) = \frac{\sin(\pi D/\lambda)}{(\pi D/\lambda)}\left(\sin\left[1.27\frac{\delta m^2}{E_\nu}(L_1-L_2)\right]\sin\left[1.27\frac{\delta m^2}{E_\nu}(L_1+L_2)\right]\right) \tag{24b}$$

The first factor comes from finite decay region (length D). Fig. 4 shows expected behavior for $\delta m^2=1$ eV^2 as a function of neutrino energy. Expected errors when there are no oscillations are also given. We expect to obtain

$$(\nu_\mu \to \nu_\mu) \qquad \delta m^2 < 0.09 \text{ eV}^2 \tag{25}$$
$$\sin^2 2\alpha < 0.08$$

E776 plans to increase the size of the phase I detector to 350 tons, build a second detector of 40 tons and place it at L=300 m. Using narrow band beam they expect to obtain

$$(\nu_\mu \to \nu_\mu) \qquad \delta m^2 < 0.3 \tag{26}$$
$$\sin^2 2\alpha < 0.09$$

3-4) Experiments at CERN[14]

Three oscillation experiments using the existing SPS neutrino detectors CDHS, CHARM and BEBC, and a new low energy PS beam at L=900 m are planned (Fig. 5). CDHS and CHARM introduce new second detectors (roughly 30 % of the big detector) at L=140 m and measure differences of ν_μ flux. Both expected limits are similar, giving

$$(\nu_\mu \to \nu_\mu) \qquad \delta m^2 \lesssim .25 \tag{27}$$
$$\sin^2 2\alpha \lesssim .12$$

BEBC plans to observe appearance of $\nu_\mu \to \nu_e$ using one detector and expects to obtain

$$(\nu_\mu \to \nu_e) \qquad \delta m^2 \lesssim .1 \tag{28}$$
$$\sin^2 2\alpha \lesssim .02$$

3-5) Experiment at LAMPF

E645 by ANL-CIT-LAMPF-OS uses sandwich of water (light or heavy) čerenkov counter and PDT modules. The detector is movable. The signatures are

$$\nu_e + n \rightarrow e^- + P \qquad \text{(Heavy Water)} \qquad (29)$$
$$\bar{\nu}_e + P \rightarrow e^+ + n \qquad \text{(Light Water)}$$

They expect to obtain

$$(\nu_e \rightarrow \nu_e) \qquad \delta m^2 \lesssim 0.3 \text{ eV}^2 \qquad (30)$$
$$(\bar{\nu}_\mu \rightarrow \bar{\nu}_e) \qquad \delta m^2 \leq 0.06 \text{ eV}^2 \qquad (31)$$
$$\sin^2 2\alpha \leq 0.008$$

We summarize present status of the world results and expected future results in Fig. 6 and Fig. 7.

4) How far can we go ?

The factor E/L in obtaining δm^2 limits favors low energy accelerators like LAMPF and BNL AGS. How far we can push the limit is a combined function of accelerator beam intensity, neutrino flux produced, neutrino energy, the size of the detector and how far we can go in the distance. I quote here one example of estimates made by our colleague[16] and plot it on the same graph to illustrate the extent of region we might search in the long future.

As long as we stick to artificial neutrino beams, there is a natural boundary in L hence in E/L. Therefore we do not expect to go much beyond the lines designated as future in Figs. 6 and 7. One way to overcome this difficulty is to use natural neutrino sources. Huge proton detectors currently under construction here at Kamioka Mine and at Utah in the U.S. could also be used to detect cosmic ν_μ and ν_e fluxes. Measurement of up down asymmetry is essentially equivalent to two detector oscillation experiment, one located near at the earth

surface, the other on the other side of the earth at $L \simeq 10^4$ kilometers. Here the difficulty is counting statistics and it may take over a year or two to produce meeningful results. Assuming containment of secondary products by neutrinos within the detector size, the neutrino energy is $\lesssim$ 2 GeV and we can obtain $L/E \sim 10^{-4}$ and in principle similar number on δm^2 limit.

Probably the ultimate oscillation limit will be given by the detection of the solar neutrino. The limit we could reach is

$$\delta m^2 \simeq E/L \simeq \frac{1 \text{ MeV}}{10^{11} \text{m}} \simeq 10^{-11} \qquad (32)$$

We give in table 1 orders of expected δm^2 limits in several different facilites.

The author is grataful for Professor R. Lanou for providing him useful materials.

References

(1) B. Pontecorvo, JETP 33 (1957) 549
Z. Maki, M. Nakagawa, S. Sakato, Prog. Theor. Phys. 28 (1962) 870

(2) C. Baltay, ν-81 II_p 295

(3) P.H. Frampton, P. Vogel, Phys. Reports 82 (1982) 339

(4) R.L. Mössbauer, ν82

(5) F. Reines et al, Phys. Rev. Lett. 45 (1980) 1307

(6) D. Silverman, A. Soni, Phys. Rev. Lett. 46 (1981) 467

(7) N. Baker et al, Phys. Rev. Lett. 47 (1981) 1576

(8) P. Nemethy et al, Phys. Rev. D23 (1981) 262

(9) FNAL/Hawaii/UCB Preprint (1982)

(10) S. Willis et al, Phys. Rev. Lett. 44 (1980) 522 and Errata 45 (1980) 1370

(11) N. Ushida et al, Phys. Rev. Lett. 47 (1981) 1694

(12) A. Astratyan et al, Phys. Lett. 105B (1981) 301

(13) M. Shaevitz, ν81

(14) H. Wachsmuth, ν82

(15) H. Chen, ν81, II_p 183

(16) R. Lanou, D.P.F. Work Shop on future of High Energy Physics and Facilities, 1982

Table 1. Fundamental limits of oscillation experiments.

Source	E_ν (MeV)	L (m)	E/L	δm^2 $(eV)^2$
HE Acc.	10^4-10^5	10^3-10^4	1-10	0.1-1
LE Acc.	10^2-10^3	10^2-10^3	.1-1	10^{-1}-10^{-2}
LAMPF	10-100	10-10^3	10^{-2}-1	10^{-1}-10^{-3}
REACTOR	2-8	10-10^2	10^{-2}-1	10^{-1}-10^{-3}
DEEP MINE	2×10^3	10^3-10^7	10^{-4}	10^{-4}
SUN	.3-7	10^{11}	10^{-11}	10^{-11}

Figure Captions

Fig. 1: General behavior of neutrino oscillation in three different regions.

Fig. 2: Limit on the disappearance $\bar{\nu}_e \to x$ obtained at Gösgen Reactor. The positive result of Reines et al, is also plotted together with Soni-Silverman's analysis (crossed points).

Fig. 3: Site of BNL neutrino oscillation experiments. E775-I is at the location x734 and E776-I is at DET.#2. In phase II both experiments plan to place second detectors close to the other's.

Fig. 4: Expected behavior of R in E775-II, the ratio of neutrino flux at two different locations. The wavy line corresponds to $\delta m^2 = 1\ eV^2$ and the error bars to no oscillation.

Fig. 5: Site plan of CERN neutrino oscillation experiments.

Fig. 6, 7: Summary of the current world results (-) on various oscillation types. Expected results in the near future is given by (---) and those in the long future by (-·-·-).

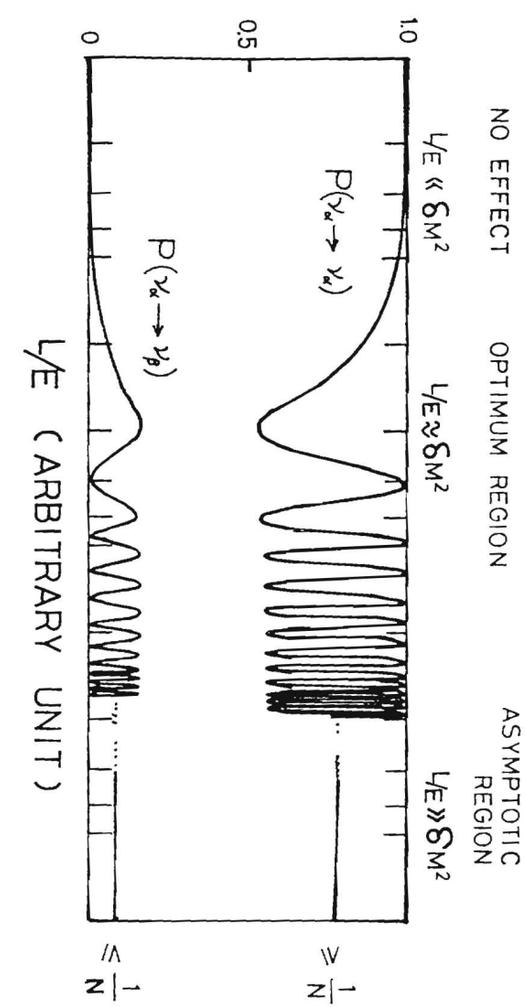

FIG. 1

FIG. 2

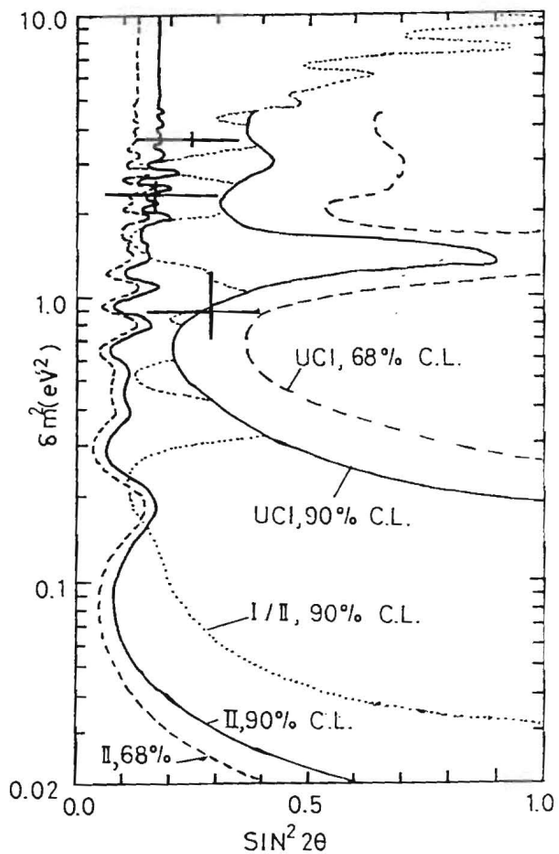
10.0
1.0
0.1
0.02
0.0
0.5
1.0
δm²(eV²)
SIN² 2θ
UCI, 68% C.L.
UCI, 90% C.L.
I / II, 90% C.L.
II, 90% C.L.
II, 68%

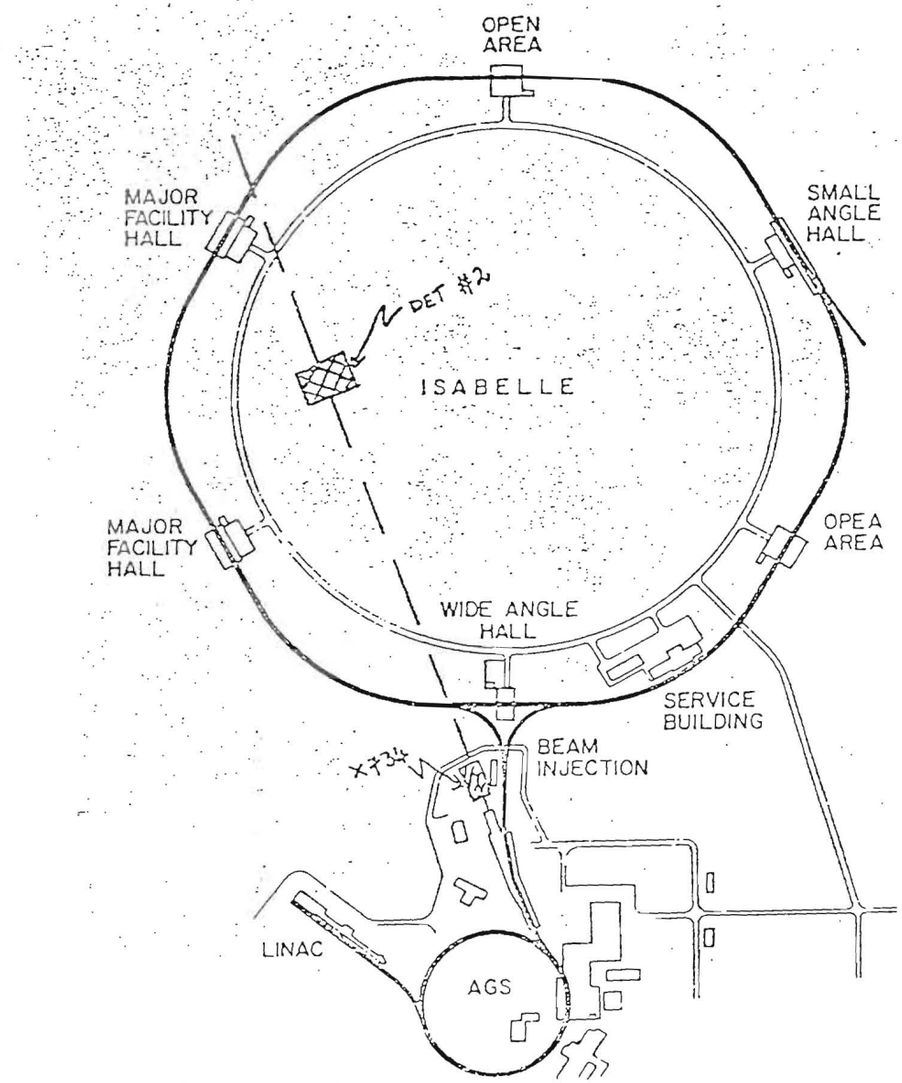
OPEN AREA
MAJOR FACILITY HALL
SMALL ANGLE HALL
DET #2
ISABELLE
MAJOR FACILITY HALL
OPEA AREA
WIDE ANGLE HALL
SERVICE BUILDING
BEAM INJECTION
LINAC
AGS

FIG. 3

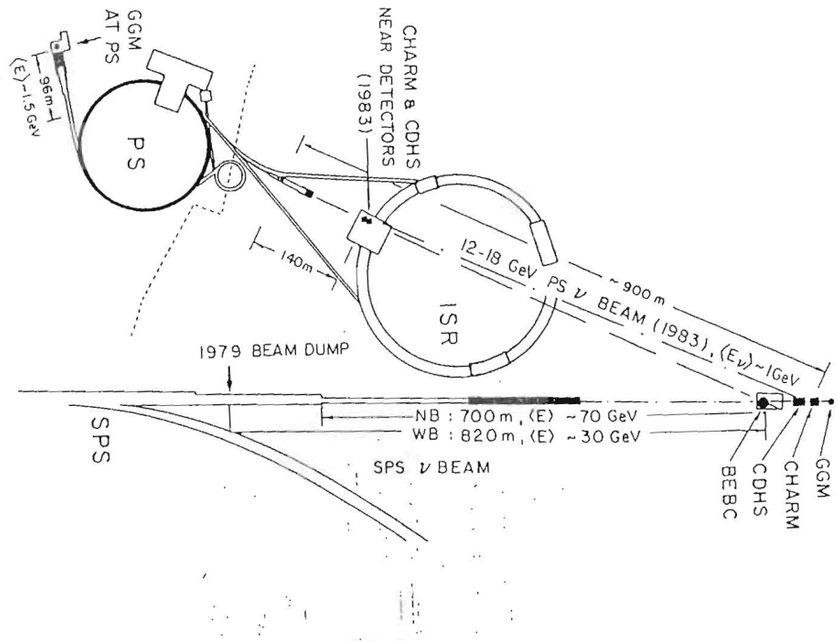
GGM AT PS
96m
⟨E⟩~1.5GeV
PS
CHARM & CDHS NEAR DETECTORS (1983)
140m
12-18 GeV PS ν BEAM (1983), ⟨Eν⟩~1GeV
~900m
ISR
1979 BEAM DUMP
NB : 700m, ⟨E⟩ ~70 GeV
WB : 820m, ⟨E⟩ ~30 GeV
SPS
SPS ν BEAM
BEBC
CDHS
CHARM
GGM

FIG. 5

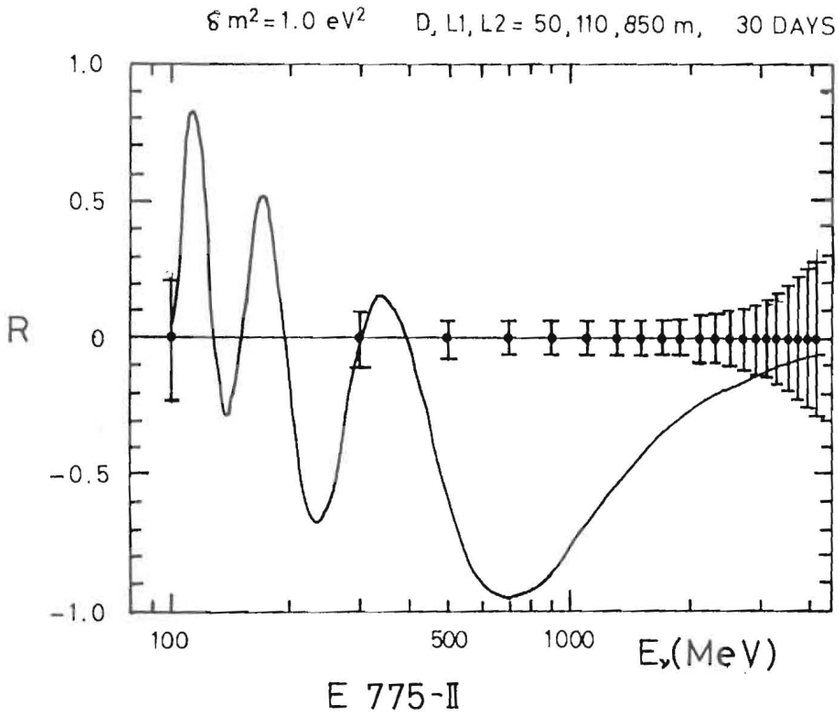
δm² = 1.0 eV²
D, L1, L2 = 50, 110, 850 m,
30 DAYS
1.0
0.5
0
−0.5
−1.0
R
100
500
1000
Eν(MeV)
E 775-II

FIG.4

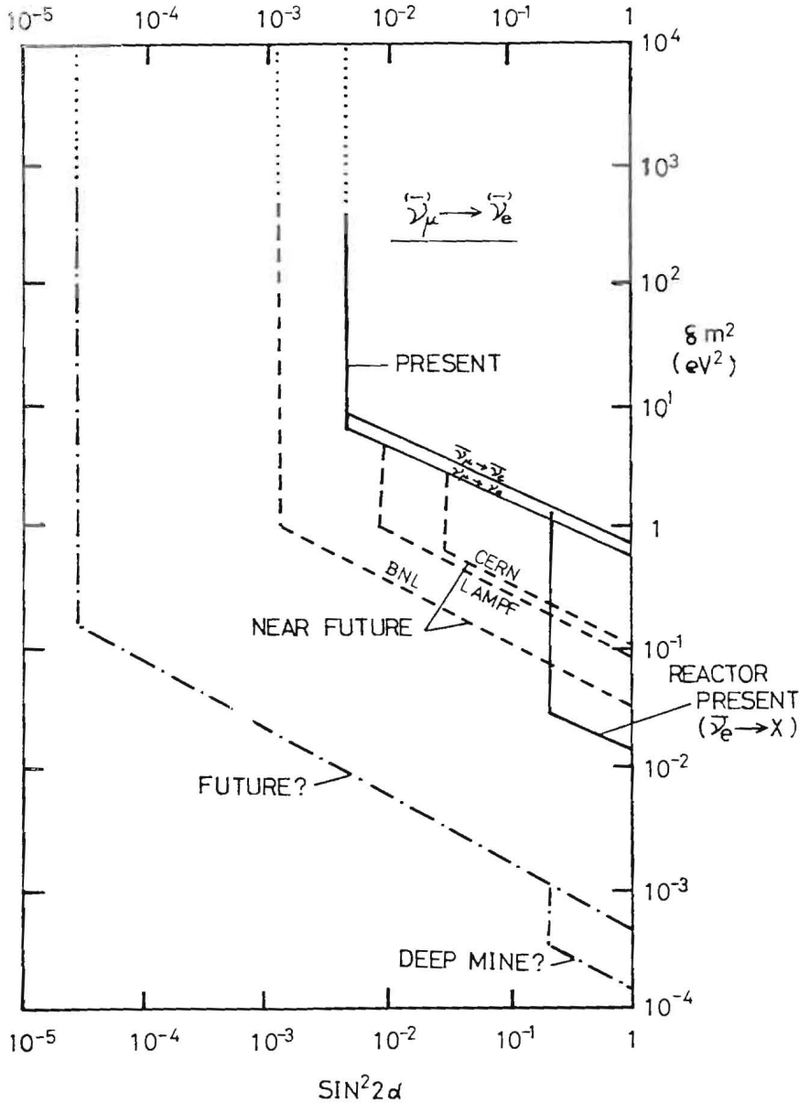
10^{-5} 10^{-4} 10^{-3} 10^{-2} 10^{-1} 1
10^4 10^3 10^2 10^1 1 10^{-1} 10^{-2} 10^{-3} 10^{-4}
δm^2 (eV^2)
$\bar{\nu}_\mu \rightarrow \bar{\nu}_e$
PRESENT
$\bar{\nu}_\mu \rightarrow \bar{\nu}_x$
$\bar{\nu}_e \rightarrow \bar{\nu}_x$
CERN
LAMPF
BNL
NEAR FUTURE
REACTOR
PRESENT
($\bar{\nu}_e \rightarrow X$)
FUTURE?
DEEP MINE?
$SIN^2 2\alpha$

FIG. 6

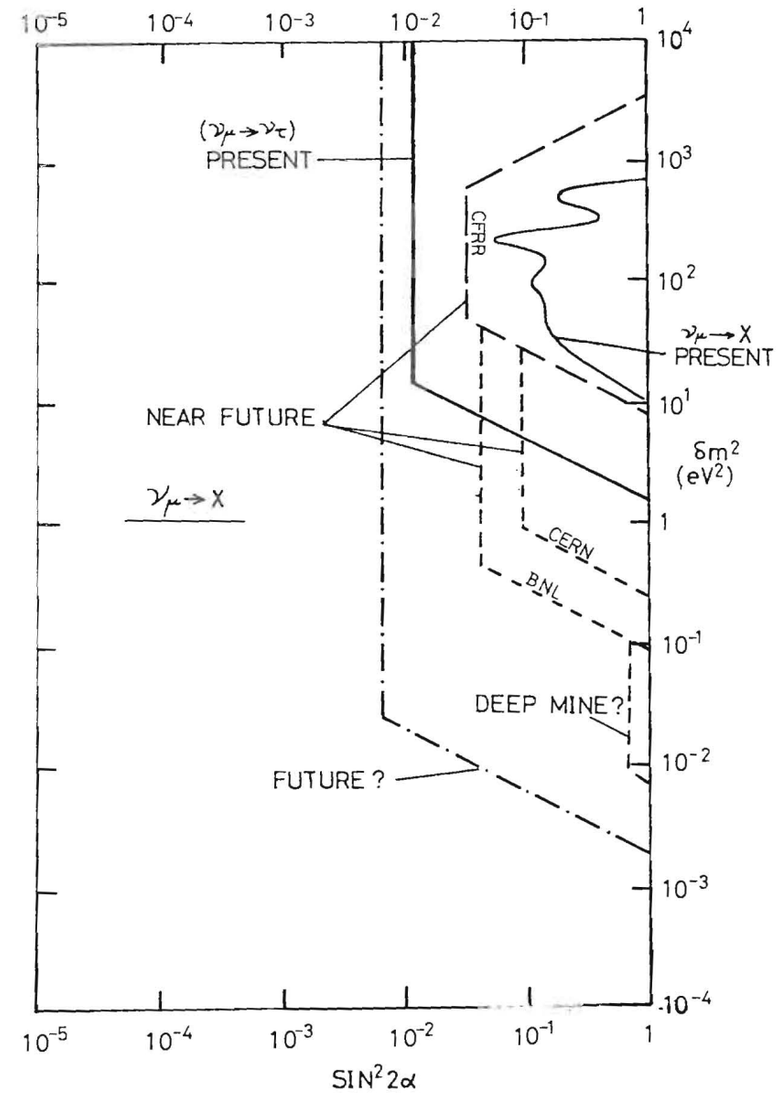
10^{-5} 10^{-4} 10^{-3} 10^{-2} 10^{-1} 1
10^4 10^3 10^2 10^1 1 10^{-1} 10^{-2} 10^{-3} 10^{-4}
($\nu_\mu \rightarrow \nu_\tau$)
PRESENT
CFRR
$\nu_\mu \rightarrow X$
PRESENT
NEAR FUTURE
$\nu_\mu \rightarrow X$
δm^2 (eV^2)
CERN
BNL
DEEP MINE?
FUTURE ?
$SIN^2 2\alpha$

FIG. 7

ELECTRON ANTINEUTRINO MASS FROM THE ß-DECAY OF ^3H

by

M. FUJIOKA

Cyclotron and Radioisotope Center, Tohoku University

Sendai, 980 Japan

Abstract

Experimental results on the mass of electron antineutrino $m_{\bar{\nu}_e}$ from the ß-decay of ^3H are briefly reviewed, and a project[1,2] is described of obtaining $m_{\bar{\nu}_e}$ by the same method using the INS (Institute for Nuclear Study, University of Tokyo) iron-free $\pi\sqrt{2}$ ß-ray spectrometer. The necessary statistics and the atomic effect on the ^3H ß-decay are discussed.

I. Introduction and review of ^3H ß-decay

Recently, possible finite mass of the neutrino has been discussed intensively both in terms of elementary-particle theory and astrophysics.[3,4] Experimentally, the information on the electron antineutrino mass $m_{\bar{\nu}_e}$ is the most accurate as illustrated in Fig. 1. The experimental results together with projects to our knowledge on $m_{\bar{\nu}_e}$

from the ^3H ß-decay are summarized in Table 1. Especially, Lubimov et al.[6] presented an indication of a finite value of $m_{\bar{\nu}_e}$, i.e., 14 eV < $m_{\bar{\nu}_e}$ < 46 eV at 99 % C.L. It is quite suggestive that this range of $m_{\bar{\nu}_e}$ is of the same order of magnitude as those estimated from grand unified theory (GUT) and astrophysics[24]; GUT based on O(10) predicts $m_\nu c^2 \sim 10$ eV, while considerations of the mean density of the universe and of the galactic halos require $m_\nu c^2 \lesssim 30$ eV and $m_\nu c^2 \gtrsim 10$ eV, respectively.[25] Since the rest mass of the neutrino if any will have a profound effect on our view of the elementary particles and of the universe, it is imperative to check the value of $m_{\bar{\nu}_e}$ presented by Lubimov et al. We are also[23] of the opinion that no substantial flaw is to be found despite scrutiny of the experimental and analytical procedures of Lubimov et al. A project of further study of $m_{\bar{\nu}_e}$ from the ^3H ß-decay is in progress as described below.

II. Present status of neutrino-mass project at INS

The most accurate method of extracting $m_{\bar{\nu}_e}$ from the ^3H ß-decay is considered to be a measurement using a large iron-free spectrometer, despite a unique advantage of being free from the so-called atomic effect in the case of ^3H implantation into a Si(Li) detector.[21] We intend to use the INS iron-free $\pi\sqrt{2}$ spectrometer[26] combined with a position-sensitive detector placed along the focal plane. In this case a successful measurement of the ^3H ß-spectrum rests upon three key points, i.e., 1) spectometer electron optics, 2) preparation of ^3H sources, and 3) the position-

sensitive detector.

II.1. Spectrometer electron optics

The INS spectrometer[26] consists of three pairs of current loops to generate required magnetic field around the central electron orbit of radius ρ = 75 cm. This spectrometer has been in use for 15 years, but mainly in the single-channel mode. A theoretical calculation of the electron trajectories by numerical integration[27] shows that the spectrometer should have a well-defined focal plane for a fractional momentum range of $|\varepsilon| \leq 2.5$ %, which is sufficient to cover the end-point region of the ^{3}H spectrum. Fig. 2 shows a bird's eye view of the spectrometer in its housing, and Fig. 3 shows an example of low-energy electron spectrum taken in a single-channel mode.[28]

For obtaining a highest luminosity we use the Bergkvist method[18] of an extended source of ^{3}H with a potential gradient as well as a position detector. An analysis of electron optics for such a configuration has been made on the basis of the second-order analytical solution.[29] More specifically, from an analysis on the third-order analytical solution an optimum configuration of source and detector has been proposed[30] for the $m_{\bar{\nu}_e}$ study of ^{3}H β-decay. Experimental verification of these theoretical predictions is in progress. As a result the iso-aberration contours of the spectrometer are shown to be the same as measured[31] 15 years ago. We do not use the aberration corrector[18] because this may cause background due to electron scattering. The geometry of the source-detector system is illustrated in

Fig. 4.

II.2. Preparation of the ^{3}H source

A large-area, uniform, thin and strong ^{3}H source is essential for the present study. Bergkvist used an "ion-pumping" method to implant ^{3}H into a thin surface layer of Al foils; this method has an advantage of stability but the specific activity of ^{3}H is ~0.1μmCi/2 g (in the following we assume an effective source thickness of 2μg/cm^2). Lubimov et al. made ^{3}H sources by evaporating ^{3}H-labeled valin (two H atoms of $C_5H_{11}NO_2$ replaced by ^{3}H); this gives a higher specific activity of ~0.5 mCi/2μg but has a disadvantage of ^{3}H release during a long run with the source placed in vacuum. Thus far we have been considering two methods of source preparation; 1) absorption of ^{3}H into a Ti metal layer[41], and 2) use of ^{3}H-labeled compound obtained, e.g., by adding ^{3}H atoms to the double bonds of organic molecules. These methods can give a specific activity up to ~1 mCi/2μg, but possible release of ^{3}H in vacuum is still a serious problem related with the background level[6] and the environmental pollution. The release rate of test sources is under study.

II.3. Position-sensitive detector

Position-sensitive gas counters have been successfully utilized as multichannel x-ray detectors or as focal-plane detectors of magnetic analysers for multichannel detection of heavy particles.[32] Good position detectors of low-energy electrons, however, had not been available until

recently, when single-wire (or plural-wires) position-sensitive proportional counters for electrons have been developed by the Kyūshū group[33] and by the INS group[34] with an intension of application to the INS iron-free spectrometer; see also ref. 35. In the former[33] the charge division is made by an analog circuit, while in the latter[34] by a digital circuit. For $E_e \geq 200$ keV a good position resolution has been obtained[36] as exemplified in Fig. 5. Since the position resolution becomes worse for lower energies, a new type of position detector, a parallel-plate avalanche counter, is under development at INS[36] in order to obtain a required resolution of $\Delta x \sim 1$ mm at $E_e \sim 20$ keV.

II.4. Expected performance of the present system

Expected performance[30] of the present system to be employed in the measurement of ^{3}H β-spectrum is shown in Table 2 in comparison with that realized by Lubimov et al. at ITEP (Inst. Theor. Exp. Phys.). Our aim is to attain an instrumental momentum resolution of $R_{instr} \sim 0.03$ % and an over-all resolution of $R_{exp} \sim 0.05$ % (corresponding to $\Delta E \sim 20$ eV at $E_e \sim 18.6$ keV), and to attain a neutrino-mass sensitivity of $\Delta m_{\bar{\nu}_e} c^2 \sim 10$ eV for checking the result of Lubimov et al.[6]

III. A simple consideration of statistics

The necessary counts, and hence the necessary ^{3}H source strength for attaining a neutrino-mass sensitivity $\Delta m_{\bar{\nu}_e} c^2$ from the end-point shape of the ^{3}H β-spectrum, and the detrimental effect of background level have been discussed.[9,18] Here we discuss this problem using a simple model of data analysis for obtaining an intuitive "feeling". Suppose that the extrapolated end-point energy E_0 is accurately known for the ^{3}H β-decay, and that we want to extract an upper limit of $m_{\bar{\nu}_e}$ from the net counts $n_0 \cdot \varepsilon \cdot t$ included between E_0 and E_0-100 eV $\equiv E_1$ (lower end-point region = ℓ.ep.r.), where n_0 is the total (net) counting rate of ^{3}H spectrum, ε is the fraction of β-rays falling in ℓ.ep.r., and t is the counting time. If we obtain the assumed constant background counting rate b from the higher ep.r. (E_0 to $E_2 = E_0 + 100$ eV) measured for the same time, we get $n_0 \varepsilon t = \Delta N - bt$, ΔN being the total counts in ℓ.ep.r., and hence $\varepsilon = (\Delta N - bt)/(n_0 t) \pm \sigma(\varepsilon)$ with $\sigma(\varepsilon) = \sqrt{n_0 \varepsilon t + 2bt}/(n_0 t)$. On the other hand the dependence of ε on $m_{\bar{\nu}_e}$ can be approximated by $\varepsilon \simeq \varepsilon(0)[1 - 1.24\,(m_{\bar{\nu}_e} c^2/100\ \text{eV})^{1.98}]$ for $0 \leq m_{\bar{\nu}_e} c^2 \leq 100$ eV, where $\varepsilon(0) \equiv \varepsilon(m_{\bar{\nu}_e} = 0)$. Thus we arrive at an estimation of the necessary net counts $n_0 \varepsilon(0) t$ as a function of the N/S ratio = $b/[n_0 \varepsilon(0)]$ and the required mass sensitivity $\Delta m_{\bar{\nu}_e}$ when $m_{\bar{\nu}_e} = 0$;

$$n_0 \varepsilon(0) t = 0.65\left(1 + \frac{2b}{n_0 \varepsilon(0)}\right)\left(\frac{100\ \text{eV}}{m_{\bar{\nu}_e} c^2}\right)^{3.96} .$$

Fig. 6 shows an analysis using this expression of the experimental spectra of Bergkvist (3 runs together) and of Lubimov et al. (16 runs). Although the present model of data analysis is too simple to be quantitative, we can understand a qualitative relation between the statistics of ^{3}H spectrum and the conclusion on $m_{\bar{\nu}_e}$; Bergkvist extracted

$m_{\bar{\nu}_e}c^2 \leq 55$ eV vs $\Delta m_{\bar{\nu}_e}c^2 \sim 21$ eV from Fig. 6, whereas Lubimov et al. obtained 14 eV $< m_{\bar{\nu}_e}c^2 < 46$ eV vs $\Delta m_{\bar{\nu}_e}c^2 \sim 11$ eV from Fig. 6.

From the above discussion suppression of the background level is seen to be quite important. Multichannel detection using a position-sensitive detector along the focal plane of a flat-type spectrometer is therefore quite promising, since the background contribution per channel is expected to be small in such a scheme.

IV. Extra-nuclear effect on the ^{3}H β-decay

Extra-nuclear effect, or so called "atomic effect"[18,37,38], on the end-point shape of the ^{3}H β-spectrum should be important for the case of magnetic or similar spectrometers where only the emerging β-particles are measured. Lubimov et al. represented the effect of excitation of the final $^3He^+$ ion by an effective level of 43 eV above the $^3He^+$ ground state (1s) with an excitation probability of 30 % (see Table 3). A convenient analytical expression for the $^3He^+$ excitation probability in the ^{3}H β-decay has been presented by Fukugita and Kubodera,[39] on the basis of which they show that an explicit account of the continuum excitation (or shake-off) results in a negligible effect on the end-point shape, thus supporting the analysis of Lubimov et al. in extracting $m_{\bar{\nu}_e}$. For a convenient reference the theoretical excitation spectrum is shown in Fig. 7; the total probability of continuum excitation (i.e., shake-off probability) is as small as 2.7 %. The theoretical spectrum

(Fig. 7) can be approximated by equivalent two or three levels as given in Table 3, where an effective level has a gaussian shape with an equivalent standard deviation; in Table 3 the width is given in half width Γ. In the two-level approximation the energy and width adopted by Lubimov et al. are smaller than the theoretical ones. Therfore, use of the theoretical spectrum will push the experimental value of $m_{\bar{\nu}_e}$ to the larger side. Recently, the experimental end-point spectrum of Lubimov et al. has been reanalysed[40] on the basis of an exact theoretical treatment of $^3He^+$ excitation and shake-off, leading to essentially no change of the resulting value of $m_{\bar{\nu}_e}$. In ref. 40 molecular or solid-state effect is also discussed qualitatively, which effect might alter the final result.

We consider that the atomic effect in its narrower sense is not an essential hindrance to the measurement of $m_{\bar{\nu}_e}$ from the ^{3}H β-decay end-point shape, and that a measurement at a higher resolution and a lower background level will substantially improve our information on $m_{\bar{\nu}_e}$. At the same time quantitative theoretical investigation of the molecular and solid-state effect on the ^{3}H β-decay is invaluable.

References

1) The members of the present project are, T. Ohshima, H. Kawakami, Y. Fujita, K. Ukai, N. Morikawa (Univ. of Tokyo), M. Fujioka, Y. Shōji (Tohoku Univ.), M. Iwahashi (Tokyo Metropolitan Univ.) and K. Hisatake (Tokyo Inst.

of Tech.).

2) T. Ohshima: Soryūshiron Kenkyū, 62(1980) 57 (in Japanese). See also, T. Ohshima: Inst. Nucl. Study rept. INS-Rep.-406, March 1981.

3) E. Fiorini ed: Proc. Neutrino '80, Neutrino Physics and Astrophysics (Plenum, N.Y. and London, 1982).

4) J. Audouze-P. Crane, T. Gaisser-D. Hegyi and J. Tran Thanh Van eds.: Proc. 16th Renc. Moriond, Astrophys. Meeting, Cosmology and Particles (Ed. Frontiéres, Preux, 1981).

5) Particle Data Group: Phys. Letters, 111B(1982, April).

6) V. A. Lubimov, E. G. Movikov, V. Z. Nozik, E. F. Tretyakov and V. S. Kosik: Phys. Letters, 94B(1980) 266.

7) J. U. Andersen, G. J. Beyer, C. Charpak, A. De Rújula, E. Elbek, H. Å. Gustafsson, P. G. Hansen, B. Jonson, P. Knudsen, E. Laegsgaard, J. Pedersen and H. L. Ravn: Phys. Letters, 113B(1982) 72.

8) S. Yasumi, these proceedings. Also, S. Yasumi, G. Rajasekaran, M. Ando, F. Ochiai, H. Ikeda, T. Ohta, P. M. Stefan, M. Maruyama, N. Hashimoto, M. Fujioka, K. Ishii, T. Shinozuka, K. Sera, T. Omori, G. Izawa, M. Yagi, K. Masumoto and K. Shima: submitted to Phys. Letters B.

9) C. S. Wu: Wisconsin Neutrino Mass Mini-Conf. and Workshop, Oct. 2-4, 1980.

10) S. G. Curran, J. Angus and A. L. Cockroft: Nature, 162 (1948) 302.

11) G. C. Hanna and B. Pontecorvo: Phys. Rev., 75(1949) 983.

12) L. M. Langer and R. J. D. Moffat: Phys. Rev., 88(1952) 689.

13) D. R. Hamilton, W. P. Alford and L. Gross: Phys. Rev., 92(1953) 1521.

14) L. Friedman and L. Smith: Phys. Rev., 109(1958) 2214.

15) R. C. Salgo and H. H. Staub: Nucl. Phys., 138A(1969) 417.

16) R. Daris and C. St.-Pierre: Nucl. Phys., 138A(1969) 545.

17) B. Röde and H. Daniel: Nuovo Cim. Letter, 5(1972) 139.

18) K.-E. Bergkvist: Nucl. Phys., B39(1972) 317, 371.

19) W. F. Piel: Nucl. Phys., A203(1973) 369.

20) E. F. Tretyakov, N. F. Myasoedov, A. M. Apalikov, V. F. Konyaev, V. A. Lubimov and E. G. Novikov: Bull. Acad. Sci. USSR, Phys. Ser., 40(1976) 1; E. F. Tretyakov: Bull. Acad. Sci. USSR, Phys. Ser., 39(1975) 583.

21) J. J. Simpson: Phys. Rev., D23(1981) 649.

22) R. Andrews: priv. commun. (1982).

23) R. G. H. Robertson, T. J. Bowles, M. Maley, J. C. Browne, J. Burritt, J. Toevs, M. Stelts, J. Helfrick, D. Knapp, A. G. Ledebuhr: Neutrino '82, Balatonfüred, Hungary, June 1982.

24) P. H. Frampton and P. Vogel: Phys. Rept., 82(1982) 339.

25) More exactly, $\sum_i m_{\nu_i} c^2 \lesssim 30$ eV and $[\sum_i (m_{\nu_i} c^2)^4]^{\frac{1}{4}} \gtrsim 10$ eV.

26) M. Fujioka and K. Hisatake: Inst. Nucl. Study Rept.,

INS-TL-89(1966) (in Japanese); M. Fujioka: Nucl. Phys., A153(1970) 337; H. Kawakami and Y. Fujita: Genshikaku Kenkyū, 25(1980) 1 (in Japanese); H. Kawakami and Y. Fujita: INS-TL-143(1982) (in Japanese).

27) M. Fujioka, H. Kawakami and M. Hirasawa: Inst. Nucl. Study Journ. INS-J, to be published. See also ref. 29.

28) M. Fujioka, M. Takashima, M. Kanbe, O. Dragoun and M. Ryšavý: Z. Phys., A299(1981) 283.

29) M. Fujioka, H. Kawakami and M. Hirasawa: Proc. 1981 INS Internat. Symp. Nucl. Rad. Detectors, Tokyo, 23-26 March, 1981, p. 584.

30) Y. Shōji, H. Kawakami, K. Hisatake, M. Fujioka and T. Ohshima: INS-TL, to be published (in Japanese).

31) M. Fujioka: Buturi, 9(1973) 788 (Phys. Soc. Japan) (in Japanese).

32) Proc. 1981 INS Symp. See also, D. A. Bromley ed.: Detectors in Nuclear Science, Nucl. Instrum. Meth. 162 no. 1-3(1979).

33) Y. Yoshida, K. Tsuji, S. Umesaki and K. Marubayashi: Nucl. Instrum. Meth., 189(1981) 423; Y. Yoshida, K. Tsuji, K. Marubayashi and Y. Matsumoto: Nucl. Instrum. Meth., 154(1978) 261.

34) Y. Fujita, H. Kawakami and H. Hosoda: Nucl. Instrum. Meth., 196(1982) 271.

35) E. J. de Graaf, A. M. Paans, M. G. Woldling and W. J. J. Spijkervet: Nucl. Instrum. Meth., 166(1979) 139; W. J. J. Spijkervet: Application of Conversion Electron Spectroscopy to Solid-State Problems, thesis, Univ. Groningen, Dec. 1980.

36) Y. Fujita: priv. commun. (1982).

37) K.-E. Bergkvist: Phys. Scripta, 4(1971) 23.

38) R. D. Scott: J. Phys., A4(1971) L105.

39) M. Fukugita and K. Kubodera: Z. Phys., C9(1981) 365.

40) J. Law: Phys. Letters, 102B(1981) 371, and references therein.

41) H. L. Adair, E. H. Kobisk and B. L. Byrum: Nucl. Instrum. Meth., 200(1982) 99.

Table 1 Experimental results and projects on $m_{\bar{\nu}_e}$ from ^3H[a)]

Year	$m_{\bar{\nu}_e}c^2$ (C.L.)	Instrument	Authors
1948	< 1 keV	Proportional counter	Curran, Angus & Cockroft[10)]
1949	< 1 keV	Prop. C.	Hanna & Pontecorvo[11)]
1952	< 250 eV	Magnetic (iron core) shaped-field spectrometer	Langer & Moffat[12)]
1953	< 500 eV	Electrostatic (spherical) integral sp.	Hamilton, Alford & Gross[13)]
1958	< 550 eV	Mass sp. (synchrometer)	Friedman & Smith[14)]
1969	< 200 eV (80 %)	Electrostatic retarding sp.	Salgo & Staub[15)]
1969	< 75 eV (68 %)	Magnetic (iron core) single-focusing sp.	Daris & St-Pièrre[16)]
1972	< 86 eV	Magnetic (iron free) $\pi\sqrt{13/2}$ sp.	Röde & Daniel[17)]
1972	< 55 eV (90 %)	Magnetic (iron core) $\pi\sqrt{2}$ sp. + aberr. corr. + extended source	Bergkvist[18)]
1973	< 100 eV	the same as ref. 12	Piel[19)]
1976	< 35 eV (90 %)	Magnetic (iron free) toroidal sp. + plural sources & det.	Tretyakov et al.[20)]
1980	14 eV < < 46 eV (99 %)	the same as preceeding	Lubimov et al.[5)]
1981	< 65 eV (95 %)	Implanted Si(Li) det.	Simpson[21)]
1980 ~		Magnetic (iron-free) $\pi\sqrt{2}$ sp. + pos. sens. det. + ext. source	the present group
1981?~		similar as preceeding	Chalk River Group[22)]
1980?~		Magnetic (iron free) toroidal sp. + atomic source + plural det.	Robertson et al.[23)]

a) For the recent review of $m_{\bar{\nu}_e}$ from the ^3H β-decay see also ref. 9.

Table 2 Comparison of the expected performance of the INS system with that realized by the ITEP system

Quantity	INS[30)]	ITEP[6)]
Transmission	0.095 %	0.8 %
Source area	110 cm^2	9 cm^2
Effective source area	42 cm^2	7.5 cm^2
Number of channels	96	3
Covered energy range	1.5 keV	0.7 keV
Luminosity	0.04 cm^2	0.06 cm^2
Data collection efficiency	3.8 cm^2	0.17 cm^2
Momentum resolution	0.05 %	0.12 %
Energy resolution at 18.6 keV	20 eV	45 eV

Table 3 Approximation of the excitation of $^3H^+$ in ^3H β-decay (including shake-off) by two or three levels

	Lubimov et al.[a)]	Two levels[b)]	Three levels[b)]
	grd (0) 70 %	grd (0) 70.2 %	grd (0) 70.2 %
E_p (Γ)	43 eV (0) 30 %	47.5 eV (77.1 eV) 29.8 %	40.8 eV (5.8 eV) 27.1 %
	———	———	88.5 eV (228 eV) 2.7 %

a) As employed in the analysis of ref. 6.

b) Approximation to Fig. 7 (see also ref. 39).

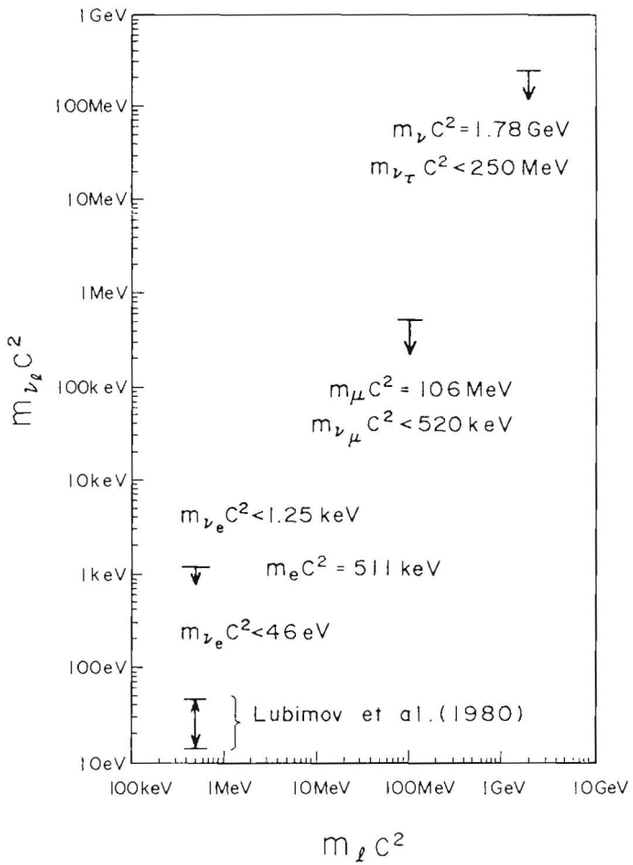

Fig. 1. Experimental results on neutrino or anti-neutrino masses; for ν_τ and ν_μ see ref. 5, for $m_{\bar{\nu}_e}$ refs. 5, 6 and for m_{ν_e} refs. 7, 8.

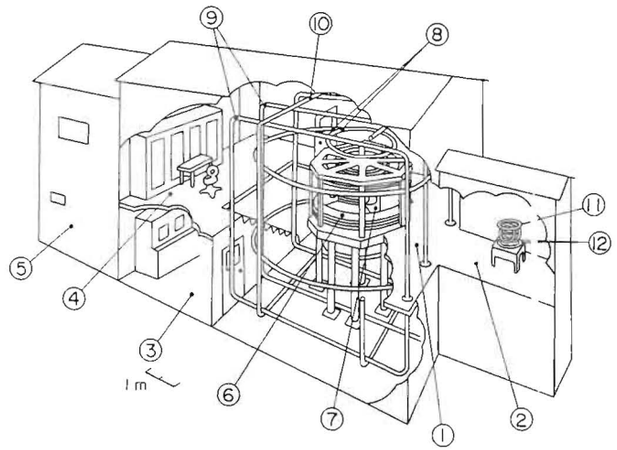

Fig. 2. INS iron-free $\pi\sqrt{2}$ spectrometer and its housing; 1) Spectrometer room, 2) Magnetometer room, 3)Power-supply room, 4) Control room, 5) Machine room, 6) Large coil, 7) Vacuum chamber, 8) Vertical H.C.(Helmholtz coils), 9) North-south H.C., 10) East-west H.C., 11) Spectrometer-field compensation coil, and 12) Magnetometer H.C.

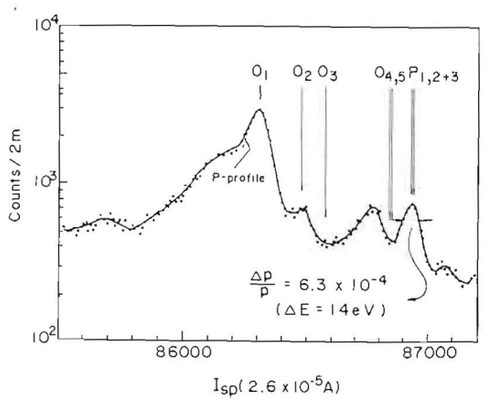

Fig. 3. Conversion spectrum of the 10.84 keV transition in ^{206}Bi in the region of O to P lines taken at instrumental momentum resolution of 0.05 % in a single-channel mode.[28]

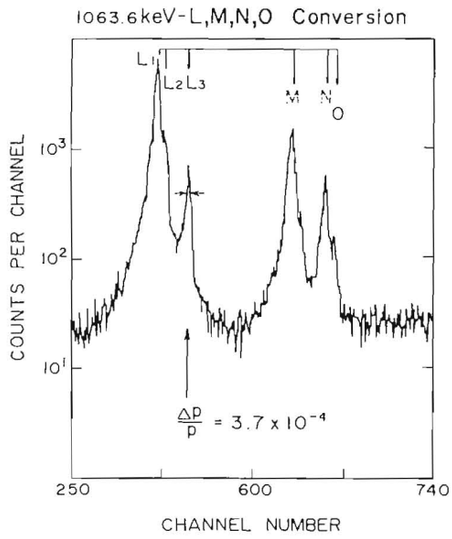

Fig. 5. Conversion spectrum of the 1063 keV transition in ^{207}Pb in a multichannel mode using a single-wire position sensitive proportional counter[36] at $R_{instr} = 3\times10^{-4}$.

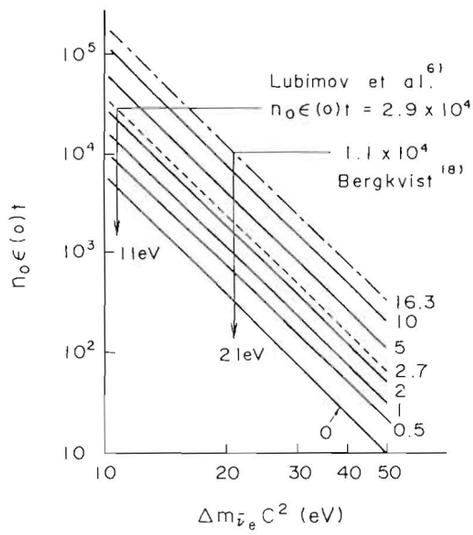

Fig. 6. Relation between required net counts $n_0\varepsilon(0)t$ in 100 eV down the end point and mass sensitivity $\Delta m_{\bar{\nu}_e}c^2$ with N/S ratio $b/(n_0\varepsilon(0))$ as a parameter.

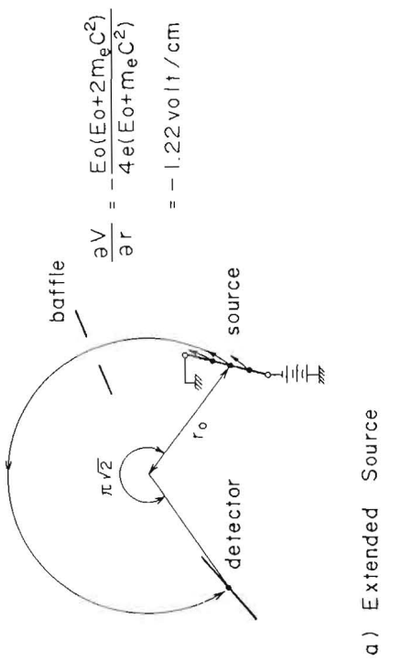

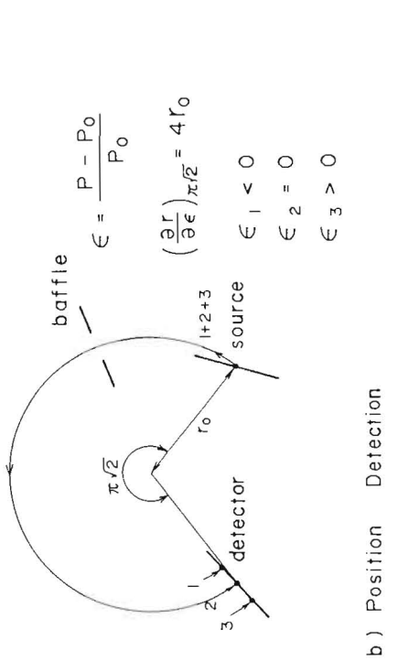

Fig. 4. Source-detector system of INS spectrometer for the measurement of ^3H β-spectrum.

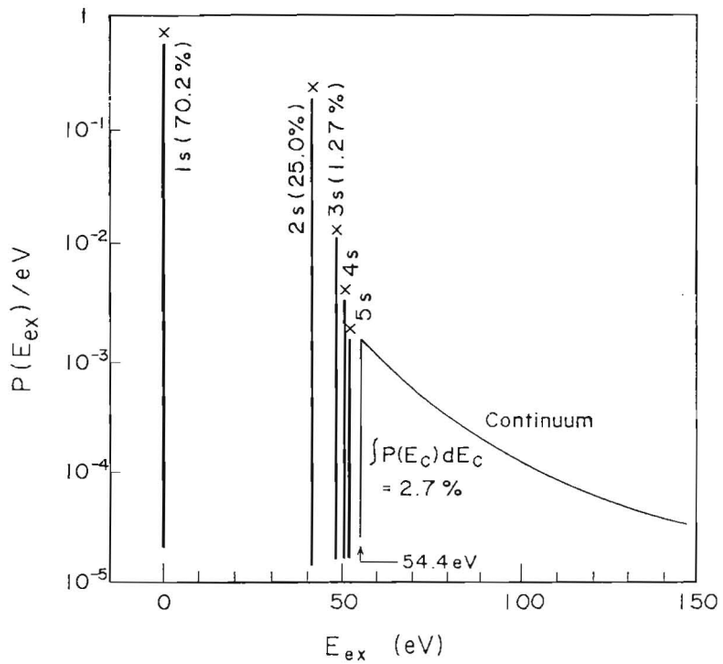

Fig. 7. Excitation spectrum of $^3He^+$ according to ref. 39. Continuum excitation corresponds to shake-off. The width of the excitation to bound states is taken to be 1 eV as a histogram.